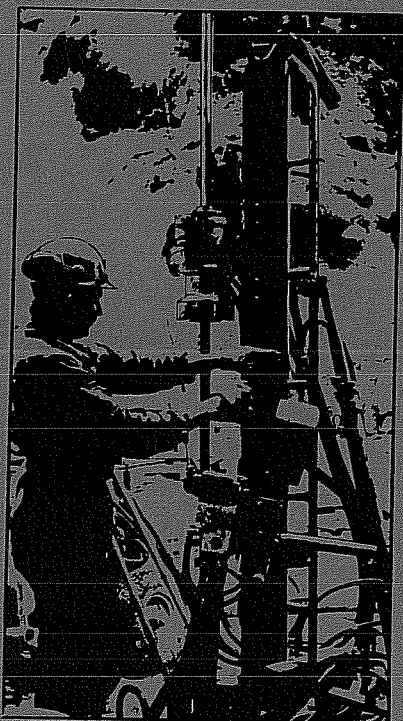


SWEDISH-AMERICAN COOPERATIVE PROGRAM ON RADIOACTIVE WASTE STORAGE IN MINED CAVERNS IN CRYSTALLINE ROCK



Technical Information Report No. 20

CHARACTERIZATION OF DISCONTINUITIES IN THE STRIPA GRANITE TIME-SCALE HEATER EXPERIMENT

Richard Thorpe
Lawrence Berkeley Laboratory
University of California
Berkeley, California 94720

July 1979

A Joint Project of

Swedish Nuclear Fuel Supply Co.
Fack 10240 Stockholm, Sweden

Operated for the Swedish
Nuclear Power Utility Industry

Lawrence Berkeley Laboratory
Earth Sciences Division
University of California
Berkeley, California 94720, USA

Operated for the U.S. Department of
Energy under Contract W-7405-ENG-48

This report was prepared as an account of work sponsored by the United States Government and/or the Swedish Nuclear Fuel Supply Company. Neither the United States nor the U.S. Department of Energy, nor the Swedish Nuclear Fuel Supply Company, nor any of their employees, nor any of their contractors, subcontractors, or their employees, makes any warranty, express or implied or assumes any legal liability or responsibility for the accuracy, completeness or usefulness of any information, apparatus, product or process disclosed, or represents that its use would not infringe privately owned rights.

Printed in the United States of America
Available from
National Technical Information Service
U.S. Department of Commerce
5285 Port Royal Road
Springfield, VA 22161
Price Code: A06

LBL-7083
SAC-20
UC-70

CHARACTERIZATION OF DISCONTINUITIES IN THE STRIPA
GRANITE - TIME-SCALE HEATER EXPERIMENT

Richard Thorpe

Lawrence Berkeley Laboratory
University of California
Berkeley, California 94720

July 1979

This report was prepared by the Lawrence Berkeley Laboratory under the University of California contract W-7405-ENG-48 with the Department of Energy. Funding for this project is administered by the Office of Nuclear Waste Isolation at Battelle Memorial Institute.

PREFACE

This report is one of a series documenting the results of the Swedish-American cooperative research program in which the cooperating scientists explore the geological, geophysical, hydrological, geochemical, and structural effects anticipated from the use of a large crystalline rock mass as a geologic repository for nuclear waste. This program has been sponsored by the Swedish Nuclear Power Utilities through the Swedish Nuclear Fuel Supply Company (SKBF), and the U.S. Department of Energy (DOE) through the Lawrence Berkeley Laboratory (LBL).

The principal investigators are L. B. Nilsson and O. Degerman for SKBF, and N. G. W. Cook, P. A. Witherspoon, and J. E. Gale for LBL. Other participants will appear as authors of the individual reports.

Previous technical reports in this series are listed below.

1. Swedish-American Cooperative Program on Radioactive Waste Storage in Mined Caverns by P. A. Witherspoon and O. Degerman. (LBL-7049, SAC-01).
2. Large Scale Permeability Test of the Granite in the Stripa Mine and Thermal Conductivity Test by Lars Lundstrom and Haken Stille. (LBL-7052, SAC-02).
3. The Mechanical Properties of the Stripa Granite by Graham Swan. (LBL-7074, SAC-03).
4. Stress Measurements in the Stripa Granite by H. Carlsson. (LBL-7078, SAC-04).
5. Borehole Drilling and Related Activities at the Stripa Mine by Pavel J. Kurfurst, T. Hugo-Persson, and G. Rudolph. (LBL-7080, SAC-05).
6. A Pilot Heater Test in the Stripa Granite by Hans Carlsson. (LBL-7086, SAC-06).
7. An Analysis of Measured Values for the State of Stress in the Earth's Crust by Dennis B. Jamison and Neville G. W. Cook. (LBL-7071, SAC-07).
8. Mining Methods Used in the Underground Tunnels and Test Rooms at Stripa by B. Andersson and P. A. Halen. (LBL-7081, SAC-08).
9. Theoretical Temperature Fields for the Stripa Heater Project by Tin Chan, Neville G. W. Cook, and Chin-Fu Tsang. (LBL-7082, SAC-09).

10. Mechanical and Thermal Design Considerations for Radioactive Waste Repositories in Hard Rock. Part I: An Appraisal of Hard Rock for Potential Underground Repositories of Radioactive Wastes by Neville G. W. Cook; Part II: In Situ Heating Experiments in Hard Rock: Their Objectives and Design by Neville G. W. Cook and Paul A. Witherspoon. (LBL-7073, SAC-10).
11. Full-Scale and Time-Scale Heating Experiments at Stripa: Preliminary Results by Neville G.W. Cook and Michael Hood. (LBL-7072, SAC-11).
12. Geochemistry and Isotope Hydrology of Groundwaters in the Stripa Granite: Results and Preliminary Interpretation by P. Fritz, J.F. Barker, and J.E. Gale. (LBL-8285, SAC-12).
13. Electrical Heaters for Thermo-mechanical Tests at the Stripa Mine by R. H. Burleigh, E. P. Binnall, A. O. DuBois, D. U. Norgren, and A. R. Oritz. (LBL-7063, SAC-13).
14. Data Acquisition, Handling, and Display for the Heater Experiments at Stripa by Maurice B. McEvoy (LBL-7062, SAC-14).
15. An Approach to the Fracture Hydrology at Stripa: Preliminary Results by J. E. Gale and P. A. Witherspoon. (LBL-7079, SAC-15).
16. Preliminary Report on Geophysical and Mechanical Borehole Measurements at Stripa by P. Nelson, B. Paulsson, R. Rachiele, L. Andersson, T. Schrauf, W. Hustrulid, O. Duran, and K. A. Magnusson. (LBL-8280, SAC-16).
17. Observations of a Potential Size-Effect in Experimental Determination of the Hydraulic Properties of Fractures by P. A. Witherspoon, C. H. Amick, J. E. Gale, and K. Iwai (LBL-8571, SAC-17).
18. Rock Mass Characterization for Storage of Nuclear Waste in Granite by P. A. Witherspoon, P. Nelson, T. Doe, R. Thorpe, B. Paulsson, J. Gale, and C. Forster (LBL-8570, SAC-18).
19. Fracture Detection in Crystalline Rock Using Shear Waves by K. H. Waters, S. P. Palmer, and W. E. Farrell (LBL-7051, SAC-19).

TABLE OF CONTENTS

	<u>Page</u>
LIST OF FIGURES.	vii
LIST OF TABLES	viii
ABSTRACT	1
1. INTRODUCTION	2
2. BACKGROUND.	5
2.1 The Time-Scale Experiment.	5
2.2 Geology of the Stripa Mine	7
3. SOURCES OF DATA.	11
3.1 Floor Mapping	11
3.2 Core Logs	13
3.3 Comparison of Data Sources	17
4. DETERMINISTIC CHARACTERIZATION OF DISCONTINUITIES	20
4.1 Methodology	20
4.2 Results	23
5. STATISTICAL CHARACTERIZATION OF DISCONTINUITIES	35
5.1 Fracture Orientations	36
5.2 Fracture Sizes	39
5.3 Fracture Spacings	44
5.4 Fracture Infilling Characteristics	47
6. DISCUSSION	53
6.1 Origin of the Fracture System	53
6.2 Current Deformations.	56
6.3 Use of the Deterministic Results	59
6.4 Limitations of Statistical Results	61

	<u>Page</u>
7. CONCLUSIONS	61
8. ACKNOWLEDGMENTS	63
9. REFERENCES	65
10. APPENDICES	67
<hr/>	
A. Borehole Fracture Logs for Time-Scale Experiment	67
B. Photographs of Time-Scale Experiment Core Samples	89
C. Stereonet Plots of Fracture Poles for Time-Scale Experiment Boreholes	99

LIST OF FIGURES

	<u>Page</u>
1. Location of Stripa Mine	2
2. General plan of test site.	5
3. Borehole layout in the time-scale drift	6
4. Sub-till geology at Stripa	8
5. Use of 1 x 1 m reference frame in fracture mapping.	12
6. Detailed map of discontinuities in the floor of the time-scale experiment drift	15
7. Fracture frequencies from detailed floor map	18
8. Core log fracture frequencies	18
9. Fracture frequencies for all fractures visible in core photographs	19
10. Generalized map of major discontinuities in the floor of the time-scale experiment drift	21
11. Subsurface profile along centerline of drift showing major discontinuities through the heater array.	24
12. Three-dimensional views of the four continuous fractures passing through the heater array	26
13. View of fracture no. 3 borehole locations, parallel to direction of shear	29
14. Contour diagram of fracture poles from time-scale experiment boreholes	37
15. Generalized fracture set boundaries corresponding to 1.5 percent contour	39
16. Generalized fracture set boundaries for analysis of mapped fracture lengths	40
17. Fracture length-frequency histograms for the three non-horizontal joint sets.	42
18. Cumulative lognormal fracture length distributions.	43
19. Vertical fracture spacing-frequency histograms for all four joint sets.	45

	<u>Page</u>
20. Cumulative lognormal distributions of fracture spacings in vertical direction	46
21. Stereographic plots of poles of fractures with the three major types of mineralization	49
22. Stereographic plots of fractures with different thicknesses	52
23. Relationship of mean fracture set orientations and measured principal stress directions	54
24. Resolution of shear and normal stresses in the mean plane of fracture set 1	57

LIST OF TABLES

1. Subsurface coordinates of fracture 1	31
2. Subsurface coordinates of fracture 2	32
3. Subsurface coordinates of fracture 3	33
4. Subsurface coordinates of fracture 4	34
5. Fracture length distribution parameters	43
6. Fracture spacing distribution parameters.	47
7. Fracture mineralization data for the Stripa core logs	48
8. Statistical mineralization data from Stripa fracture logs	52
9. Thickness data for fracture infillings	53
10. Shear and normal stresses on the mean planes of the four fracture sets	58

ABSTRACT

The report describes the methodology and results of a detailed study of geologic discontinuities associated with the time-scale heater test at the Stripa mine in Sweden. Mapping of the floor of the experiment tunnel coupled with observation of core samples from beneath the drift indicate that four N-striking shear fractures dip steeply through the 6x10x25-m rock mass. Oblique-thrust faulting has produced displacements of up to 2 m on one of the surfaces, and its inferred 3-D configuration is consistent with observed slickensiding. Resolution of locally measured principal stresses on the shear plane yields a theoretical shear direction that also coincides with the slickensiding.

Four distinct joint sets exist locally, one of which coincides with the shear fractures. Another lies nearly horizontal, and two others are steeply inclined. Fracture length and spacing distributions for the four joint sets are shown to be lognormal. Two of the sets lie perpendicular to principal stress directions. The fact that one of these two joint sets apparently post-dates other fracturing and is normal to the minimum principal stress suggests that it is due to isostatic rebound.

1. INTRODUCTION

In June of 1977, Lawrence Berkeley Laboratory (LBL), and the Swedish Nuclear Fuel Safety Program (KBS) initiated a cooperative research program to study the suitability of crystalline rocks for storage of nuclear waste. Within the program are several different experimental projects, which are described by Witherspoon and Degerman (1978), Cook and Witherspoon (1978), and Gale and Witherspoon (1978). The field site for the research is located in south central Sweden (Fig. 1), at the Stripa mine. The history of mining

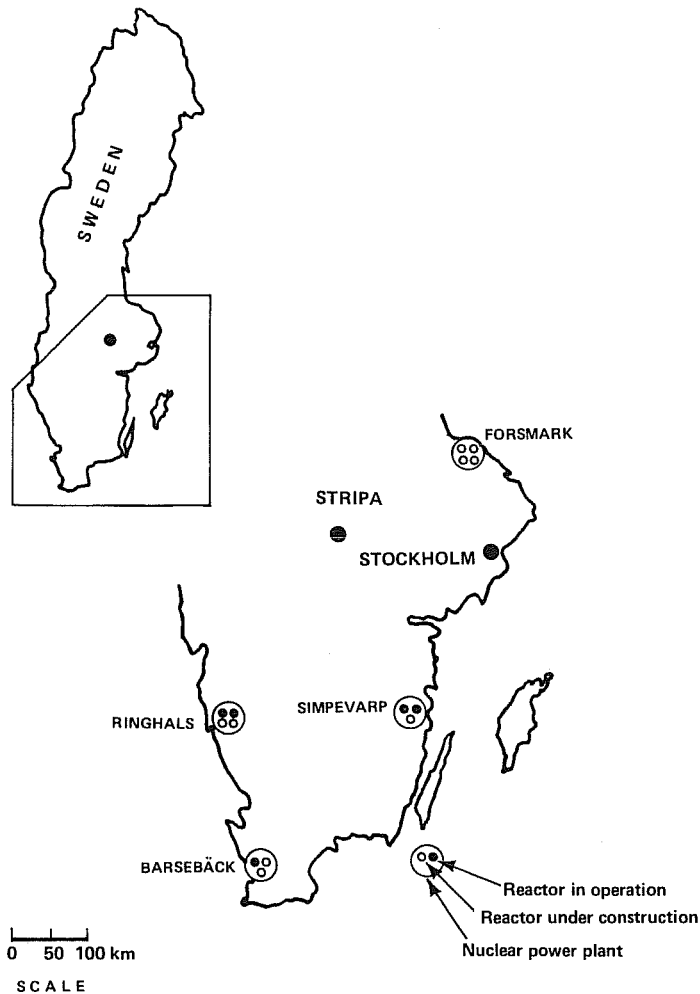


Fig. 1. Location of Stripa Mine.

in the area and at Stripa is centuries old; iron ore production at the mine ceased early in 1977, however. Since that time the mine has been operated as an underground experimentation site under the auspices of the parent organization of KBS, the Swedish Nuclear Fuel Supply Company (SKBF).

The field studies involve two disciplines, subsurface hydrology and thermomechanical behavior within massive fractured granite. Both aspects of the program require characterization of the fracture system because of its recognized importance to the stability of mined openings and the movement of fluids within the rock mass (Office of Waste Isolation 1977). The scope of characterization, however, depends on the extent of the rock mass influenced by the individual experiments. The heater experiments affect localized rock volumes of up to about a thousand cubic meters, whereas the hydrologic research involves volumes several orders of magnitude larger. While the latter requires a statistical approach to define the fracture network, the heater experiments require a more detailed study in which significant fractures are delineated in the subsurface. This report describes results of such a study for the "time-scale" experiment, which is one of the two underground heater tests of Stripa. A similar report is being prepared concerning the other heater test, which is termed the "full-scale" experiment. The two experiments and their respective geological studies differ sufficiently in scope, methodology, and results to warrant this separation. The common objective of the reports, however, is to define the position and nature of major discontinuities in the heated regions. The ability to accomplish this depends largely on the quality and amount of subsurface geologic data available for each region. In a general

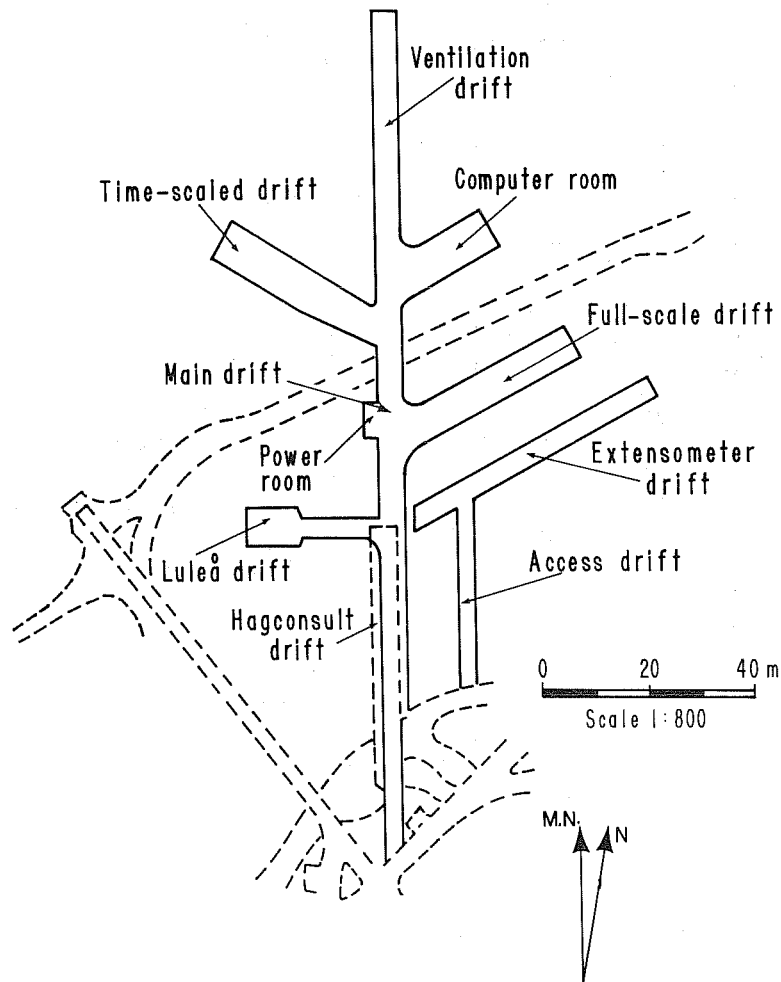
sense, the degree of detail which can be acquired is commensurate with the subsurface sampling, i.e., the "density" of instrumentation boreholes. Because the full-scale experiment is concerned with near-field effects, instrumentation drilling is dense near the heaters, and a detailed geological description can be made. For the time scale test, however, characterization is more general because although the zone of influence is larger, the sampling density is less.

In seeking to define the fracture system in the time-scale heater test, this report presents a limited amount of discrete discontinuity data coupled with a statistical evaluation of the local fracture network. In this manner the highly fractured rock between the delineated features can be represented stochastically. Throughout the report the general term "discontinuity" refers to natural fractures, joints, faults, dikes, or shear zones; "fracture" denotes any discontinuity except the dikes. Fractures without detectable displacement are termed joints; fractures with obvious slickensides are "shear fractures." Characteristics of the fractures, such as types and thicknesses of infilling, sizes, and spacings, will be discussed mainly statistically. Based on rather limited geological information about the Stripa area, some hypotheses regarding the origin of the fracture system will be offered. The potential influence of the discontinuities on local hydrology or the rock mass response to heating are beyond the scope of the report.

2. BACKGROUND

2.1 The Time-Scale Experiment

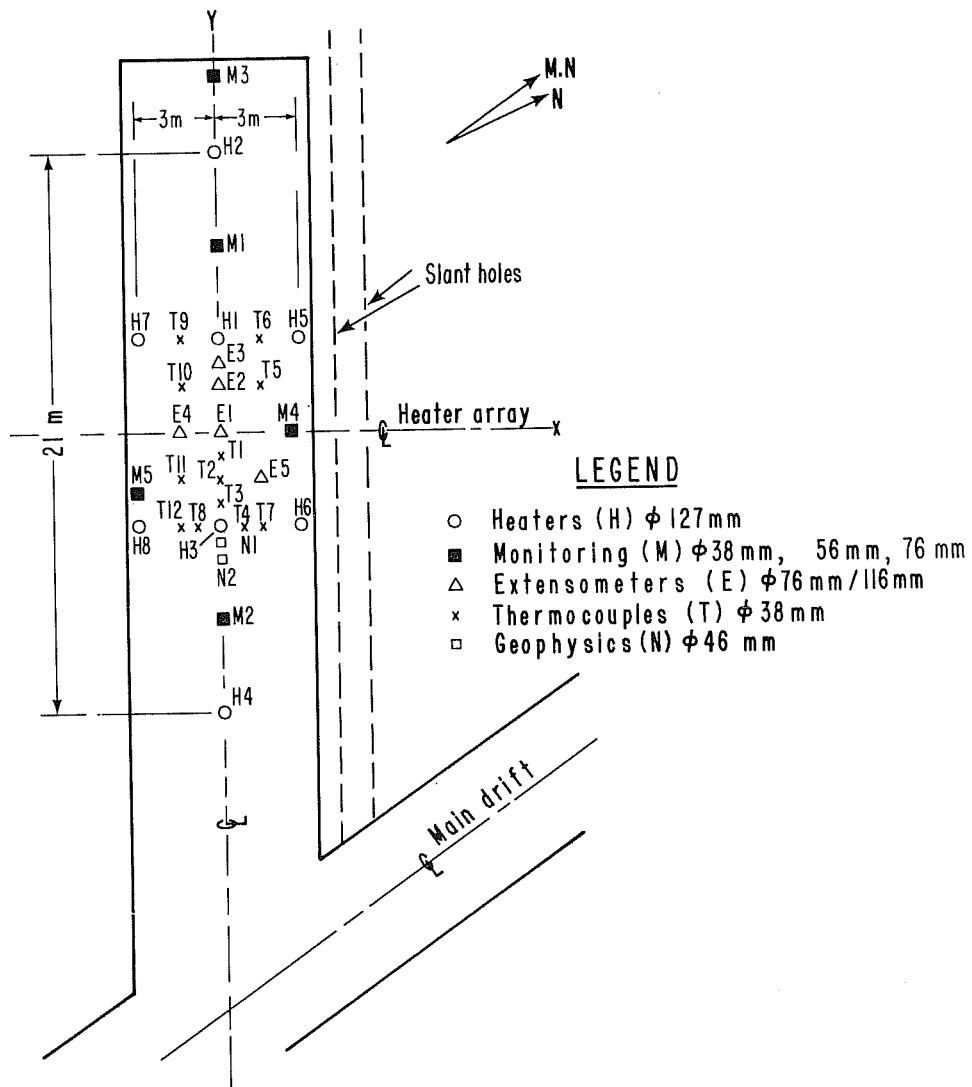
The heater experiments are located approximately 335 m below the surface in massive granite adjacent to the Stripa ore body. A layout of the underground site is shown in Fig. 2. The time-scale experiment is designed to simulate the interactive thermal effects of an array of waste canisters over a period of 12 years. Theoretically, this can be accom-



XBL 787-1983

Fig. 2. General plan of test site.

plished in a 1-year period by scaling the dimensions and power outputs of the heaters by a factor of $1/3.5$. Since heat conduction involves the ratio of time to squared length, the laws of similitude correspondingly shorten the time scale by $1/(3.5)^2$, or approximately $1/12$. The array consists of eight 1-m-long heaters arranged in the pattern shown in Fig. 3. The midplane of the array is located approximately 10 m below the drift floor,



XBL 787-1986A

Fig. 3. Borehole layout in the time-scale drift.

which should be outside the zone of stress alteration produced by the 5-m-diameter tunnel. Over the life of the experiment, the outer isotherms produced by the heaters should approach flattened ellipsoidal shapes. The principal objective of the test is to investigate this simulated far-field response to heating and thus improve numerical modeling capabilities. Also of interest are the local effects between the heaters.

To monitor this rock mass behavior, a number of vertical displacement, temperature, and stress-strain measurements are being recorded at various locations in the boreholes shown in Fig. 3. The most pronounced deformations in the rock mass should occur in the central portion of the heater array where temperatures will be the highest; therefore, instrumentation is concentrated in that area.

In addition to the geomechanical instrumentation, in situ fluid pressures are being monitored in two 45-m boreholes situated alongside the heater array, as shown in Fig. 3. As described by Gale and Witherspoon (1978), each borehole is separated into five equal intervals by hydraulic packers so that any change in the fluid pressure profile can be detected and recorded electronically. The vertical N- and M-holes of Fig. 3 are used for periodic geophysical monitoring of the heated rock mass. For a complete discussion of this aspect of the instrumentation, refer to Nelson et al. (1979).

2.2 Geology of the Stripa Mine

The Stripa mine geology has been studied by the Swedish Geological Survey (SGU), and reported by Olkiewicz et al. (1978). Figure 4 shows

the surficial geologic setting in the area of the mine. The ore body lies in a synclinal trough whose axis plunges about 20° to the ENE. The ore has a relatively high iron content, and is composed predominantly of inter-banded hematite and quartz with some magnetite concentrations. It is stratiformly bound within gray to brownish Precambrian metavolcanic rock, which in European terminology is broadly classed as "leptite." A smaller ore body lies parallel to the main ore and stratigraphically below it. The southern limb of this parallel ore is missing above the 200-m mine level, while below that depth both limbs are present. Just below each of the ore bodies the leptite is clearly layered, while above it is not. The iron ore is the youngest component of the leptite and occurs as reddish brown masses. A number of diabase and amphibolite dikes transect the leptite and are visible in the mine levels.

The underground test site is located in a massive granite body in contact with the north limb of the leptite syncline. The contact is quite irregular, but in its area in the mine it strikes ENE and dips steeply to the SE. The actual heater experiments are being conducted approximately 150 m within the granite, at a depth of about 340 m. The granite most likely post-dates the leptite and is probably connected with one of several post-orogenic Precambrian plutons in the region. Due to relatively mild tectonism since the intrusion, there are no gneissic structures in the granite. The granite is generally unfoliated and varies from gray to light red in color. Composition of the reddish variety has been reported by Olkiewicz et al. (1978).

Quartz	44%
Plagioclase	39%
Microcline	12%
Chlorite	3%
Muscovite	2%
Accessory Minerals:	zircon, opaques

The gray type of granite which predominates in the test areas has a somewhat higher microcline percentage and less plagioclase. Grain sizes vary from 1 to 5 mm, with an average of 3 mm. Associated with the granite are widely spaced pegmatite and aplitic dikes less than 1 m in thickness. The youngest dikes are diabase, nearly vertical, and strike NNE.

Although little has been written on the tectonic features in the mine, previous investigations at Stripa (Geijer 1938) have differentiated the fractures in the ore body into two categories. One category is related to shearing between layers produced by the fold deformation, and the other is described by Geijer as more recent and "steeply dipping" (no average strike direction mentioned). The fold-related fractures in the ore body tend to be steeply inclined and strike in an ENE direction, although these are also nearly horizontal faults.

Major fractures throughout the various drifts in the granite formation have been broadly surveyed by SGU and reported by Olkiewicz et al. (1978). Compilations of fractures over an extensive area show a clear dominance of those that dip steeply to the north, except in the heater experiment areas, where many fractures dip to the south. Two general strike directions

persist, according to Olkiewicz et al. (1978). One is evenly distributed from north to east; and the other is concentrated between northwest and west. These surveys indicate that the great majority of the fractures are visibly closed, and water seepage consists only of damp surfaces or slow drips. Fracture filling materials are primarily chlorite, and occasionally calcite.

3. SOURCES OF DATA

The work of Olkiewicz et al. (1978) provides a general description of geologic discontinuities in the underground test area. The interpretation of the time-scale experiment, however, demands a more detailed characterization over a smaller area. Locating the positions of discrete major features beneath the drift floor required (1) a detailed floor map of surficial discontinuities, and (2) complete core logs describing subsurface features. The majority of the subsurface interpretation for the time-scale drift could not be performed on site, hence secondary information included (a) stereo-photographs of the floor and walls of the drift, and (b) color photographs of the logged core samples taken from the drift. The data bases are described further below.

3.1 Floor Mapping

Underground-fracture surveys typically involve mapping features from the walls and roofs of drifts (Knill and Jones 1965; Kendorski and Mahtab 1976). In order to trace individual features beneath the drift, it was necessary to inspect the floor--a task that required much preparatory work. First, the newly excavated 6x6x32-m entry was scaled of loose rock and thoroughly cleaned to facilitate geological mapping. Next, a 1x1-m horizontal

grid was painted on the floor, oriented parallel to the drift centerline, and hence tied into the overall mine survey system. Mine elevations were measured at the painted coordinates to provide some representation of the irregular floor topography, which has a relief of 0.5 m or less.

The floor was mapped square-by-square, starting at the end of the drift and progressing back toward the entrance. To facilitate the process and improve accuracy, a 1x1-m square frame, with 0.1-m graduations along its side, was positioned over the grid points, as depicted in Fig. 5. This allowed fracture positions to be visually estimated within each square

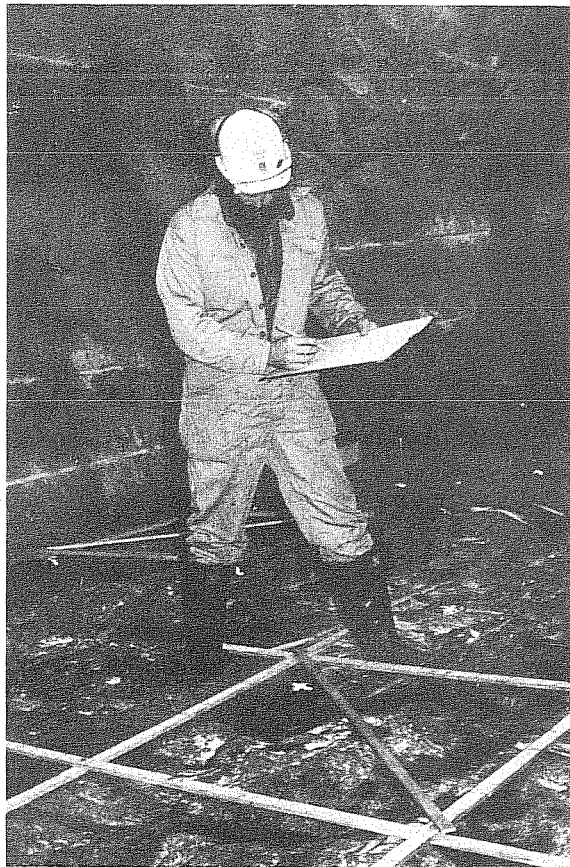


Fig. 5. Use of 1x1-m reference frame in fracture mapping.

to an accuracy of about ± 5 cm. Features were sketched onto a 20:1 base map, which represents the outcrop boundaries of fractures, veins, and dikes. The map thus corresponds to what could be traced directly from a photomosaic, except that much more detail can be recorded in field mapping. With this method the topography of the drift floor tends to be reflected in the irregular traces of mildly dipping fractures. In most cases of nearly horizontal features, however, much of the coated surface was exposed and mapping in two dimensions was troublesome. For this reason, and also because of geometrical biasing, nearly horizontal features (less than about 30° dip) were not included in the floor map.

Virtually all other steeply dipping features with trace lengths greater than about 0.3 m were mapped. Normally, the dip angles of major discontinuities were determined; for minor fractures only relative dip directions were recorded. The mapped traces of all fractures represent average strikes, assuming mild surface relief. Type and thickness of fracture coating and changes in rock were briefly noted during mapping. The resulting detailed floor map is shown in Fig. 6 and discussed further in Section 4.

3.2 Core Logs

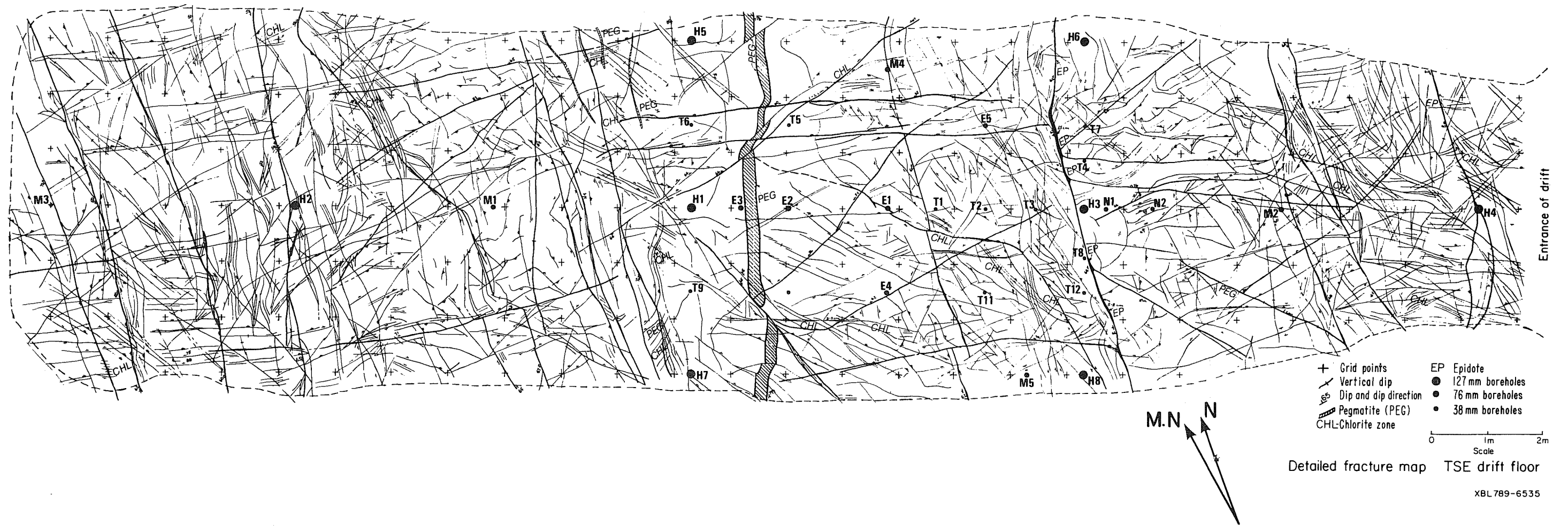
Thirty-two instrumentation and heater boreholes were drilled vertically in the time-scale drift to an average depth of about 12 m. Core samples oriented with respect to the drift centerline were taken from seventeen of the holes that were 76 mm or greater in diameter. These include the E, M, and H holes, concentrated in the central portion of the heater layout (Fig. 3). In addition to the vertical boreholes, two inclined 76-mm-diameter

holes are drilled downward alongside the heater array such that they cross the transverse axis of the array at the heater midplane. A complete discussion of the drilling and sampling process is given by Kurfurst, Hugo-Persson, and Rudolph (1978).

Fracture logs of all core samples were prepared in tabular form and contain the following data.

- rock description
- depth and types of discontinuities
- surface characteristics of discontinuities, including planarity, roughness, and weathering
- orientations of discontinuities with respect to core axis and drift centerline direction (excepting non-oriented core).

Logs for the oriented core are included in Appendix A. Thin sealed fractures, typically filled with chlorite, were not usually logged. For this work, fractures that were open in the core were assumed to be relatively weaker than all others, and hence more significant from an engineering standpoint. However, this apparent weakness probably was also a function of the drilling and handling technique. To illustrate, several fractures that were opened by rough handling showed distinct slickensiding, which should represent planes of weakness in the rock mass. It is reasonable that the cohesion of a fracture can vary across its surface, so a fracture sealed in the core sample may not necessarily be closed elsewhere. Hence, important features may not always be sampled consistently when drilling technique varies and only open fractures are logged. The significance of this bias in the fracture logging remains to be investigated.



+ Grid points
 V Vertical dip
 D Dip and dip direction
 PEG Pegmatite (PEG)
 CHL-Chlorite zone
 EP Epidote
 ● 127 mm boreholes
 ● 76 mm boreholes
 ● 38 mm boreholes
 0 1m 2m
 Scale
 Detailed fracture map TSE drift floor
 XBL 789-6535

Fig. 6. Detailed map of discontinuities in the floor of the time-scale experiment drift.

Since the interpretive part of this study was not conducted at the test site, the sealed fractures in the core could be identified later only by examining photographs of the cores. Reduced copies of these photographs are shown in Appendix B. Several of these pictures provided crosshole correlations of major sealed discontinuities, as discussed further in Section 4.

3.3 Comparison of Data Sources

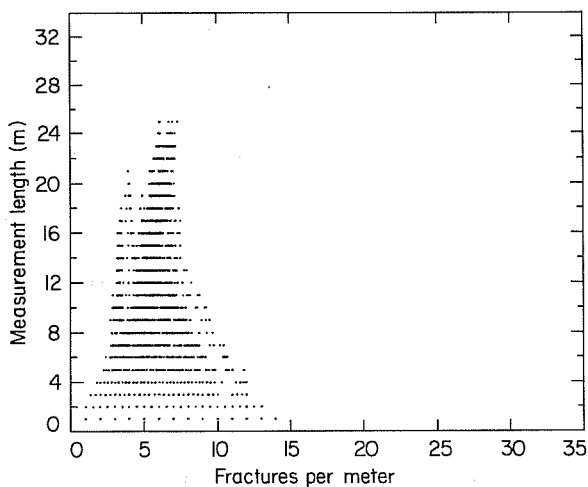
In synthesizing surface and subsurface information, it is desirable to have data bases that are consistent in terms of their relative fracture frequency. It is assumed here that if sampling frequencies are similar, the same class of fracture is being compared. To demonstrate the compatibility between the fracture mapping and the core logging, the average fracture frequency was plotted for various sample lengths. For the detailed fracture map, sample lines were taken 1 m apart in the longitudinal and transverse directions, which is comparable to the spacing of the boreholes. Fracture frequency was computed as the total number of fractures counted over a given sample length, divided by the sample length. For example, if a 2-m sample line had five fractures crossing it over the first meter and seven over the second, three frequencies would be recorded: five and seven fractures per meter for two 1-m sample lengths and $12/2$, or six fractures per meter for the overall 2-m length. Results from the floor map are presented in Fig. 7, which shows a maximum frequency of about fourteen fractures per meter, and an average frequency of about six fractures over the entire floor.

A similar plot of the borehole fracture log data has been developed

by dividing the number of consecutive logged fractures by the distance between the first and last. In this instance the measurement length is variable. If, for example, a log showed three fractures at successive depths of 1.0, 1.2, and 1.5 m, three frequencies would be calculated:

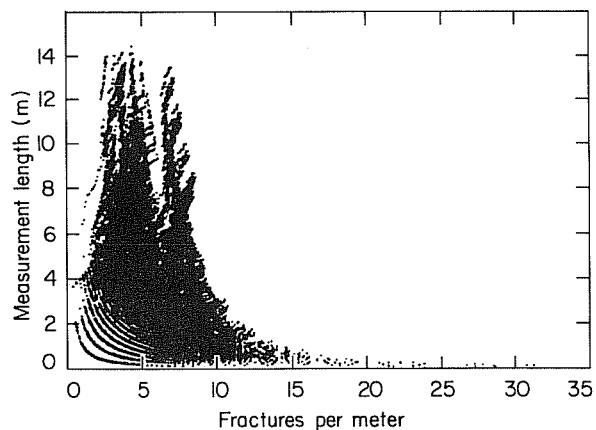
- (a) $2/(1.2-1.0) = 10$ fractures/meter (0.2 m measurement length)
- (b) $2/(1.5-1.2) = 6.67$ fractures/meter (0.3 m measurement length)
- (c) $3/(1.5-1.0) = 6$ fractures/meter (0.5 m measurement length).

If the number of consecutive fractures is varied from two up to the total number in a particular log, a distribution of frequencies is obtained for that hole. Figure 8 is a composite plot of such data for all of the time-scale fracture logs. The peculiar shape of the data near the origin results from dividing a discrete number of fractures by random lengths; i.e., $f(x) = n/x$. The bimodal shapes of both distributions are probably due to variations in drilling techniques and borehole sizes, which cause different numbers of fractures to open upon retrieval of the core. The maximum



XBL 799-11313

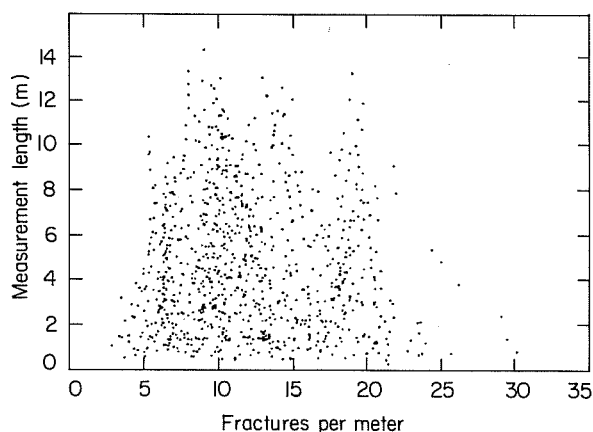
Fig. 7. Fracture frequencies from detailed floor map.



XBL 799-11314

Fig. 8. Core log fracture frequencies.

frequency for measurement lengths of 1 m is about 14, which is commensurate with the frequency shown in Fig. 7. Both distributions have similar overall shapes and average frequencies of about six fractures per meter--hence the data bases are judged to be compatible. Neither can give an indication of the actual fracture frequency in the granite, however. This can be accomplished by examining the core photographs in detail, counting all fractures, regardless of length, thickness, or degree of openness. All visible fractures in the photos were counted over random core lengths, and the computed frequencies are plotted in Fig. 9. Comparing Fig. 9 with the previous figures indicates that the actual fracture frequency in the rock mass is likely to be two to three times greater than that observed in the core logs or fracture map. The disparity can be rationalized by recognizing that both data bases used in this study preferentially sample the more significant fractures, that is, those which are longer (>0.3 m) and weaker (open in the core).



XBL 799-11315

Fig. 9. Fracture frequencies for all fractures visible in core photographs.

4. DETERMINISTIC CHARACTERIZATION OF DISCONTINUITIES

4.1 Methodology

Determination of the three-dimensional network of discontinuities was basically a process of correlating major observed surface features with the core information. Because of the discontinuous nature of rock joints, this was considered possible for only a few prominent and continuous features, i.e., the fractures and the single pegmatite dike shown in Fig. 10. These were therefore delineated first in the detailed surficial map of the floor (Fig. 6). Criteria for this designation were length, surficial continuity, and filling thickness. Fractures which extended over many meters or which were traceable throughout the floor, walls, and roof of the drift were considered significant and likely to extend to depths comparable to their observed or mapped lengths. Fractures which tend to offset other features, as well as being relatively long, were considered to be most extensive in area. The fractures in Fig. 10 typically have mineralization thicknesses ranging from several millimeters to several centimeters, as opposed to a millimeter or less for the majority of the fractures shown in Fig. 6.

The subsurface (subfloor) positions of the major features in the floor map were estimated by assuming the surfaces were planar, then calculating expected positions in the nearby boreholes. The equation of such a fracture plane in cartesian coordinates is given by

$$A (x - x_0) + B (y - y_0) + C (z - z_0) = 0,$$

where x_0 , y_0 , and z_0 are coordinates of a known, or mapped point in a plane and A , B , and C are the direction cosines of the normal vector to

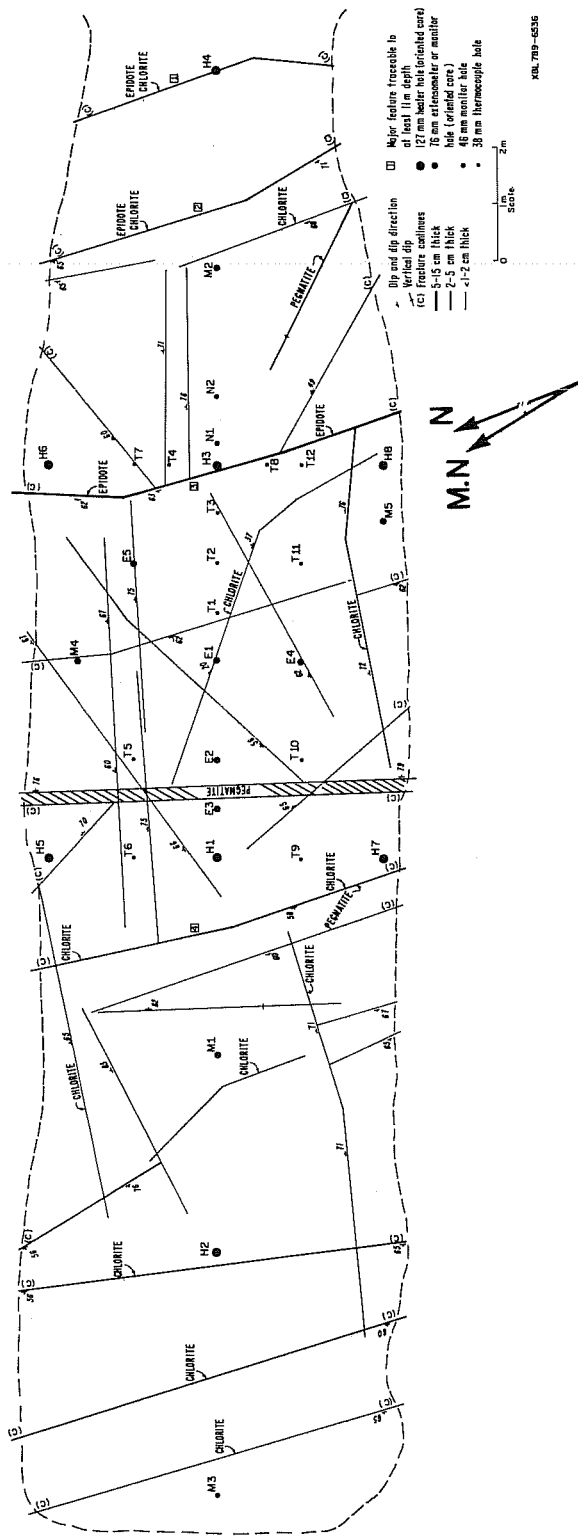


Fig. 10. Generalized map of major discontinuities in the floor of the time-scale experiment drift.

the plane. Letting x and y be the horizontal coordinates of a particular vertical borehole, then solving for z , gives the elevation at which the plane should intersect the borehole. Fractures described in the core log or observed in the core photographs could then be compared with the extrapolation. Since fractures generally are not perfectly planar, the actual intercept (if present) was usually some distance above or below the extrapolated position. To account for a fracture's waviness and to help delineate the zone in which it might be found, the extrapolation was made from several different points along the mapped fracture trace. Selection of the most reasonable candidate fracture in the core was a trial-and-error process based on (1) its proximity to the extrapolated positions, (2) similarity of surface and subsurface orientations, and (3) similarity of filling characteristics. Further correlation of a fracture to deeper locations was made in the same manner, using local borehole orientations and hole-to-hole extrapolation. Fractures were projected to a maximum depth of about 13 m below the drift floor, or 3 m below the midplane of the heater array. Since few boreholes extended to this depth, further extrapolations would have been speculative at best. Likewise, the lateral extent of fractures was extrapolated only 1 m beyond the periphery of the heater array. Boundary coordinates for the fractures were estimated as the mean of mathematical projections from nearby mapped or correlated locations.

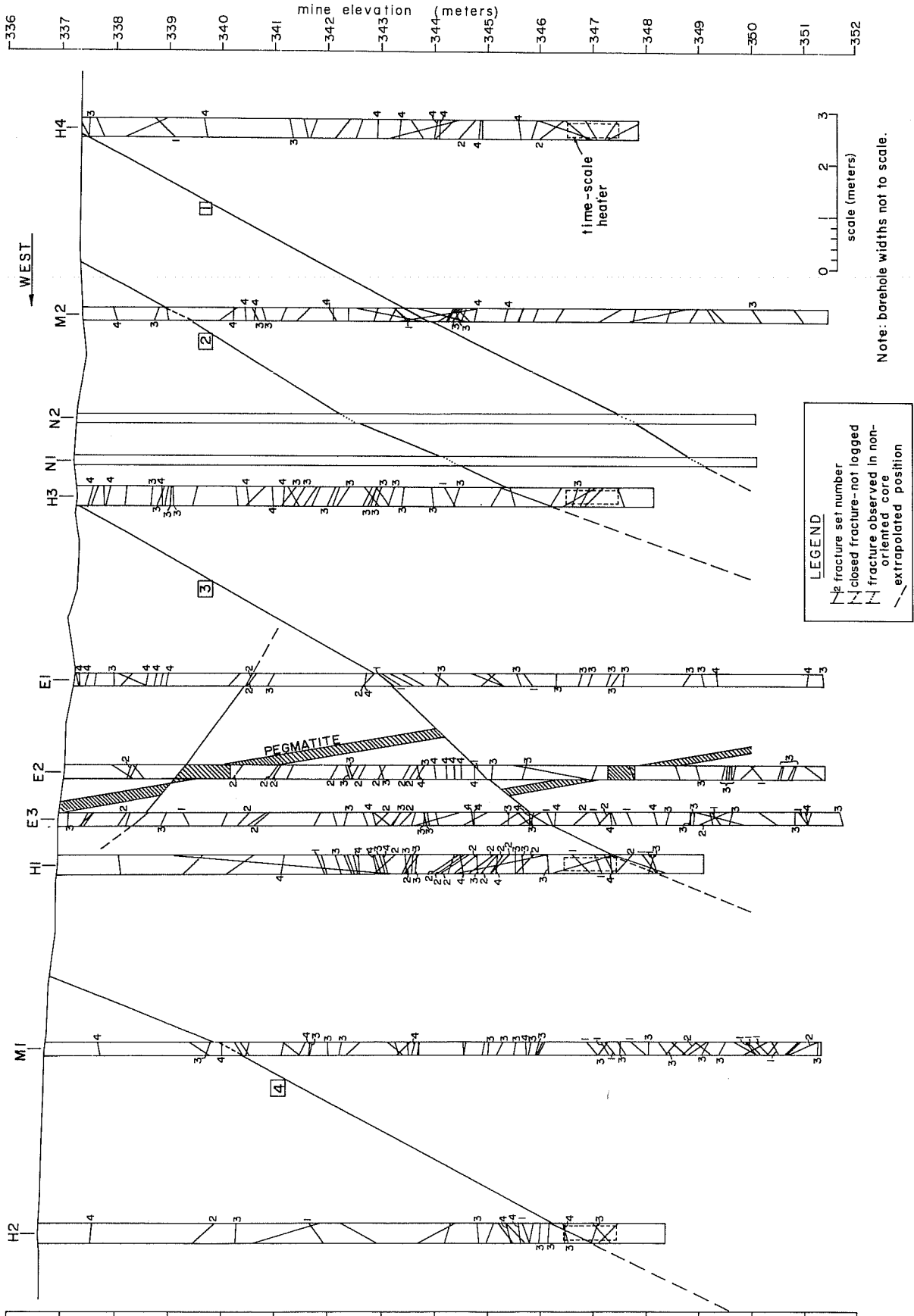
Surface-to-subsurface correlations provided what can be considered "first order" attempts to find major continuous features. The second and more speculative type of correlation attempted to delineate major fractures not intersecting in the drift. Because of the vertical orien-

tation of boreholes, these types of fractures would be primarily sub-horizontal. Despite the large number of fractures in the core samples, reasonable evidence of single fractures continuing from one borehole to the next was difficult to find.

4.2 Results

Following the trial-and-error procedure described above, it was possible to delineate the subsurface locations of four of the major through-going fractures shown in the floor map. These are members of a set which strikes N-S and dips 55° to 70° to the west. The boxed numerals in Fig. 10 indicate the four fractures in the floor map. In general, they tend to offset or truncate other features. The most prominent feature, a fracture labeled 3, is visible near the H3 borehole and strikes transverse to the centerline. The outcrop of this fracture is marked by a relatively thick coating of epidote and chlorite. Over most of its expression the infilling is 1 to 2 cm thick, but in at least two areas where other fractures intersect it, the epidote thickness reaches 5 to 15 cm. Slickensides are visible on the fracture walls, oriented at roughly S60W. Because of this clear evidence of movement, it is designated here as a "shear fracture."

The other three fractures which were traced into the subsurface are similar in orientation and infilling mineralogy. Their mapped expressions are thinner and more irregular, however, and may actually represent narrow zones of fracturing. Figure 11 shows the four fractures in a vertical profile through the centerline of the heater array. This is perhaps the simplest and most useful profile, since the apparent dip of the fractures is

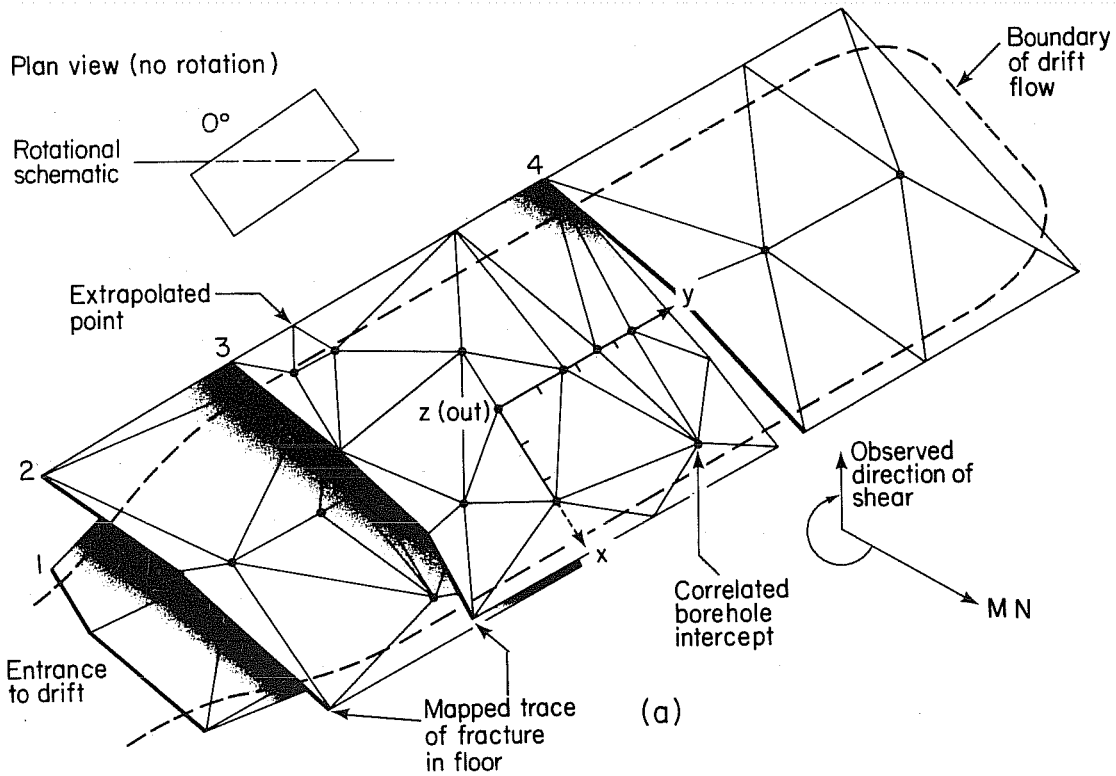


XBL 7811-12833

Fig. 11. Subsurface profile along centerline of drift showing major discontinuities through the heater array.

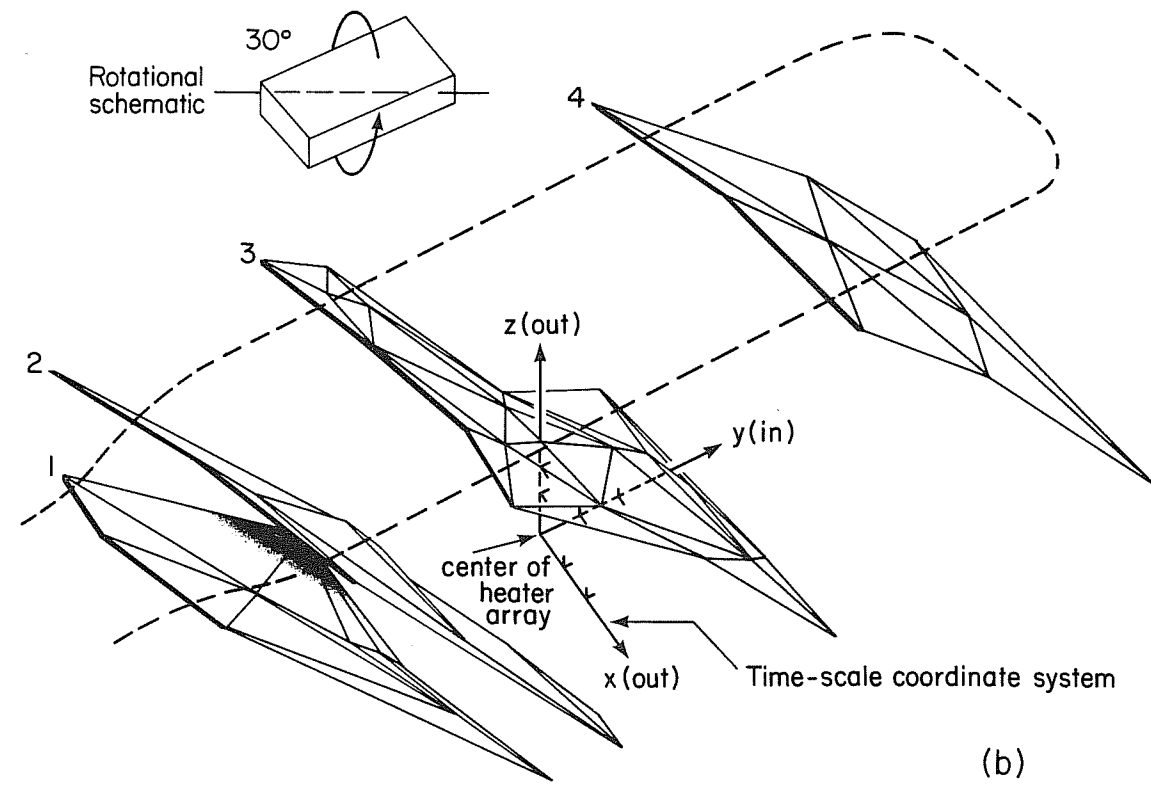
very near the true dip, and their spatial relationship to the majority of the heaters and instrumentation boreholes can be seen easily. Correlated intercepts from boreholes not on the centerline can be combined with points on the centerline profile to produce three-dimensional representations of the fracture surfaces. The correlated borehole locations and the extrapolated boundary points for a particular fracture form the vertices of contiguous triangles, whose composite gives an approximation of the overall surface waviness.

Figure 12 shows a series of orthographic projections of the four fractures. Beginning with the plan view oriented as shown in Fig. 12a, the figure is rotated about the observer's horizon in Figs. 12b and 12c. The horizontal axis of rotation has been selected approximately perpendicular to the direction of shearing observed on fracture 3. At an inclination of about 45° above the horizontal the projected width of this fracture reaches a minimum, which is consistent with the small amplitude of waviness one would expect to observe in the direction of shearing. The amplitude does not appear to be zero, however, because (1) the boundary points are only extrapolated, and (2) the lines connecting the points have been arbitrarily assigned. Since the boundary points were determined from local (borehole) fracture orientations, they may not conform well with the average trend of all borehole intercepts. Hence, the true linearity of the surface in the direction of shearing can be better assessed by ignoring the extrapolated points. This has been done in Fig. 13 for the 45° view in Fig. 12c. The overlap of points in Fig. 13 suggests that sliding is kinematically possible in the viewing direction

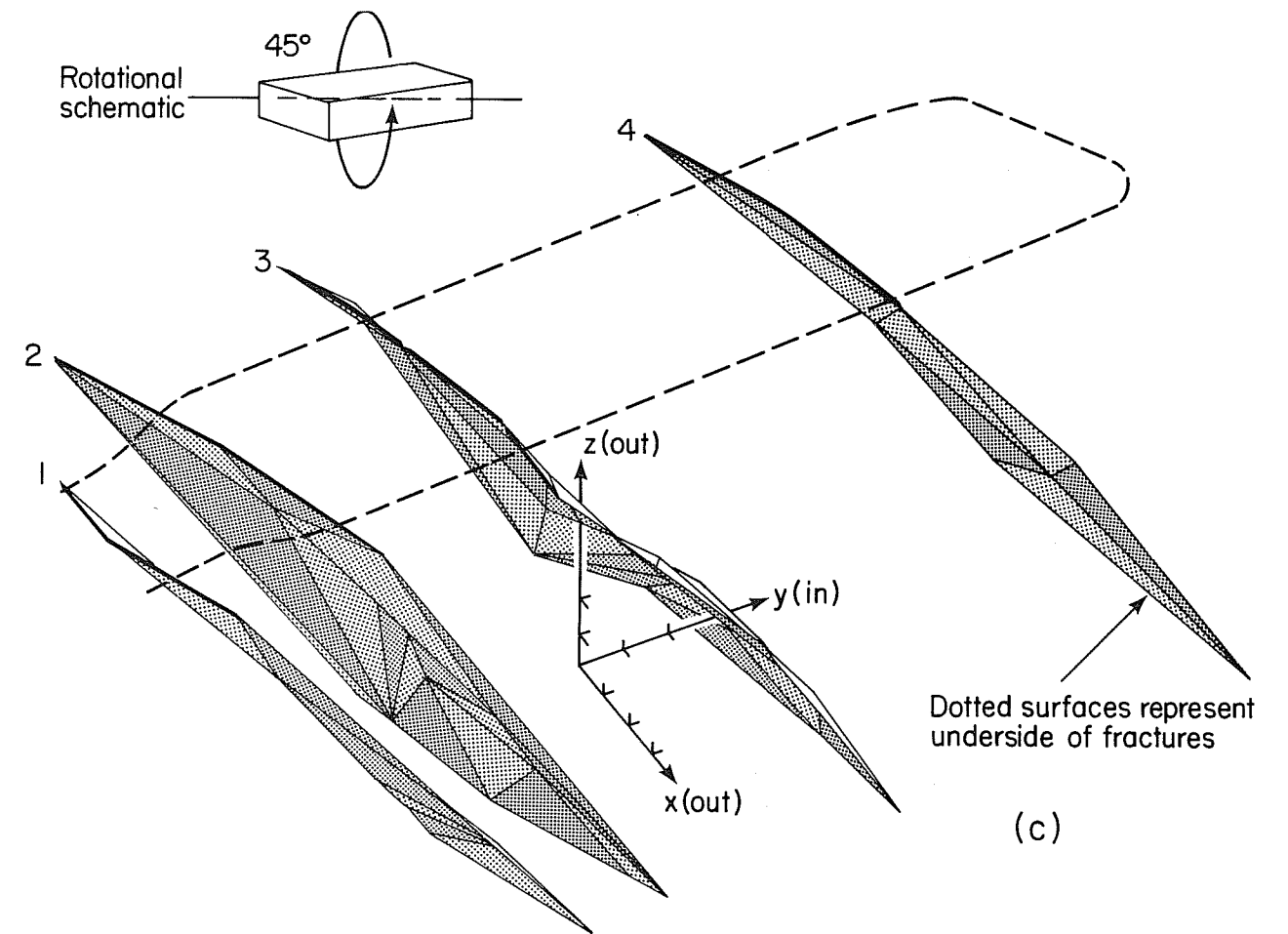


XBL 799-11316

Fig. 12. Three-dimensional views of the four continuous fractures passing through the heater array.



XBL 799-11317



XBL 799-11318

Fig. 12 (continued)

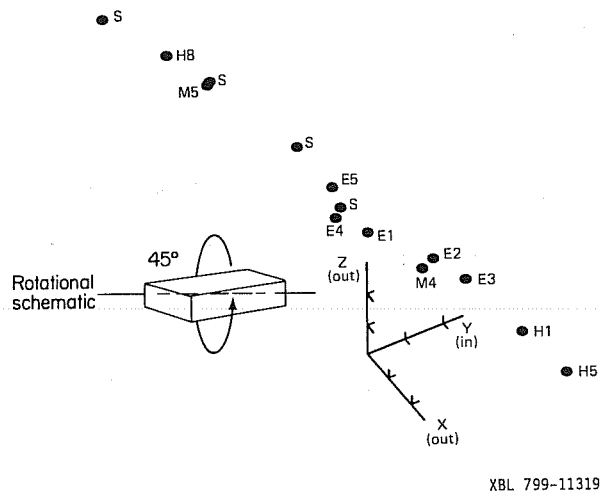


Fig. 13. View of fracture no. 3 borehole locations, parallel to direction of shear. Extrapolated points are excluded. Points labeled "S" represent mapped surface locations.

and, therefore, the credibility of the three-dimensional configuration shown is strengthened.

Along with the four major fractures, a 20-cm-thick pegmatite dike passes transversely through the time-scale heater array, as shown in Figs. 6, 10, and 11. It is one of a series of widely spaced dikes which strike NNE and dip steeply to the east. Grain size of the pegmatite averages about 1 cm. Much of the fracturing post-dates the pegmatite, as seen by the offsets in its detailed mapping. Most of the offsets are less than about 20 cm and, at depth, it is difficult to infer such small irregularities from available borehole data. However, from hole-to-hole correlation, it is evident that an offset of about 2.0 m in the pegmatite must occur at a depth of about 8 m. Fracture 3 is most likely responsible for this faulting, as depicted in Fig. 11. Based on the offset and slicken-

siding, the type of movement is oblique-thrust, with the direction indicated in Figs. 12 and 13.

A compilation of all subsurface points that define the four major fractures is given in Tables 1 through 4. The fact that some sealed fracture locations and orientations were estimated from core photographs makes the results no less reliable in light of the previous discussion concerning cohesive strength of a fracture surface. This is illustrated by the intersection of fracture 3 with the H8 borehole (Table 3). Although the surface expression of the fracture near H8 is extremely clear, and one would expect to find a very prominent trace of it at a depth of 1 to 2 m in the core, only a sealed, unlogged fracture of the appropriate orientation was discovered in that interval. This observation and similar occurrences shown in the tables, indicate that what may appear to be a significant discontinuity in one area may be less obvious a short distance away.

The three-dimensional fracture delineations described above may not represent reality, however. Major features could actually be composed of one or more closely spaced fractures, as evidenced by the many fracture zones shown in Fig. 6. Our limited subsurface information allows us to assume only discrete, single-surface representations of the major features. More detailed data from future in situ hydrologic or geophysical tests in the time-scale drift could either confirm or refute this assumption.

The four continuous faults certainly do not constitute a complete characterization of the fracture system. Virtually thousands of other fractures can be identified in the drift, most of them discontinuous with

Table 1. Subsurface coordinates of fracture 1.

Borehole number	Observed location						Observed orientation (degrees)	How identified in core sample	Remarks	
	Mapped at surface	Borehole depth (m)	Local (TSE) coordinates (meters)			Dip				Dip azimuth
			X	Y	Z					
	X		3.0	- 9.5	8.60	60	310	--	1-3 cm epidote; highly fractured zone	
	X		- .3	-10.6	8.65	~60	330	--	1-3 cm epidote & chlorite; curved portion	
	X		-2.0	-10.6	8.65	~60	330	--	1-3 cm; several other parallel fractures	
M2		6.27	0	- 7.0	3.37	60	330	Log	2-cm sealed epidote 20	
N2		10.45	0	- 4.7	-0.7	~70	--	Photo	Dip azimuth uncertain	
N1		11.73	0	- 3.9	1.98	~65	--	Photo	Dip azimuth uncertain	
H6		10.5	3	- 3.5	-0.7	~60	320-340	Photo	Several sealed 1-2 cm parallel fractures	
			0	- 4.5	-3.0	--	--	--	Extrapolated from N1 & N2	
			-4	- 3.6	-3.0	--	--	--	Extrapolated from M2 surface	
			4	- 2	-3.0	--	--	--	Extrapolated from H6	

Table 2. Subsurface coordinates of fracture 2.

Borehole number	Observed location					Observed orientation (degrees)		How identified in core sample	Remarks
	Mapped at surface	Borehole depth (m)	Local (TSE) coordinates (meters)			Dip	Dip azimuth		
			X	Y	Z				
			4.0	-6.81	9.8	~68	310	--	Extrapolated horizontally from mapped exposure
	X		- .48	-8.14	9.7	65 -70	310	--	2-5 cm epidote & chlorite; highly fractured zone of light-colored granite
			-4.0	-9.7	9.7	~71	310	--	Extrapolated horizontally from mapped exposure
M2		1.8	0	-7	7.84	60 -70	~330	Photo	Sealed, parallel fracture zone below
N2		5.2	0	-4.7	4.6	60 -70	--	Photo	Sealed, <1 cm; orientation uncertain
N1		7.1	0	-3.9	2.7	60 -70	--	Photo	Zone of sealed fractures; orientation uncertain
H3		8.39	0	-3.5	1.4	70	315	Log	Open, >1 mm; several other parallel fractures above & below; all chlorite
H6		7.04	3	-3.5	2.73	63	320	Log	Open, >1 mm; several other parallel fractures above & below; all chlorite
E5		10.64	1.5	-1.78	- .86	75	~300	Log & photo	Many sealed parallel fractures in 0.5-m zone above
M5		12.75	-3.0	-2.5	-3.0	~60	320	Photo	Sealed, <1 cm; several others with 0.3 m
M4		13.86	2.5	0	-4.16	55	340	Photo	Sealed, 1 cm; dip uncertain
			0	-1.92	-3.0			--	Extrapolated from H3
			4	- .32	-3.0			--	Extrapolated from H6, E5 & M4
			-4	-2.7	-3.0			--	Extrapolated from M5

Table 3. Subsurface coordinates of fracture 3.

Borehole number	Observed location						How identified in core sample	Remarks	
	Mapped at surface	Borehole depth (m)	Local (TSE) coordinates (meters)			Observed orientation (degrees)			
			X	Y	Z	Dip			Dip azimuth
			4.0	-3.01	9.7	~60	~330	--	Extrapolated horizontally from mapped exposure
	X		1.75	-2.87	9.7	63	320	--	10-15 cm epidote; curved portion
	X		-1.0	-3.58	9.7	64	310	--	5-10 cm epidote
			-4.0	-4.62	9.8	~65	~310	--	Extrapolated horizontally from mapped exposure
E5		2.15	1.5	-1.78	7.63	60	315	Log	Open; 1 mm chlorite
H8		0.94	-3.0	-3.5	8.88	~65	~325	Photo	Sealed; 2-3 cm thick
M5		2.33	-3.0	-2.5	7.43	70	315	Log	Open; 1 mm chlorite
M4		4.76	2.5	0	4.93	55	325	Log	Open; 1-5 mm epidote
E1		5.83	0	0	3.94	50	315	Log	Open; 1-2 mm chlorite; parallel fracture 10 cm below
E4		6.82	-1.5	0	3.11	65	295	Log	Open; 1 mm chlorite (questionable correlation)
E2		7.76	0	+1.75	2.19	55	305	Log	Open; 1 mm chlorite
E3		8.97	0	+2.62	1.1	60	305	Log	Open; 1 cm chlorite; shear azimuth ≈ 240-250
H1		10.85	0	+3.5	- .76	70	325	Log	Open; 1 mm chlorite
H5		9.70	3.0	+3.5	0.20	~25	~330	Photo	Sealed; 1 cm
			4.0	+1.75	3.28	--	--	--	Extrapolated from M4, H5 & surface
			4.0	+5.0	-3.0	--	--	--	From H5
			1.5	+4.7	-3.0	--	--	--	From H5 & H1
			-4.0	+3.7	-3.0	--	--	--	From H1 & 3
			-4.0	+1.25	-1.04	--	--	--	From E2, E3, E4 & M5
			-4.0	-3.0	8.11	--	--	--	From M5, H8 & surface

Table 4. Subsurface coordinates of fracture 4.

Borehole number	Observed location					Observed orientation (degrees)		How identified in core sample	Remarks
	Mapped at surface	Borehole depth (m)	Local (TSE) coordinates (meters)			Dip	Dip azimuth		
			X	Y	Z				
M1 H2	X		4.0	+5.63	10.0	60	315	--	Extrapolated horizontally from mapped exposure
			0.35	+4.73	10.1	56	315	--	2-5 cm chlorite
			-4.0	+3.5	9.9	60	315	--	Extrapolated horizontally from mapped exposure; highly fractured zone; chlorite
		3.52	0	+7.0	6.80			Photo	Sealed; 1 cm thick; multiple fractures
		9.98	0	+10.5	0.46			Log	
		4.0	+8.8	5.08	--	--	--	--	Extrapolated from surface, M1 & H2
		4.0	+12.85	-3.0	--	--	--	--	From H2
		-4.0	+11.45	-3.0	--	--	--	--	From H2
	-4.0	+8.8	2.03	--	--	--	--	From H2, M1 & surface	

respect to the four shear fractures. Although subsurface correlation of the secondary features is, thus, difficult, attempts were made in this study to determine the subsurface expressions of all features shown in Fig. 10. This proved very difficult below about 5 m from the surface. The majority of the discontinuous surficial features were either truncated, or they extended out of the zone of heating by that depth, and thus their delineation near the surface would be largely superfluous. Alternatively, the steeply dipping fractures shown in Fig. 10 that strike parallel to the drift were impossible to detect at depths of 8 to 12 m, since they seldom intersected the vertical boreholes. As mentioned previously, mathematical and graphical attempts to correlate sub-horizontal features between boreholes were unsuccessful. While this supports the claim that few continuous fractures pass through the experiment, it is clear that a more general approach is required to characterize the local rock mass. Accordingly, fracturing in the regions between the four main faults will be described statistically in the following section.

5. STATISTICAL CHARACTERIZATION OF DISCONTINUITIES

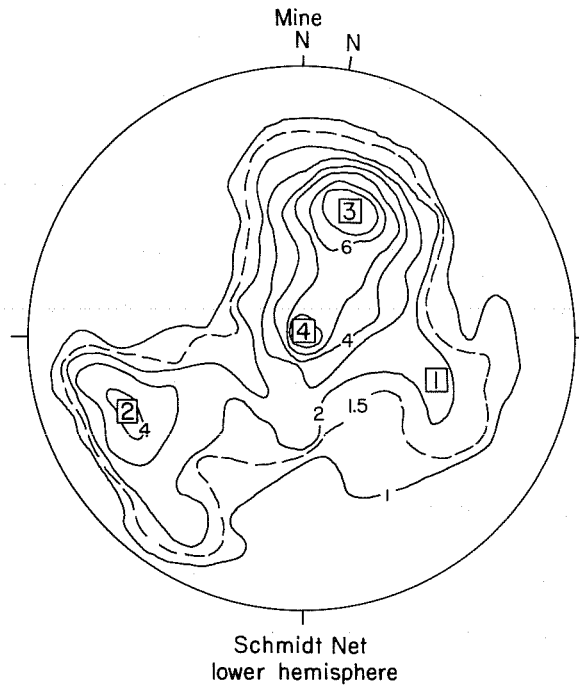
In lieu of precise determination of actual fracture locations in the subsurface, the best approach is to combine all available data into a statistical model of the fracturing by describing the discontinuous fractures between the major continuous features according to distributions of size, spacing, and orientation. To provide an adequate sampling base, all vertical borehole data have been combined, and therefore possible variations in the discontinuous system are not represented. Using the results presented here--that is, by combining the four continuous features,

the pegmatite dike, and a discontinuous fracture network--a generalized model of the local rock mass can be synthesized. It is beyond the scope of this report to formulate a numerical simulation, which properly belongs with the interpretation of thermomechanical or hydrological test data. Three important fracture parameters, orientation, size, and spacing, as well as infilling characteristics are discussed below.

5.1 Fracture Orientations

A distribution of orientations can be developed by stereographically plotting the normal vectors (poles) of all fracture planes logged in the boreholes. Using a counting circle of 10° radius (1.5 percent area) on the surface of the unit sphere, the original plot of poles can be discretized and contoured. Fig. 14 shows the resulting contour map, plotted on an equal-area projection, for 827 fractures in the time-scale vertical boreholes. Contour intervals represent the percentage of fractures per 1.5 percent area. As labeled in the figure, there are three distinct fracture sets, plus a fourth which is less certain. Although localized statistical variations in fracture orientations are not analyzed here, stereonet plots of fracture planes from individual core logs are provided for reference in Appendix C.

Set 1, though poorly defined, is significant because it roughly corresponds in orientation to the four major features described above. Set 2 also corresponds to fractures already identified by the surface mapping, that is, those striking nearly parallel to the drift centerline and dipping steeply to the northeast. While most joints in set 2 are clustered about the mean pole as shown, the distribution is noticeably skewed toward the south. This



XBL 799-11320

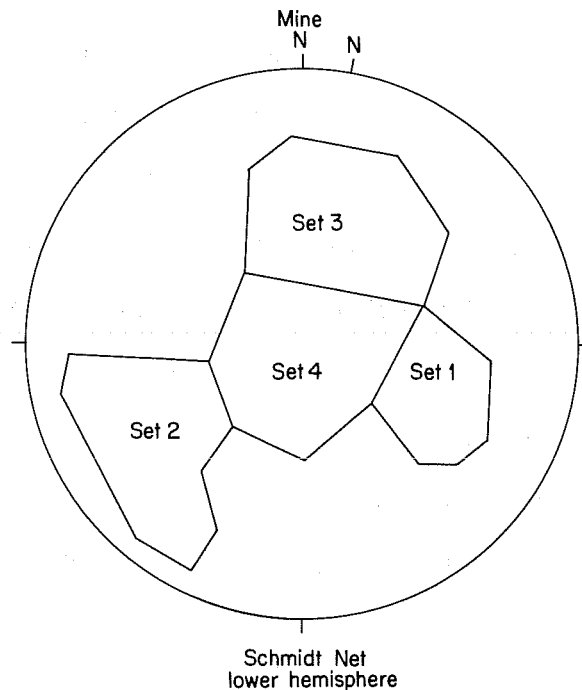
Fig. 14. Contour diagram of fracture poles from time-scale experiment boreholes. Contour intervals represent percentage of points per 1.5 percent area (10 degrees counting radius), based on a total of 827 points. Numbers in boxes show mean orientations of respective joint sets.

"shoulder" could actually be a fifth joint set, but for simplicity it is considered part of set 2. Sets 3 and 4 are more evenly distributed about their means. Set 4 is generally parallel to the floor, and therefore it is not represented in floor mapping. Visual inspection of the walls of the underground site, however, has shown this set to be pervasive throughout the granite. Joint set 3 is the predominant cluster in Fig. 14 in terms of sampling frequency, yet relatively few of these fractures appear in the detailed fracture map. This lack of correspondence probably arises from the lower-bound length of fractures in the map; that is, most joints in this set

probably have trace lengths less than 0.5 m, and thus they were not routinely mapped. Fracture lengths are discussed further in Section 5.2.

Mathematical distributions for the four fracture-set orientations have not yet been developed. Although their mean pole directions are evident, it is clear that sets 1 and 2 do not conform to a simple spherical normal distribution; that is, there is covariance between the solid angle and azimuth of poles relative to the mean pole direction. In contrast, sets 3 and 4 appear to be normally distributed, but their contours overlap to form a bimodal distribution. Because of these non-uniformities, a more complete statistical analysis of the four fracture-set distributions will be reported in the future.

Several simplifying assumptions can be made in order to study fracture size and spacing variations. First, it is possible to approximate the boundaries of each cluster in Fig. 14. The average, or random, density of 827 poles on the hemisphere is 12.5 poles per contouring circle, which corresponds to the 1.5 percent interval in Fig. 14. This is taken as the "significance threshold" of the clusters, and forms a logical boundary. The individual cluster boundaries are therefore comprised of the 1.5 percent contour plus arbitrary boundaries drawn between sets. In this manner, the significant concentration of poles (> 1.5 percent contour) is delimited into the four sets, as shown in Fig. 15. The boundaries have been linearized in order to facilitate the assignment of appropriate set numbers to fractures in the core logs and floor map. The major assumption here is that the fracture sets do not overlap. Note that orientation distribution functions



XBL 799-11321

Fig. 15. Generalized fracture set boundaries corresponding to 1.5 percent contour.

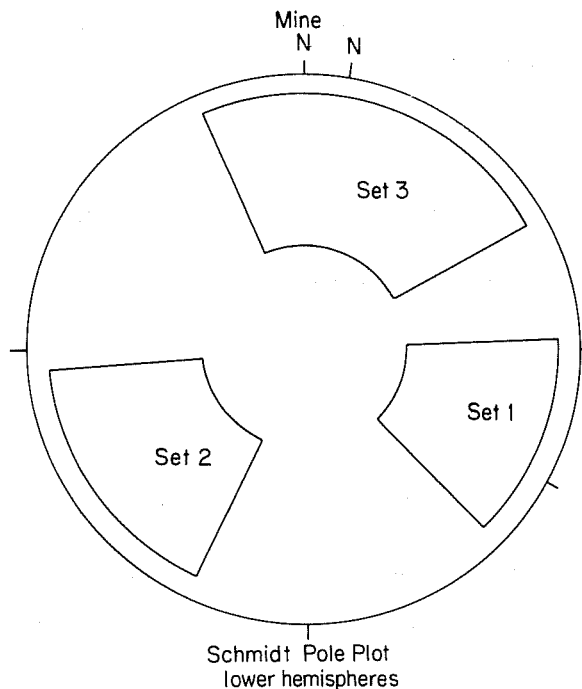
have not been defined for the sets; the sizes and spacings of fractures within a set are assumed to be independent of orientation.

5.2 Fracture Sizes

In order to estimate their sizes, discontinuous fractures are assumed to be disc-shaped with a distribution of diametral lengths. This characterization has previously been adopted for analysis of joint traces (Barton 1978). The detailed fracture map supplies trace lengths, provided that fracture set groupings can be made according to the following discussion. The angles of dip for minor fractures were not routinely measured during the floor mapping. However, sets can be generalized according to dip direction,

and hence pole direction. Using Fig. 15 to indicate the appropriate ranges of pole azimuths, fracture set boundaries can be broadened as shown in Fig. 16. Dip angles of fracture planes range from about 30° to 80° for each of sets 1, 2, and 3, which yield limits on pole inclinations as shown. These angular limits arose from the fact that (1) subhorizontal fractures were not usually mapped, and (2) dips of 80° to 90° were considered vertical and were so designated in the map. Using Fig. 16, the fracture sets in the floor can be identified to within 10° to 20° of their configurations in Fig. 15. Due to the bias against subhorizontal fractures, set 4 was not included in this survey.

Trace lengths of fractures falling within the Fig. 16 boundaries were



XBL 799-11322

Fig. 16. Generalized fracture set boundaries for analysis of mapped fracture lengths.

scaled from Fig. 6 to the nearest 0.1 m. Length-frequency histograms for these tabulated data are shown in Figs. 17a, b, and c for sets 1, 2, and 3, respectively. The probability p of equaling or exceeding each of the given fracture lengths can be calculated according to the Weibull plotting position formula:

$$p = \frac{m}{n + 1},$$

where n is the number of observations, and m is the rank of the fracture length, the longest having $m = 1$ and the shortest having $m = n$. Plotting these data in lognormal probability form yields the cumulative frequency distributions shown in Fig. 18. The best linear fit through the data is provided by the lognormal distribution function, the equation for which is given by Chow (1964):

$$\log x = \overline{\log x} + K \cdot \sigma_{\log x} \quad (1)$$

The variable x is the fracture length in meters, $\overline{\log x}$ is the logarithmic mean, and the standard deviation for the distribution is $\sigma_{\log x}$. The K term is related to the normal probability function by

$$P(X \geq x) = \frac{1}{\sqrt{2\pi}} \int_{-\infty}^K \exp(-K^2/2) dK \quad (2)$$

Values of the exceedence probability, $P(X > x)$, for various values of K can be found in normal probability tables from most statistical handbooks. For clarity, the linear K axis is plotted alongside the probability axis in Fig. 18. Nonlinearity at the ends of each set of data is due to the lower bound on mapped fracture lengths (about 0.3 m) and the upper

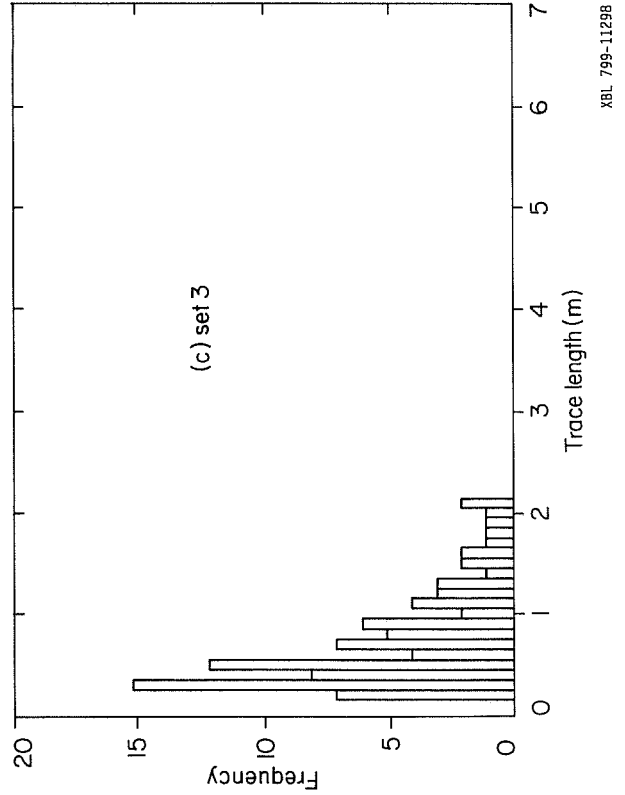
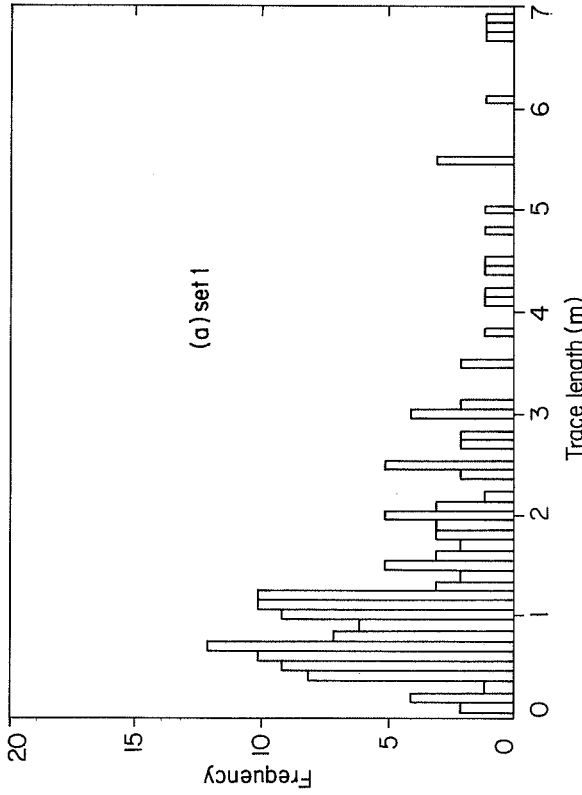
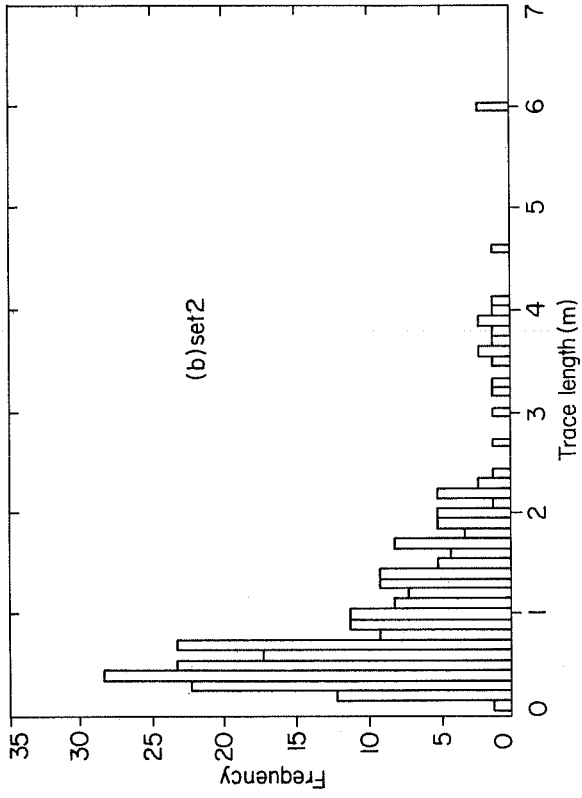
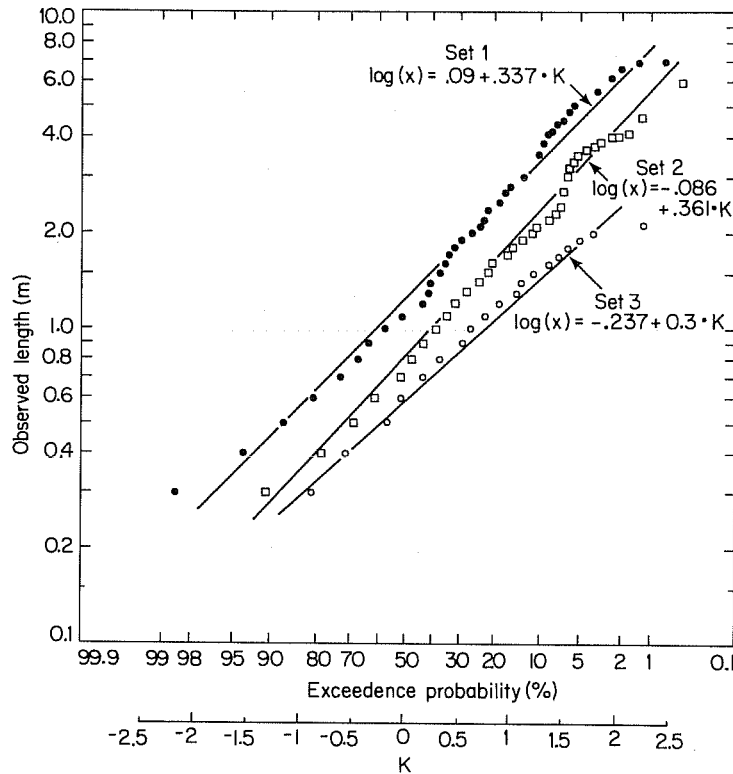


Fig. 17. Fracture length-frequency histograms for the three non-horizontal joint sets.



XBL 799-11323

Fig. 18. Cumulative lognormal fracture length distributions.

bound set by the dimensions of the drift (e.g., about 7 m for set 1). For purposes of representing the local fracturing, however, the relevant range of lengths is given adequately by the three distributions. As shown in Fig. 18, least squares fitting of Eq. (1) to the sets of data gives the respective mean and standard deviation values listed in Table 5.

Table 5. Fracture length distribution parameters.

Set no.	Mean length (m)	Standard deviation (m)
1	1.25	2.20
2	0.81	2.29
3	0.58	2.00

The cumulative distributions of Fig. 18 give the exceedence probabilities, rather than the discrete probabilities, for given lengths of fractures. In other words, Fig. 18 shows that there is a 50 percent chance of finding a fracture in set 1 whose length is greater than 1.25 m, but only a 10 percent chance of finding one greater than about 3.4 m. To determine the probability of finding a fracture of some given length, the probability density function

$$p(x) = \frac{1}{\sigma_y e^y \sqrt{2\pi}} \exp \left[-\frac{(y-\bar{y})^2}{2\sigma_y^2} \right] \quad (3)$$

must be used, where $y = \log x$ and σ_y and \bar{y} are from Table 5.

5.3 Fracture Spacings

Fracture data from the vertical boreholes were used as a basis for analyzing the spacings between fractures of the four sets. For each core log, spacings relative to the core axis (i.e., vertical) were computed for consecutive fractures of the same set. For the analysis, fracture sets were delimited according to the boundaries shown in Fig. 15. For example, if three successive fractures in set 4 were found at depths of 1.5, 2.0, and 3.0 m in a given borehole, two spacings, 0.5 m and 1.0 m, would be recorded. Fractures of any other set lying within 1.5 to 3.0 m would, of course, be ignored. Following this computation procedure for all core logs, the histogram plots shown in Figs. 19a-d were developed.

Again using the lognormal probability distribution, the exceedence probabilities are represented by Figs. 20a and b. In order to determine

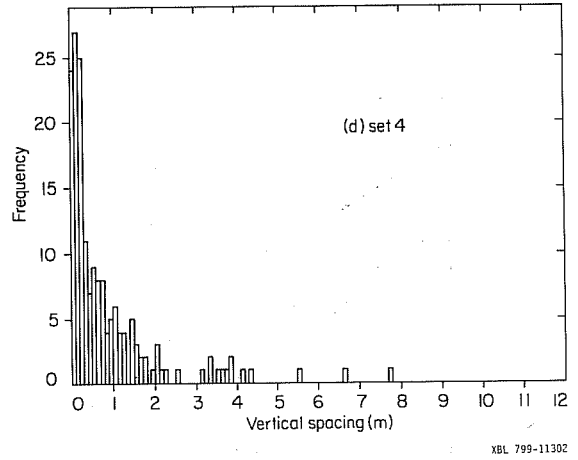
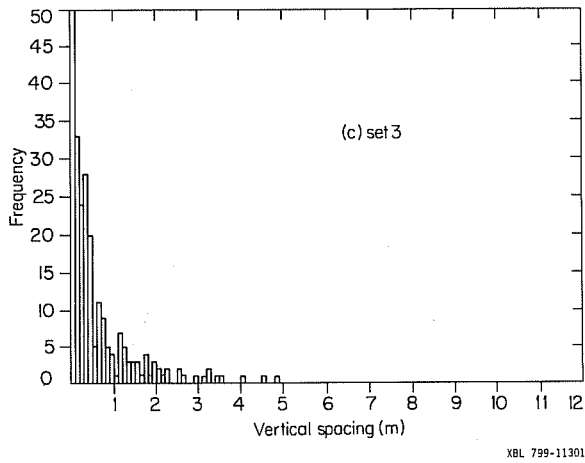
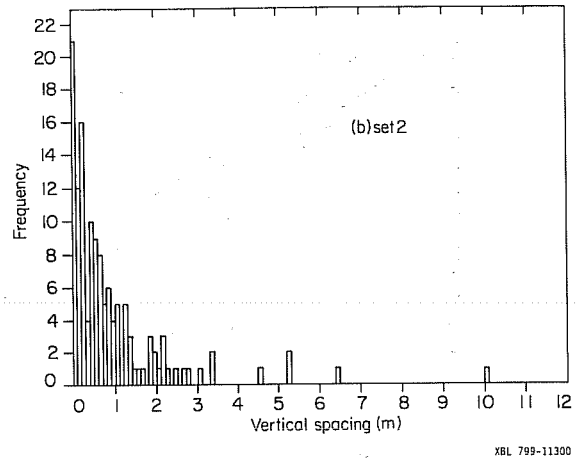
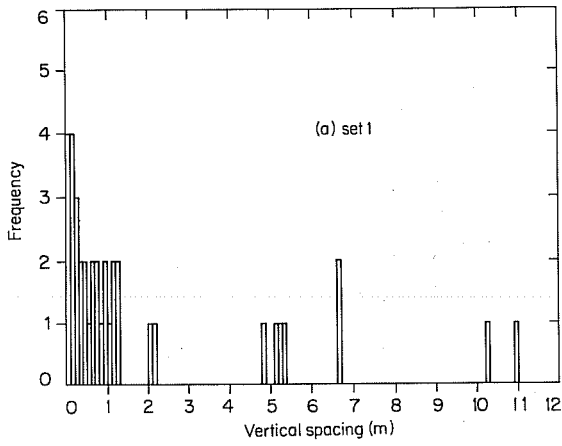


Fig. 19. Vertical fracture spacing-frequency histograms for all four joint sets.

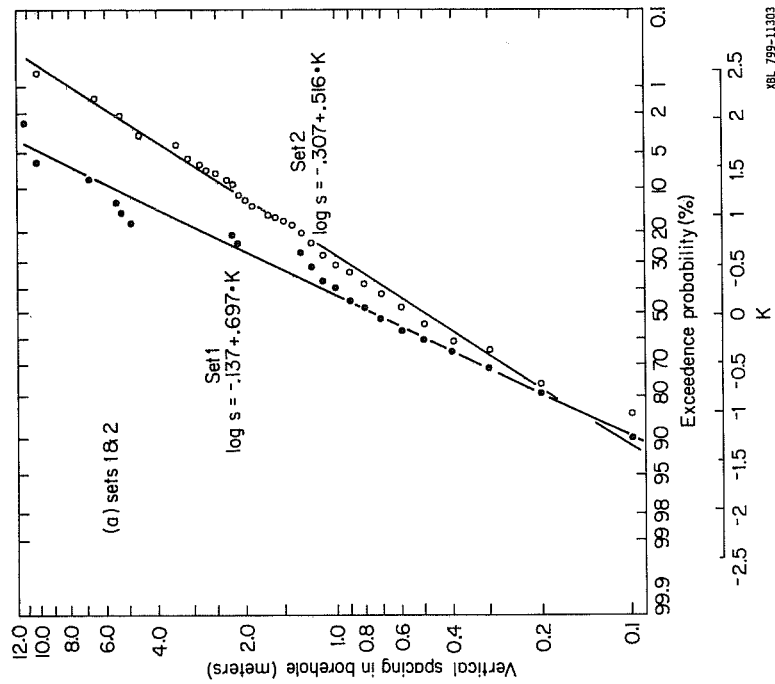
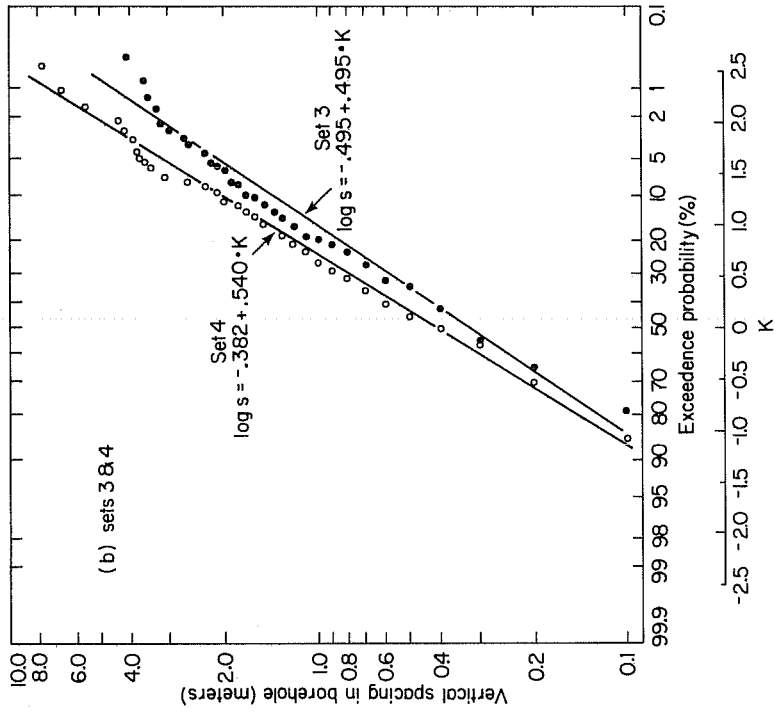


Fig. 20. Cumulative lognormal distributions of fracture spacings in vertical direction.

the perpendicular spacings between parallel-dipping fractures it is necessary to multiply the observed spacings by the cosine of the dip angle (Terzaghi 1965). Since the orientations of fractures vary within a set, however, the dip of the mean fracture plane must be used to estimate the correct spacing. Parameters describing the vertical and corrected spacings are listed in Table 6.

Table 6. Fracture spacing distribution parameters.

Set no.	Mean vertical spacing (m)	Standard deviation	Mean dip angle ($^{\circ}$)	Normal spacing
1	0.73	4.98	41	0.55
2	0.50	3.28	59	0.25
3	0.32	3.13	39	0.25
4	0.42	3.47	0	0.42

Vertical spacing distributions in Figs. 20a and b appear to be less linear than fracture length distributions in Fig. 18. This nonlinearity and the more pronounced irregularities in the plotted data are most probably due to the sampling bias of the core logs; that is, sealed fractures were not routinely logged. The lognormal distributions fit the data well enough, however, to be useful in statistical representations of fracturing. Equation (3) should be used as the stochastic generator for discrete fracture spacings.

5.4 Fracture Infilling Characteristics

The most common mineralization observed in the fractures is chlorite, second is calcite, and third is epidote.* Other minerals identified in the

*Current mineralogical-petrological studies will determine more definitively the nature of fracture-filling material.

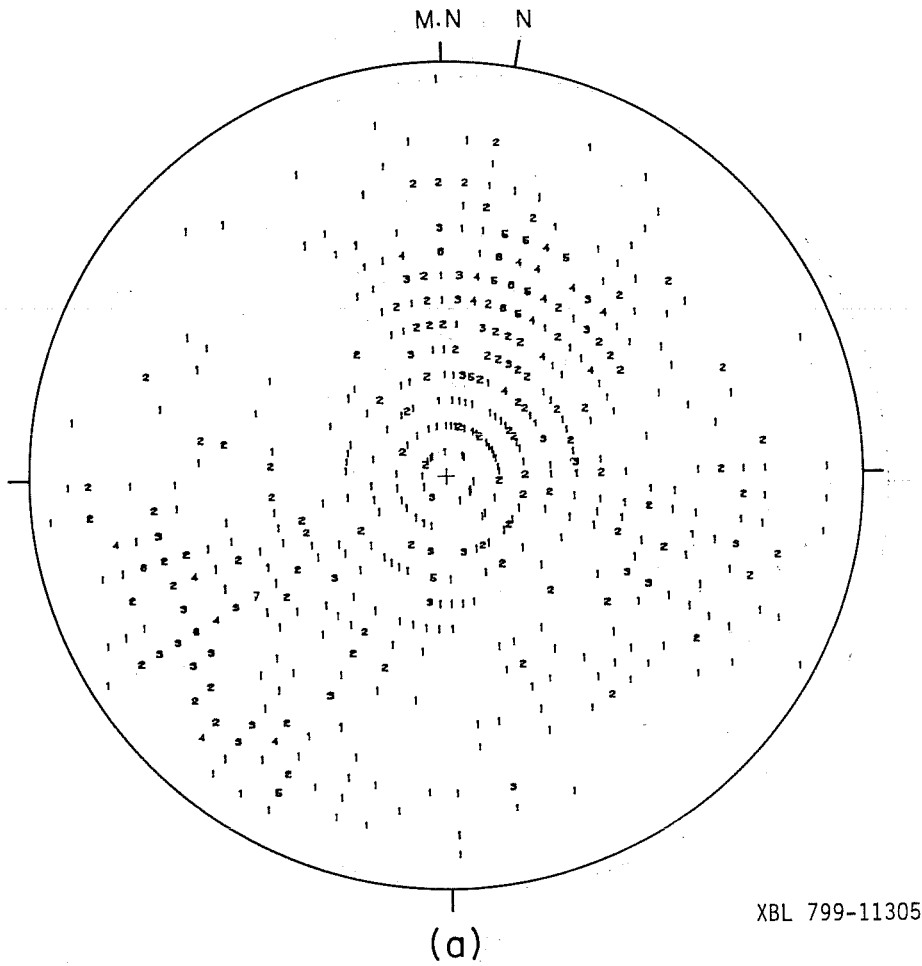
core logs include mica, pyrite, and fluorite. Based on the 827 natural fractures logged in the vertical boreholes, the percentage occurrences are given in Table 7. It is common for a fracture to have two or more types of mineralization, and no predominance of a filling in a particular fracture is indicated.

In order to correlate the types of infilling with the fracture sets, equal-area stereonet plots of poles to fracture exhibiting the three major types are given by Figs. 21 a, b, and c. Percentage occurrence data for each set are summarized in Table 8. Chlorite is common to all four fracture sets, while calcite tends to be most concentrated in sets 2 and 3. Epidote is most commonly associated with sets 1 and 2, but less frequently found in sets 3 and 4.

A similar presentation of fracture infilling thicknesses shows that the great majority are less than a millimeter wide. Figure 22a, b, and c shows the orientation distributions of fractures of increasing thickness. These data are summarized in the form of exceedence, or cumulative probabilities, in Table 9. Comparison of Figs. 15 and 22c indicates that set 1

Table 7. Fracture mineralization data for the Stripa core logs.

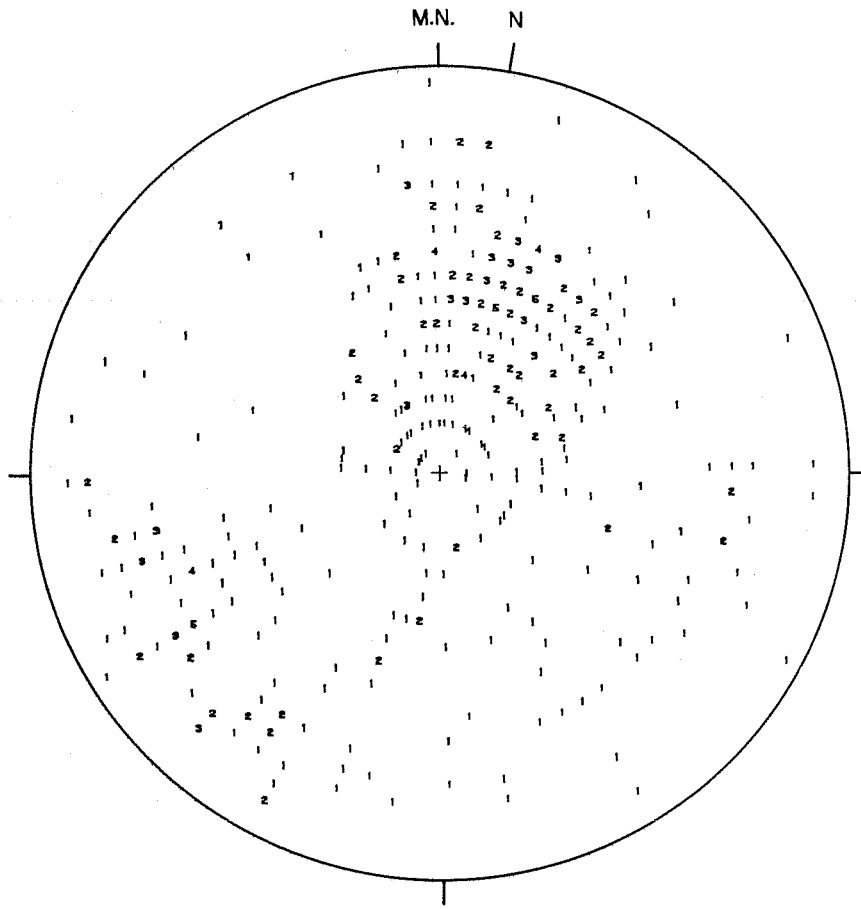
<u>Mineralization</u>	<u>Number of occurrences</u>	<u>Percentage of 827 (%)</u>
Chlorite	758	91.7
Calcite	406	49.1
Epidote	62	7.5
Mica	16	1.9
Pyrite	9	1.1
Flourite	7	0.8



XBL 799-11305

Schmidt equal-area pole plot
Chlorite mineralization
Lower hemisphere
758 points

Fig. 21. Stereographic plots of poles of fractures with the three major types of mineralization.

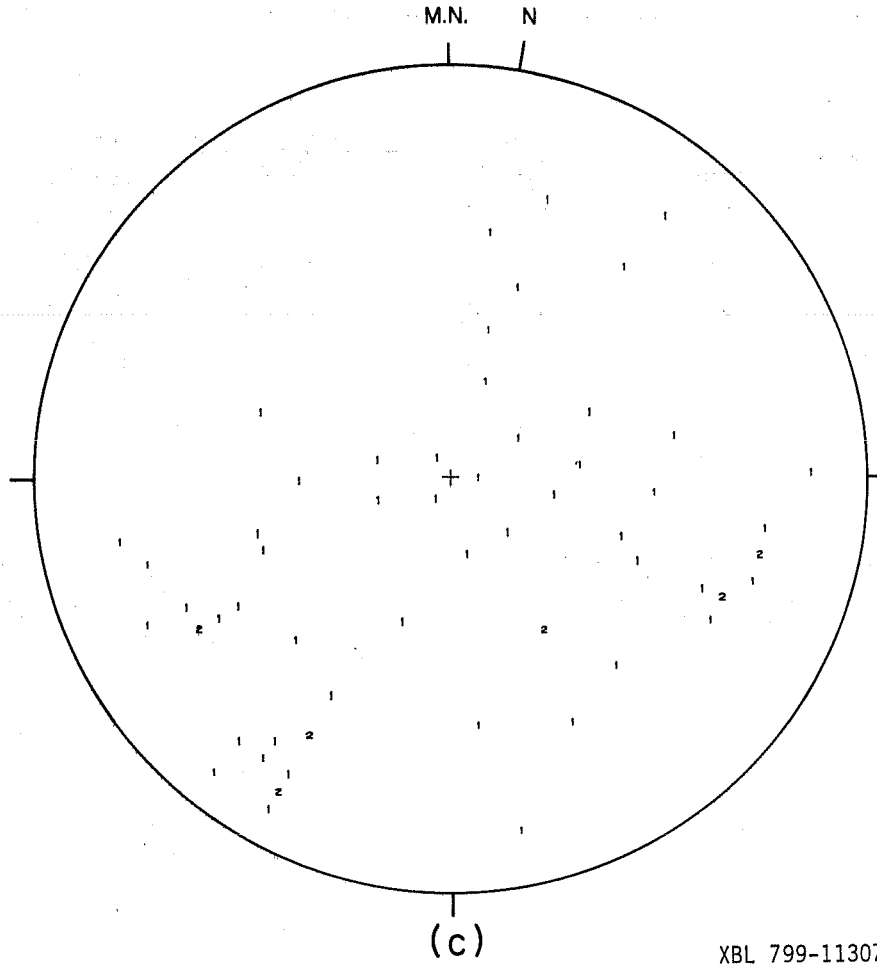


(b)

XBL 799-11306

Schmidt equal-area poleplot
Calcite mineralization
Lower hemisphere
406 points

(Fig. 21 continued)



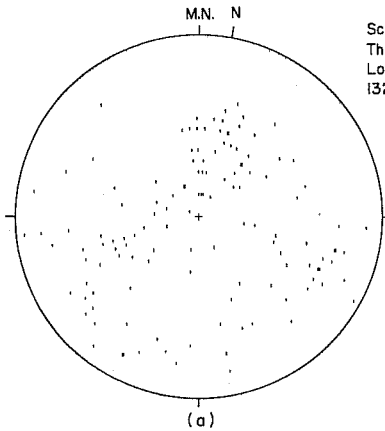
XBL 799-11307

Schmidt equal-area pole plot
Epidote mineralization
Lower hemisphere
62 points

(Fig. 21 continued)

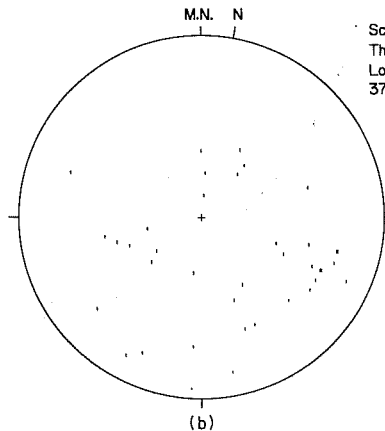
Table 8. Statistical mineralization data from Stripa fracture logs.

Set number	Total number in set	Number and percentage of occurrences		
		Chlorite	Calcite	Epidote
1	53	46 (87%)	14 (26%)	7 (13%)
2	154	147 (95%)	72 (47%)	20 (13%)
3	254	244 (96%)	151 (63%)	7 (3%)
4	191	172 (90%)	83 (43%)	11 (6%)



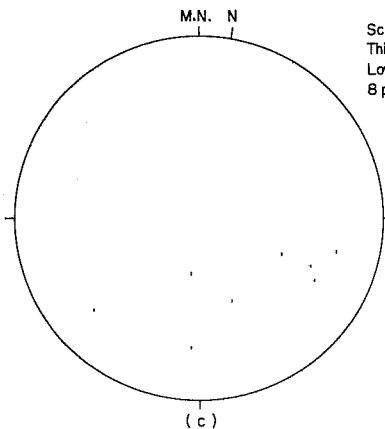
Schmidt equal-area pole plot
Thickness > 1mm
Lower hemisphere
132 points

XBL 799-11308



Schmidt equal-area pole plot
Thickness > 2mm
Lower hemisphere
37 points

XBL 799-11309



Schmidt equal-area pole plot
Thickness > 5mm
Lower hemisphere
8 points

XBL 799-11310

Fig. 22. Stereographic plots of fractures with different thicknesses.

Table 9. Thickness data for fracture infillings.

Set number	Total number in set	Number and percentage of occurrences		
		1 mm	2 mm	5 mm
1	53	13 (25%)	8 (15%)	3 (6%)
2	154	30 (19%)	7 (5%)	1 (1%)
3	254	35 (14%)	5 (2%)	0 (0%)
4	191	21 (11%)	4 (2%)	1 (1%)

comprises the thicker fractures, which also agrees with the delineation of major features from the floor map (Fig. 10). Sets 3 and 4 generally have the smallest percentages of fractures thicker than 1.0 mm.

6. DISCUSSION

6.1 Origin of the Fracture System

The geology and tectonics of the granite mass at Stripa are complex and difficult to interpret due to the lack of previous study from which to draw. An understanding of the regional geological setting and a general idea of the morphology of the rock mass are necessary in order to theorize on the origin of the fracture system, and are currently being investigated. Although discussion of possible origins of the discontinuities is very speculative at this time, the following information might stimulate study into possible connections between the existing stresses and fracture pattern in the underground test area.

Carlsson (1978) has reported the results of stress measurements in the OV1 drift (Fig. 2), whose average principal stress components show a close directional relationship with the fracture sets in the time-scale drift (Fig.

14). A plot of mean fracture-set poles and the major principal stress vectors is shown in Fig. 23. The mean poles of sets 1 and 3 are about perpendicular to the major principal stress direction, σ_1 , and the pole of set 3 corresponds to the minimum principal stress, σ_3 . Furthermore, the mean plane of set 2 is oriented virtually perpendicular to the major principal stress. Such orthogonalities are common in fracture networks in rock (Ramsey 1967), but because of historical changes in the tectonic regime, the observed fracturing need not be morphologically related to the existing state of stress. Nevertheless, the following speculation about joint origins is an attempt to explain the close correlation of the local stress field with the extensive fracturing in the time-scale drift.

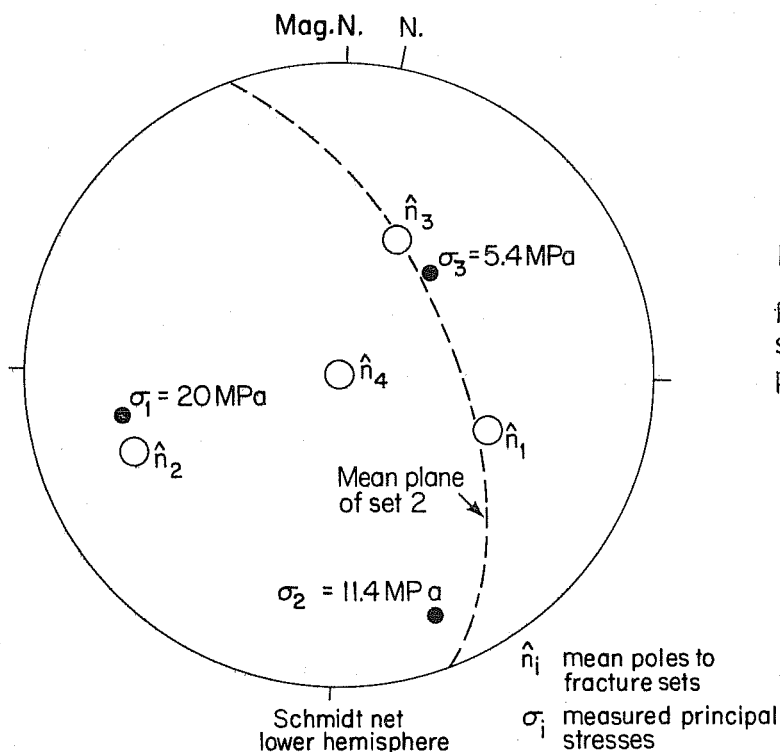


Fig. 23.

Relationship of mean fracture set orientations and measured principal stress directions.

It can be reasoned that joint sets 1, 2, and 4 are related to the intrusion and subsequent cooling of the granite body. The presence of epidote and chlorite on these fractures, as opposed to only calcite, suggests such a hydro-thermal environment. The core samples and floor map show that the surfaces of the joints of set 2 are generally irregular and rough, indicating that they are extension (tension-related) features. Such fracturing should occur parallel to the maximum compressive stress. Here, the opposite is true and, therefore, the stresses which initiated these fractures must have been different from the stress which has been measured. Although it is speculative to reconstruct this previous stress field, the orientation of set 2 implies that the major principal stress should have been nearly orthogonal to that which now exists. It is visualized that such a large shift in the local state of stress could have been associated with cooling isotherms in the pluton, which in turn would have been related to the overall shape and orientation of the body. For example, if a mass of cooling granite were striking parallel to the maximum principal stress, then the maximum stress within the rock mass due to cooling should be perpendicular to the long dimensions of the body. Of course, the applicability of such a model here is uncertain because very little is known at this time about the intrusion process or the geometry of the rock mass at Stripa. All that can be stated now is that the granite-leptite contact appears to strike roughly parallel to the mean pole of joint set 2 and σ_1 , which may be indicative of such a thermal fracture mechanism.

The above discussion does not imply that the existing state of stress is the same as that at the time of intrusion. The most recent change in

stress resulted from glacial loading, consisting of 2 to 3 km of ice (Press and Siever 1974). Certain factors indicate that fracture set 3 may be associated with the current isostatic uplift from this loading: (1) the set's orientation with respect to σ_3 , (2) the predominance of only calcite fracture infillings, as opposed to hydrothermal minerals, (3) the relatively short trace lengths and close spacings of joints, and (4) the observation that these joints tend to pass continuously across the other fractures in the core samples. An alternate explanation of joint set 3 is that it results from a distorted stress field produced by the mine itself. Verification of this mechanism depends on further stress measurements and fracture studies far from the mine stopes.

6.2 Current Deformations

Deformation within the Stripa granite is continuing, as evidenced by the faulting of certain fractures in set 1. It has been shown in Section 4 that the configuration of at least one of these faults is consistent with the observed direction of slickensiding. The relationship between this shearing and the existing state of stress can be analyzed by resolving the principal stress vectors in Fig. 23 into shear and normal components on the mean plane of set 1. This is done stereographically in Fig. 24 by first finding the resultant stress direction, $\hat{\sigma}_r$; then passing a plane through this resultant and the mean normal of set 1, \hat{n}_1 . The intersection of this plane and the set 1 plane (containing the dip vector, \hat{d}_1) is the direction of the shear stress, \hat{s}_1 , on the joints. The azimuthal direction of \hat{s}_1 is given by the vertical plane containing it, and this turns out to be 242° , which agrees with the observed direction of shearing (240° , see Section 4). Stress magnitudes on this mean plane have been calculated,

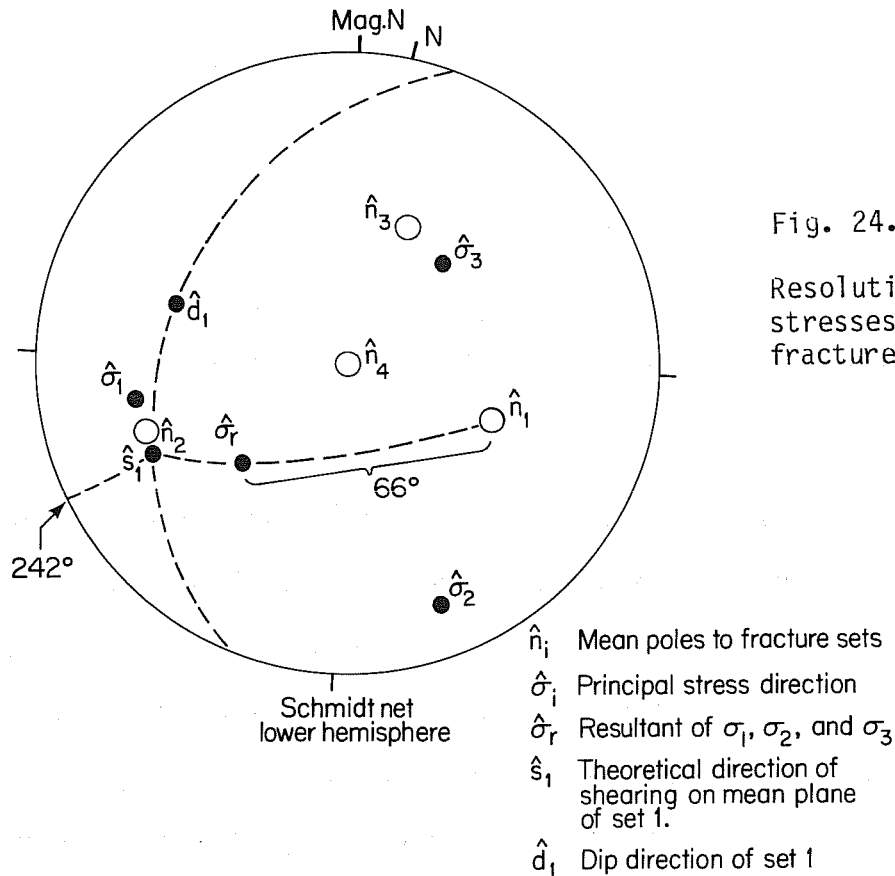


Fig. 24.

Resolution of shear and normal stresses in the mean plane of fracture set 1.

XBL 799-11312

and the resulting ratio of shear-to-normal stress is 2.25. For sliding equilibrium the friction angle of the set 1 faults must be at least $\arctan(2.25) = 66^\circ$, assuming no cohesion. The friction angle must be somewhat less, however, because a certain amount of cohesion does indeed exist on the faults, as discussed in Section 4.

Stresses on the mean planes of the other three fracture sets can be similarly resolved, and their magnitudes are given in Table 10. The highest shear-to-normal stress ratio is found on set 3, which indicates that the friction angle and/or the cohesive strength is high enough to maintain equilibrium. Recognizing that set 3 is relatively discontinuous, its "cohesion" derives from the strength of the intact granite. Table 10 also

Table 10. Shear and normal stresses on the mean planes of the four fracture sets.

<u>Set number</u>	<u>Shear stress (MPa)</u>	<u>Normal stress (MPa)</u>	<u>Theoretical azimuth of shearing (°)</u>	<u>Shear/normal</u>
1	21.56	9.60	242	2.25
2	10.35	21.21	127	0.49
3	23.08	4.91	218	4.70
4	15.17	18.08	224	0.84

lists the theoretical azimuths of shearing on all of the mean planes. Many of the fractures logged in the core samples show signs of slickensiding and, based on a limited re-examination of the core, the actual directions do not agree with those in Table 10. The observed azimuth directions vary from about 230° to 280° , which is generally in the direction of shearing on set 1. While these directions need not be precisely aligned with the major faulting, it is clear that the present tectonic movements are being controlled by the set 1 shear fractures. This is to say, when sliding occurs along a set 1 fault, the stresses on the other fracture planes are temporarily altered from those shown in Table 10 until new equilibrium positions are reached.

Rather than conclude that none of the fractures were formed by shear failure, we hypothesize that the existing shear planes originated as tensile failure surfaces, which were then propagated by tectonic stresses until those oriented in similar directions became interconnected and formed faults. While the predominant faulting is currently associated with set 1 fractures, propagation of the set 3 surfaces due to the current state of stress might create an entirely new mode of shear deformation in the distant future. This is plausible in light of the high shear-to-normal stress ratio on these

planes. Alternatively, if the local state of stress were substantially altered (e.g., by large-scale heating or further mining), such that set 3 fractures would be propagated, the likelihood of faulting along these planes would be enhanced.

The degree to which certain fractures are currently open may be indicated not only by the occurrence of slickensides, but also by the type of infilling. As discussed previously, epidote is probably a post-intrusion product of hydrothermal solutioning. Chlorite is common to virtually all fractures, and is thought to be deposited as an alteration product of the feldspars and muscovite on the fracture walls. Of the three predominant minerals, calcite is probably the most recently deposited (Wollenberg 1979), and might indicate the location of the main hydraulic flow paths. The calcite fractures are clustered in sets 2 and 3. The shear fractures extending through the time-scale experiment also have significant calcite coatings in addition to chlorite and epidote, so it is probable that major fractures in set 1 also constitute flow channels in the rock mass.

6.3 Use of the Deterministic Results

We envision that the major features in the time-scale experiment can be analyzed numerically by modeling individual discontinuities to simulate the mechanical behavior of a rock mass (as discussed by Goodman 1976), provided their strength properties are known.

As discussed in Chapter 4, because of the paucity of subsurface information near the ends of the heater array, the configurations of the major fracture surfaces are not completely indisputable: fracture number 3 has been delineated with the most confidence; fractures 1, 2, and 4 are less

certain. The surficial expressions of fractures 1, 2, and 4 are more complex, and are most likely associated with zones of fracturing which have undergone relatively less shearing.

Fracture 3 shows the most pronounced shear deformation, and is undoubtedly the most significant discontinuity through the experiment. Due to the observed and inferred waviness, however, its mode of shear deformation is limited mainly to slip along an azimuth of about 240° from true north. Considerably more energy would be required to shear the fault in other directions, because the amount of dilation (aperture opening) would be greater. Because the infilling thickness is quite irregular, which may be due to the dilation from past shearing, the relative amounts of mineralization vary over the surface. Calcite and chlorite are pervasive, but the epidote thickness can vary from less than a centimeter to about 15 cm, with an average thickness of about 2 cm, based on the data in Table 3. Epidote is harder than chlorite, however, and probably has less influence on the mechanical behavior of the rock mass.

The pegmatite dike shown in Fig. 6 is obviously a discontinuous feature, although the small-scale offsets of less than about 20 cm should be neglected, since they cannot be accurately defined at depth. It is therefore recommended that the dike be modeled as a 10- to 20 cm-wide tabular body striking perpendicular to the long axis on the array, as shown in Figs. 10 and 11. The only major offset in the dike which can be confidently inferred from the borehole data is that caused by shear fracture number 3.

6.4 Limitations of Statistical Results

The statistical data reported here are lacking in certain respects. First of all, to be useful in a stochastic analysis, the non-uniform distributions of the fracture plane orientations should be quantified. Secondly, the major assumption of the fracture size and spacing analyses is that these parameters are independent of each other. In fact, the detailed fracture map shows that this is not exactly correct because of the occurrence of fracture zones. In these areas, for example, it is possible to find closely spaced long fractures. For proper representation, this relationship needs to be investigated. Thirdly, the statistical data represent the whole experimental area, rather than selected areas. The data base used here is probably insufficient for a proper statistical analysis; potential variations in the orientation, length, and size parameters over different zones in the drift should be investigated. Fourthly, the relationship between fracture size or spacing and infilling characteristics needs attention. Ideally, a complete statistical characterization should facilitate the simulation of fracture networks in the areas between the major continuous features. Until such a characterization can be reported, it is suggested that the mean orientation, size, and spacing values reported in Section 5 be adopted for purposes of modeling or interpretation of thermal data.

7. CONCLUSIONS

On the basis of available data, four major continuous fracture surfaces and a faulted pegmatite dike have been delineated to a depth of about 13 m below the experiment drift. The most prominent of these features is a shear fracture which dips steeply through the central portion of the

heater array, and obliquely thrust-faults the pegmatite at a depth of about 8 m. The inferred offset is about 2 m, N60W.

The methodology by which these continuous features were identified, outlined in this paper, appears sound in light of the consistency of the fracture configurations and the observed shearing direction. Based on the available subsurface data, however, the method cannot be expected to yield detailed information on the network of discontinuous fractures. This aspect has required a statistical approach, from which it is concluded that there are four principal sets of fractures. The mean orientations of these sets have been determined, and the distributions of fractures about the means are described qualitatively. The spacing and size distributions of fractures of the given sets have been shown to conform to the lognormal probability distribution, assuming that these parameters are independent.

Speculations have been made concerning the origins of the fracture sets. Because of the close alignment of the fracture sets and the locally measured principal stress directions, it is reasoned that some fracturing results from cooling of the granite following emplacement and other fracturing is due to much more recent isostatic uplift. The local state of stress has probably changed over time, and it is hypothesized that the current stresses have induced the most recent extension fracturing, as well as faulting along the major continuous fractures in the time-scale drift. Mine excavations may also have some influence on the stress field, but this is unsubstantiated at present.

8. ACKNOWLEDGMENTS

A number of persons must be recognized for their help in preparing this report. Individuals who participated in the fracture mapping included S. Abrahamsson, K. Almén, L. Andersson, T. Dauggard, L. Jacobsson, and U. Jacobsson. B. Kanehiro, W. Klauber, and D. McCarthy provided assistance in the interpretation of the fracture data. T. Pfeiffer did the fine illustration work for the report. The contributions of all these individuals are gratefully acknowledged. A special note of thanks is given to Dr. J. E. Gale for his continuing guidance in the project.

9. REFERENCES

- Barton, C.M. 1978. Analysis of Joint Traces. Proceedings, 19th U.S. Symposium on Rock Mechanics, Reno, Nevada.
- Carlsson, Hans. 1978. Stress Measurements in the Stripa Granite. Lawrence Berkeley Laboratory report LBL-7078, SAC-04. Berkeley, California.
- Chow, V.T. 1964. Handbook of Applied Hydrology. New York: McGraw-Hill, Inc.
- Cook, Neville G.W., and P.A. Witherspoon. 1978. Mechanical and Thermal Design Considerations for Radioactive Waste Repositories in Hard Rock. Part II: In Situ Heating Experiments in Hard Rock: Their Objectives and Design. Lawrence Berkeley Laboratory report LBL-7073, SAC-10. Berkeley, California.
- Gale, J.E., and P.A. Witherspoon. 1978. An Approach to the Fracture Hydrology at Stripa: Preliminary Results. OEDC Seminar on In Situ Heating Experiments in Geological Formations, Stripa, Sweden, Sept. 12-15. Also Lawrence Berkeley Laboratory report LBL-7079, SAC-15. Berkeley, California.
- Geijer, P. 1938. Stripa Odalfaeltsgeologi (Stripa Mine District Mapping). Stripa Mine Archives, Stripa, Sweden.
- Goodman, R.E. 1976. Methods of Geological Engineering in Discontinuous Rocks. St. Paul, Minnesota: West Publishing Company.
- Kendorski, F.S., and M.A. Mahtab. 1976. Fracture Patterns and Anisotropy of San Manuel Quartz Monzonite. Bulletin of Association of Engineering Geologists 13 (1): 23-52.
- Knill, J., and K. Jones. 1965. "The Recording and Interpretation of Geological Conditions in the Foundations of the Roseires, Karifa, and Latiyan Dams. Geotechnique 15: 94-124.
- Kurfurst, Pavel J., T. Hugo-Persson, and G. Rudolf. 1978. Borehole Drilling and Related Activities at the Stripa Mine. Lawrence Berkeley Laboratory report LBL-7080, SAC-05. Berkeley, California.
- Nelson, P., B. Paulsson, R. Rachiele, L. Andersson, T. Schrauf, W. Hustrulid, O. Duran, and K. Magnusson. 1979. Preliminary Report on Geophysical and Mechanical Borehole Measurements at Stripa. Lawrence Berkeley Laboratory report LBL-8280, SAC-16. Berkeley, California.
- Office of Waste Isolation. 1977. Movement of Fluids in Largely Impermeable Rocks. Seminar held at University of Texas at Austin, January 27-29.

- Olkiewicz, A. J., K. Hansson, K-E. Almen, and G. Gidlund. 1978. Geological and Hydrogeological Documentation of the Stripa Test Station. KBS Technical report 63. Stockholm, Sweden.
- Press, F., and R. Siever. 1974. The Earth. San Francisco: W.H. Freeman and Co.
- Ramsay, J.G. 1967. Folding and Fracturing of Rocks. New York: McGraw-Hill, Inc.
- Terzaghi, R.D. 1965. Sources of Error in Joint Surveys. Geotechnique. 15:
- Witherspoon, P.A., and O. Degeman. 1978. Swedish-American Cooperative Program on Radioactive Waste Storage in Mined Caverns. Lawrence Berkeley Laboratory report LBL-7049, SAC-01. Berkeley, California.
- Witherspoon, P.A., J. Gale, P. Nelson, T. Doe, R. Thorpe, C. Forster, and B. Paulsson. 1979. Rock Mass Characterization for Storage of Nuclear Waste in Granite. Proc. 4th ISRM Congress, Montreaux, Switzerland.
- Wollenberg, H. 1979. Lawrence Berkeley Laboratory, Berkeley, California. Personal communication.

10. APPENDICES

APPENDIX A. Borehole Fracture Logs for Time-Scale Experiment

EXPLANATION OF FRACTURE LOGS

- DEPTH - Represents depth to midpoint of fracture surface (nearest cm).
- ROCK TYPE - The term "granite" is a general descriptor here, referring more specifically to quartz monzonite. Minor variations of this classification are not detailed.
- DISCONTINUITIES AND BREAKS
- NATURAL - Naturally occurring fracture; usually open in situ and containing some mineralization.
- INDUCED - Break caused by drilling.
- UNCERTAIN - May be a natural fracture; however, its openness in situ is very questionable.
- OPEN/CLOSED - Refers to condition of fracture in core and, by inference, to its condition in situ.
- OTHER - Refers to a discontinuity other than a fracture.
- ROUGHNESS - Amplitude of small-scale irregularities with wavelengths < 1-2 cm. Larger scale roughness is denoted as "irregular."
- WEATHERING - Degree of alteration of wall rock:
- HW - Highly weathered
 - MW - Moderately weathered
 - SW - Slightly weathered
 - NW - Non-weathered

MINERALIZATION

- TYPE - Coded by occurrence, not predominance.
 Main types are chlorite (K), calcite (C), and epidote (E). Others include:
 iron pyrite (I)
 mica (M)
 fluorite (F)
 quartz (Q).
- COLOR - Black (BK), Blue (B), Brown (BN), Green (G), White (W),
 Yellow (Y).
- THICKNESS - Very approximate; "hairline" fractures are about
 1/2-mm thick.
- HARDNESS - Soft (S) - scratch with plastic
 Moderately hard (MH) - scratch with iron
 Hard (H) - scratch with steel.

ORIENTATION

- BETA ANGLE - Azimuth of apparent dip, looking down hole.
 ALPHA ANGLE - Acute angle between fracture and core axis.

- REMARKS - Slickensiding (shearing) is indicated, along with
 azimuth (B).

E1		DISCONTINUITIES AND BREAKS					MINERALIZATION				ORIENTATION		REMARKS	
DEPTH (M)	ROCK TYPE	CONDITION			SURFACE CHARACTERISTICS		TYPE	COLOR	THICK- NESS (MM)	HARD- NESS	BETA (DEG)	ALPHA (DEG)		
		1-INDUCED 2-NATURAL	3-UNCERTAIN 1-OPEN	3-OTHER 2-CLOSED	1-PLANAR	3-IRREGULAR 2-CURVED							ROUGH- NESS (MM)	WEATH- ERING
.07	GRANITE	1		1	1		HU	KC	BK	5	MH	250	65	SEVERAL INDUCED FR
.11	GRANITE	1		1	2		HU	KC	BKG	1	MH	255	75	
.24	GRANITE	1		1	1		HU	KH	BKG	1	MH	10	75	
.40	GRANITE	1		1	3		HU	KC	BKW	4	MH	65	70	
.74	GRANITE	1		1	1		HU	KC	BKG	1	MH	95	70	
.96	GRANITE	3		1	2		SU	KH	BKW	.5	H	40	40	PARTLY INDUCED
1.09	GRANITE	1		2				E		4		165	25	SEALED FRACTURE
1.35	GRANITE	3		1	1		HU	C		.5	H	50	75	PARTLY INDUCED
1.38	GRANITE	2		2	3		HU					360	85	
1.51	GRANITE	1		1	3		HU	KC		.5	H	10	80	
1.63	GRANITE	1		1	2		HU	KC	G	2	M	290	60	SHEARED
1.74	GRANITE	1		1	2		HU	KE	BK	1	MH-H	315	75	
2.79	GRANITE	2		2	3									
2.99	GRANITE	1		1	2		HU	KC	BKGW	1	S-MH	295	25	
3.28	GRANITE	1		1	1		HU	KCE	BKGW	1	MH	310	50	SHEARED
3.33	GRANITE	1		1	2		HU	KC	BKG	.5	MH	300	35	
3.69	GRANITE	1		1	1		HU	KC	BK	.5	MH	60	45	
4.20	GRANITE	2												
5.45	GRANITE	1		1	1		HU	KC	GW	.5	MH	55	75	
5.51	GRANITE	1		1	1		HU	K	G	.5	MH	300	30	
5.83	GRANITE	1		1	1		HU	KC	GW	2	S	165	40	
5.93	GRANITE	1		1	1		HU	K	G	.5	MH	165	35	
6.11	GRANITE	1		1	1		HU	K	G	.5	MH	145	23	
6.33	GRANITE	1		1	1		HU	K	G	.5	MH	180	30	
6.82	GRANITE	1		1	1		HU	K	G	.5	MH	75	45	
6.87	GRANITE	1		1	1		HU	K	G	.5	MH	130	30	
7.71	GRANITE	1		1	3		HU	C	W	.5	MH	210	20	
7.74	GRANITE	1		1	1		HU	KC	BK	.5	MH	35	35	CALC FR ALONG CORE
7.87	GRANITE	1		1	2		HU	KC	BK	.5	MH	150	35	
8.32	GRANITE	1		1	1		HU	KC	BK	.5	MH	115	50	
8.50	GRANITE	1		1	1		HU	KC	BK	.5	MH	170	55	
9.03	GRANITE	1		1	3		HU	K	BK	.5	MH	90	65	
9.49	GRANITE	1		1	1		HU	KC	BK	.5	MH	65	55	
9.68	GRANITE	1		1	1		HU	KC	BKG	.5	MH	65	50	
10.02	GRANITE	1		1	1		HU	KC	BKG	.5	SH	60	55	SHEARED
10.15	GRANITE	1		1	1		HU	KC	BKG	.5	MH	50	45	V-FORK, TWO CRACKS
10.31	GRANITE	1		1	1		HU	KC	BKG	.5	MH	75	70	
10.49	GRANITE	2												
11.49	GRANITE	1		1	3		HU	KC	BKG	.5	MH	50	45	
11.79	GRANITE	1		1	2		HU	E	G	1	H	100	35	PARTLY INDUCED
11.87	GRANITE	2												
12.06	GRANITE	1		1	3		SU	KE		.5	MH	120	75	
12.30	GRANITE	2												
13.27	GRANITE	2												
13.76	GRANITE	1		1	1		HU	KC	BKG	.5	MH	65	75	SHEARED
14.06	GRANITE	1		1	1		HU	K	BKB	2	MH	100	60	(END)

E2		DISCONTINUITIES AND BREAKS						MINERALIZATION				ORIENTATION		REMARKS					
		CONDITION			SURFACE CHARACTERISTICS														
DEPTH (M)	ROCK TYPE	1- NATURAL	2- INDUCED	3- UNCERTAIN	1- OPEN	2- CLOSED	3- OTHER	1- PLANAR	2- CURVED	3- IRREGULAR	ROUGH- NESS (MM)	WEATH- ERING	TYPE	COLOR	THICK- NESS (MM)	HARD- NESS	BETA (DEG)	ALPHA (DEG)	REMARKS
.02	GRANITE	1	1	1		2	SW	CE	GW	.5	M			GW	.5	M	270	10	
.27	GRANITE	2	2																
1.09	GRANITE	1	1	1		1	HU	KC	GW	.5	S			GW	.5	S	190	35	SHEARED
1.21	GRANITE	1	1	1		2	HU	K	G	.5	S			G	.5	S	300	55	
1.28	GRANITE	1	1	1		1	HU	K	G	.5	S			G	.5	S	300	45	
1.39	GRANITE	1	1	1		1	HU	K	G	.5	S			G	.5	S	235	35	
2.16	GRAN/PEG	1	1	1		2	HU	KCE	GW	1	S			GW	1	S	350	50	
2.44	PEGHATITE	2	2																
3.10	PEG/GRAN																		
3.25	PEG/GRAN	3		1		3	HU	KH	GW	.5	S			GW	.5	S	300	35	PARTLY INDUCED
3.44	GRANITE	2		3		3	SW	K	G	.5	S			G	.5	S	80	25	PARTLY INDUCED
3.91	GRANITE	1	1	1		2	HU	KE	G	.5	S			G	.5	S	300	35	
3.98	GRANITE	1		1		3	SW	KE	G	.5	S			G	.5	S	300	40	PARTLY INDUCED
4.32	GRANITE	1	1	2		3	HU	KE	G	.5	S			G	.5	S	280	20	
5.05	GRANITE	1	1	1		1	HU	K	G	.5	S			G	.5	S	300	45	
5.31	GRANITE	1	1	1		1	HU	K	G	.5	S			G	.5	S	115	55	SHEARED
5.36	GRANITE	1	1	1		1	HU	K	G	.5	S			G	.5	S	115	55	SHEARED
5.44	GRANITE	1	1	1		1	HU	KC	GW	.5	S			GW	.5	S	70	35	
5.57	GRANITE	1	1	1		2	HU	K	G	.5	S			G	.5	S	300	45	
5.94	GRANITE	1	1	1		2	HU	K	G	.5	S			G	.5	S	300	45	
5.94	GRANITE	3		1		2	SW	K	G	.5	S			G	.5	S	110	50	
6.40	GRANITE	1	1	1		3	HU	K	G	.5	S			G	.5	S	300	45	
6.54	GRANITE	1	1	1		2	HU	K	G	.5	S			G	.5	S	300	40	SHEARED
6.62	GRANITE	1	1	1		2	HU	K	G	.5	S			G	.5	S	140	75	
6.67	GRANITE	1	1	1		1	HU	K	G	.5	S			G	.5	S	60	40	
6.94	GRANITE	1	1	1		1	M-HU	K	G	.5	S			G	.5	S	120	75	SHEARED
7.15	GRANITE	1	1	1		1	M-HU	K	G	1	S			G	1	S	110	80	SHEARED
7.30	GRANITE	1	1	1		2	HU	K	G	.5	S			G	.5	S	100	75	DIRECTION UNCERTAIN
7.43	GRANITE	1	1	1		3	SW	K	G	.5	MH			G	.5	MH	95	75	
7.65	GRANITE	1	1	1		2	HU	KC	GW	.5	MH			GW	.5	MH	95	80	
7.76	GRANITE	1	1	1		2	HU	K	G	.5	S			G	.5	S	155	45	
7.98	PEGHATITE	1	1	1		3	HU	KC	GW	.5	S			GW	.5	S	80	65	
8.20	PEG/GRAN																		NO FRACTURE
8.59	GRANITE	1	1	1		4	HU	KC	GW	.5	MH			GW	.5	MH	60	60	
8.78	GRANITE	2	2																NUMEROUS SEALED CHLOR FR 9.00-9.30
9.09	GRANITE	1	1	1		2	HU	KC	G	1	S			G	1	S	155	10	
9.91	GRANITE	1	1	2		2	HU	K	G	1	S			G	1	S	300	55	
10.10	GRAN/PEG																		NO FRACTURE
10.61	PEGHATITE	1	1	2		3	HU	KC	GW	.5	MH			GW	.5	MH	260	25	
10.63	PEG/GRAN																		
11.32	GRANITE	2	2																
11.48	GRANITE	3		1		2	SW	C	W	.5	MH			W	.5	MH	240	55	
11.85	GRANITE	1	1	1		2	HU	K	G	.5	MH			G	.5	MH	105	45	
12.34	GRANITE	1	1	2		2	HU	K	G	.5	MH			G	.5	MH	80	40	
12.40	GRANITE	1	1	1		2	HU	KC	GW	.5	MH			GW	.5	MH	85	45	
12.45	GRANITE	1	1	1		3	HU	K	G	.5	MH			G	.5	MH	85	60	
12.49	GRANITE	1	1	1		2	HU	K	G	.5	MH			G	.5	MH	90	55	SHEARED
12.54	GRANITE	1	1	1		3	HU	K	G	.5	S			G	.5	S	75	50	
12.79	GRANITE	1	1	1		3	SW	C	W	.5	MH			W	.5	MH	55	30	
12.96	GRANITE	1	1	1		2	HU	K	G	.5	S			G	.5	S	175	50	
13.41	GRANITE	1	1	2		3	HU	KC	GW	.5	MH			GW	.5	MH	70	50	
13.45	GRANITE	1	1	1		1	HU	KC	GW	.5	S			GW	.5	S	70	55	SHEARED
13.62	GRANITE	1	1	1		3	HU	KC	GW	.5	MH			GW	.5	MH	45	55	
13.67	GRANITE	1	1	1		2	HU	KC	GW	1	MH			GW	1	MH	55	60	
14.03	GRAN/PEG	1	1	1		4	SW	K	G	.5	MH			G	.5	MH	205	35	

E3		DISCONTINUITIES AND BREAKS					MINERALIZATION				ORIENTATION		REMARKS				
		SURFACE CHARACTERISTICS					TYPE	COLOR	THICKNESS (MM)	HARDNESS	BETA (DEG)	ALPHA (DEG)					
DEPTH (M)	ROCK TYPE	1-NATURAL	2-INDUCED	3-UNCERTAIN	1-OPEN	2-CLOSED							3-OTHER	1-PLANNED	2-CURVED	3-IRREGULAR	ROUGHNESS (MM)
.05	GRANITE		2														
.20	GRANITE		1			1		2			2	HU	K	G	.5	MH	85 70
.51	GRANITE		1			1		1			2	HU	K	G	1	MH	315 55
.54	GRANITE		1			1		1			2	HU	KC	GW	.5	MH	295 25
.58	GRANITE		1			1		1			2	HU	KC	GU	.5	S	285 20
1.20	GRANITE		1			1		1			3	HU	KC	GU	.5	S	310 45
1.30	GRANITE		1			1		1			2	HU	KC	GU	.5	S	290 45
1.44	GRANITE		2														INDUCED
1.53	GRANITE		1			1		1			2	HU	KC	GU	.5	S	340 40
1.97	GRANITE		1			1		1			1	SU	KC	BU	.5	S	40 60
2.40	GRANITE		3					3			1	HU			.5		150 60
3.12	GRANITE		1			1		1			1	HU	C	U	.5		20 65
3.47	GRANITE		1			1		1			2	HU	K	G	.5	S	300 30
3.73	GRANITE		1			1		3			1	HU	K	G	.5	S	300 20
3.81	GRANITE		1			1		1			2	HU	K	G	.5	S	310 30
3.90	GRANITE		2			2											
4.86	GRANITE		1			1		1			1	HU	KC	GU	1	MH	305 50
5.15	GRANITE		2														SHEARED
5.19	GRANITE		1			1		2			2	HU	KC	GU	.5	MH	125 65
5.39	GRANITE		1			1		1			2	HU	KC	GU	.5	S	75 45
5.76	GRANITE		1			1		1			3	HU	KC	GU	.5	S	160 70
5.92	GRANITE		1			1		1			1	HU	K	G	.5	S	165 75
6.06	GRANITE		1			1		1			2	HU	KC	GU	.5	MH	310 35
6.06	GRANITE		1			1		1			3	SU	K	G	.5	MH	205 40
6.20	GRANITE		2			2											THROUGH 1/2 OF CORE UPTAKE DEPTH 6.30
6.32	GRANITE		1			1		3			2	SU	KC	GU	.5	MH	45 45
6.33	GRANITE		1			1		1			2	HU	K	G	.5	MH	60 40
6.49	GRANITE		1			1		1			3	HU	KC	GU	.5	S	300 30
6.65	GRANITE		1			1		1			1	HU	KC	GU	.5	MH	75 40
6.85	GRANITE		1			1		1			2	HU	KC	GU	.5	S	85 40
6.87	GRANITE		1			1		1			3	HU	K	G	.5	MH	115 65
6.87	GRANITE		2			2											SUBPARALLEL TO CORE
6.93	GRANITE		1			1		1			2	SU	K	G	.5	MH	125 75
7.09	GRANITE		1			1		1			2	HU	KC	GU	.5	S	305 12
7.09	GRANITE		1			1		1			2	SU	KC	GU	.5	MH	130 70
7.75	GRANITE		1			1		1			1	HU	K	G	.5	MH	100 80
7.72	GRANITE		1			1		1			2	SU	K	G	.5	MH	115 75
7.75	GRANITE		1			1		1			2	HU	KC			MH	300 15
7.86	GRANITE		2			2											
8.40	GRANITE		1			1		3			3	HU	K	G	.5	MH	80 70
8.42	GRANITE		1			1		1			2	HU	KC	GU	.5	S	50 25
8.70	GRANITE		1			1		3			4	SU	C	U	.5	MH	250 20
8.71	GRANITE		1			1		3			3	SU	KC	GU	.5	MH	280 35
8.80	GRANITE		1			1		1			3	HU	KC	GU	.5	MH	100 85
8.80	GRANITE		1			1		1			2	HU	KC	GU	.5	S	315 25
8.85	GRANITE		1			1		1			2	HU	KC	GU	.5	S	50 70
8.97	GRANITE		1			1		1			2	HU	KC	GU	.5	S	155 30
9.18	GRANITE		1			1		1			2	SU	K	G	.5	MH	145 60
9.29	GRANITE		3					1			2	SU	K	G	.5	H	295 80
9.76	GRANITE		1			1		1			3	HU	KC	GU	.5	S	300 25
10.09	GRANITE		1			1		1			2	HU	KC	GU	.5	MH	195 65
10.21	GRANITE		1			1		1			3	HU	KC	GU	.5	S	300 30
10.21	GRANITE		1			1		3			2	HU	K	G	.5	MH	90
10.34	GRANITE		1			1		1			2	SU	K	G	.5	MH	145 80
10.39	GRANITE		1			1		1			2	HU	KC	GU	.5	MH	140 65
10.68	GRANITE		1			1		1			3	HU	KC	GU	1	MH	160 65
11.17	GRANITE		1			1		1			2	HU	KCI	BNGW	.5	MH	190 75
11.40	GRANITE		1			1		2			2	HU	KC	GU	.5	MH	75 45
11.83	GRANITE		1			1		3			3	HU	KCI	BNGW	.5	MH	90 60
11.83	GRANITE		1			1		1			2	HU	K	G	.5	MH	285 55
11.90	GRANITE		1			1		1			3	HU	KC	GU	.5	S	85 45
12.22	GRANITE		1			1		1			3	HU	K	G	.5	S	130 70
12.25	GRANITE		1			1		1			2	HU	KC	GU	.5	S	320 20
12.31	GRANITE		1			1		1			1	HU	K	G	.5	S	160 55
12.35	GRANITE		1			1		1			1	HU	K	G	.5	S	175 15
12.59	GRANITE		1			1		3			2	HU	KC	GU	.5	S	75 50
13.27	GRANITE		1			1		3			2	HU	KCIM	BNGW	.5	S	175 35
13.80	GRANITE		1			1		1			1	SU	KI	BNG	.5	M	90 65
13.94	GRANITE		1			1		3			3	SU	KC	GU	.5	S	185 55
14.01	GRANITE		1			1		3			2	SU	CI	BNGW	.5	S	155 75
14.07	GRANITE		1			1		3			2	HU	K	G	.5	S	305 60
14.67	GRANITE		1			1		1			1	HU	KC	U	.5	S	110 50

E4		DISCONTINUITIES AND BREAKS					MINERALIZATION					ORIENTATION		REMARKS
		CONDITION		SURFACE CHARACTERISTICS			TYPE	COLOR	THICKNESS (MM)	HARDNESS	BETA (DEG)	ALPHA (DEG)		
DEPTH (M)	ROCK TYPE	1-NATURAL	2-UNCERTAIN 2-INDUCED	3-OPEN	3-OTHER 2-CLOSED 1-PLANAR	3-IRREGULAR 2-CURVED							ROUGHNESS (MM)	WEATHERING
.13	GRANITE	1	1	1	1	2	SW	KCS	G	.5	H	55	20	
.75	GRANITE	1	1	1	2	3	NW	K	G		MH	100	80	
.77	GRANITE	1	1	1	2	3	NW	K	G		MH	75	75	SHEARED
.93	GRANITE	1	1	1	1	1	NW	K	G		H	125	30	
1.15	GRANITE	1	1	1	1	1	NW	K	G	.5	S	355	35	MECHANICALLY OPENED
1.50	GRANITE	1	1	1	1	3	NW				H	170	65	
1.94	GRANITE	1	1	1	1	1	SW	K	G	.5	MH	135	30	PARTLY INDUCED
2.16	GRANITE	1	1	1	1	2	SW	K	G	.5	S	140	35	SHEARED
2.66	GRANITE	1	1	1	1	2	SW	KC	G	.5	S	130	55	SHEARED
2.79	GRANITE	1	1	1	1	1	SW	K	G		MH	240	15	APPROX DEPTH
3.37	GRANITE	2												PARTLY INDUCED
3.41	GRANITE	2												CORE LOST 3.37-3.41
3.86	GRANITE	1	1	1	1	3	SW	K	G	.5	S	130	30	CHANGE TO 62MM CORE
4.11	GRANITE	1	1	1	2	2	SW	K	G	.5	S	140	50	SHEARED
4.19	GRANITE	1	1	1	1	3	KC	K	G	1	S	120	40	SHEARED, CURVED
4.74	GRANITE	1	1	1	2	2	SW	KC	GW	2	S	135	40	SHEARED
4.78	GRANITE	1	1	1	1	1	SW	KC	GW	.5	S	120	50	BOTH SHEARED, ONE
4.89	GRANITE	1	1	1	1	1		K	G	.5	H	180	50	OR TWO FRACTURES
5.07	GRANITE	2												IN BETWEEN THESE
5.34	GRANITE	1	1	1	1	3	NW	K	G	.5	S	220	75	
5.57	GRANITE	1	1	1	1	2	NW	KH	W	.5	S	290	70	
5.65	GRANITE	1	1	1	1	2	NW	K	G	.5	S	110	30	SHEARED
5.74	GRANITE	1	1	1	3	3	NW	K	G	.5	S	265	10	
5.80	GRANITE	1	1	1	1	2	SW	K	G	.5	S	340	40	
6.11	GRANITE	1	1	1	3	2	NW	KC	GW	.5	S	115	30	
6.40	GRANITE	1	1	1	1	2	NW	K	G	.5	S	110	30	2 FR, OTHER A=90
6.50	GRANITE	1	1	1	1	1	NW	K	G	.5	S	345	30	PARTLY INDUCED
6.50	GRANITE	1	1	1	3	3	SW	K	G	.5	S	270	80	
6.82	GRANITE	1	1	1	1	2	NW	K	G	.5	S	145	25	PART INDUCED, V-FORM
6.85	GRANITE	1	1	1	1	3	NW	K	G	.5	S	335	40	
6.93	GRANITE	1	1	1	3	2	NW	K	G	.5	S	340	45	
7.32	GRANITE	1	1	1	1	1	NW	K	G	.5	S	150	40	
7.51	GRANITE	1	1	1	3	2	NW	K	G	.5	S	20	85	
7.65	GRANITE	1	1	1	3	2	NW	K	G	.5	S	300	70	
7.87	GRANITE	1	1	1	3	2	NW	K	G	.5	S	270	55	V-FORM
7.24	GRANITE	1	1	1	3	2	NW	K	G	.5	S	280	50	
8.40	GRANITE	1	1	1	1	3	NW	K	G	.5	S	290	60	
9.00	GRANITE	2												
9.08	GRANITE	1	1	1	1	1	NW	K	G	.5	S	300	45	
9.30	GRANITE	1	1	1	1	1	NW	KC	GW	.5	S	280	80	
9.63	GRANITE	1	1	1	3	2	NW	KC	GW	.5	S	100	60	V-FORM
9.73	GRANITE	1	1	1	1	1	NW	K	G	.5	S	300	60	
10.16	GRANITE	1	1	1	2	2	NW	K	G	.5	S	270	70	
10.35	GRANITE	3												
10.72	GRANITE	1	1	1	1	2	NW	K	G	.5	S	280	40	
10.77														3 CM PEGMATITE
11.26	GRANITE	1	1	1	1	3	NW	KC	GW	.5	S	65	20	
11.26	GRANITE	1	1	1	2	2	SW	K	G	.5	S	70	55	
11.62	GRANITE	1	1	1	3	3	S-NW	KC	GW	.5	MH	70	55	PART INDUCED
11.79	GRANITE	1	1	1	1	2	SW	KC	BKG	.5	MH	260	50	SHEARED
12.30	GRANITE	1	1	1	1	2	NW	K	BK	.5	MH	245	65	SHEARED
12.94	GRANITE	1	1	1	1	1	SW	C	G	.5	MH-H	250	60	SHEARED
13.14	GRANITE	1	1	1	1	2	NW	K	BKG	.5	MH	250	70	SHEARED
13.83	GRANITE	1	1	1	1	1	SW	KI	BKBN	.5	MH	280	60	
13.97	GRANITE	1	1	1	3	2	SW	KCI	BK	.5	H	270	50	
14.02	GRANITE	1	1	1	1	3	NW	KI	BKBNW	.5	H-S	275	30	
14.08	GRANITE	1	1	1	3	2	NW	K	BK	.5	MH	290	60	
14.17	GRANITE	1	1	1	3	2	NW	K	BK	.5	MH	310	60	SHEARED
14.24	GRANITE	1	1	1	1	2	NW	K	BK	.5	H	300	65	SHEARED
14.32	GRANITE	1	1	1	3	1	NW	K	BK	.5	MH	280	70	SHEARED (END)

E5		DISCONTINUITIES AND BREAKS					MINERALIZATION					ORIENTATION		REMARKS
DEPTH (M)	ROCK TYPE	CONDITION			SURFACE CHARACTERISTICS		WEATH- ERING	TYPE	COLOR	THICK- NESS (MM)	HARD- NESS	BETA (DEG)	ALPHA (DEG)	
		1-NATURAL	3-UNCERTAIN 2-INDUCED	1-OPEN 2-CLOSED	3-OTHER 1-PLANNED	3-IRREGULAR 2-CURVED 1-PLANAR								
.25	GRANITE	1	1	1	1	HU	K	BKG	.5	MH	50	40		
.31	GRANITE	1	1	1	2	HU	K	BKG	.5	MH	325	75	SULFIDE	
.54	GRANITE	1	1	2	1	HU	K	BKG	.5	MH	50	60		
.56	GRANITE	1	1	1	1	HU	K	BKG	.5	H	255	15		
.57	GRANITE	1	1	1	1	HU	KC	BKW	.5	MH	65	30	PARTLY OPEN	
.86	GRANITE	1	1	2	2	SU	KC	BK	.5	MH	90	50	GRAPHITE FILLING	
.88	GRANITE	1	1	1	1	SU	KC	BK	.5	S-MH	280	25	GRAPHITE	
.98	GRANITE	1	1	2	2	HU	KC	BL	.5	S-MH	310	60	GRAPHITE FILLING	
1.19	GRANITE	1	1	3	1	HU	KC	BK	.5	MH	305	30	GRAPHITE FILLING	
1.40	GRANITE	2												
1.70	GRANITE	2												
2.15	GRANITE	1	1	1	1	HU	KC	BKG U	.5	S-MH	165	30		
2.34	GRANITE	3		3	2	SU	K	BKG	.5	MH	45	55	MOSTLY INDUCED	
2.48	GRANITE	1	1	3	2	SU	K	BKG	.5	MH	180	50		
2.49	GRANITE	1	1	1	1	SU	K	BKG	.5	MH			PARTLY INDUCED	
3.48	GRANITE	1	1	1	1	HU	KC	BKG	.5	S-MH	60	30		
3.62	GRANITE	2												
3.79	GRANITE	1	1	2	2	SU	K	BK	.5	MH	55	55		
3.93	GRANITE	1	1	3	2	HU	I	BN	.5	MH	80	80		
3.98	GRANITE	1	1	1	1	SU	KC	BK	1	MH	55	50		
4.02	GRANITE	1	1	1	1	SU	KC	G	1	MH	60	50		
4.17	GRANITE	1	1	1	1	HU	K	G	1	MH	70	80		
4.34	GRANITE	1	1	1	1	HU	KC	BNW	1	MH	80	55		
4.66	GRANITE	1	1	2	1	HU	KC	GW	.5	MH	80	60		
4.97	GRANITE	1	1	3	1	HU	KC	BKW	1	MH	85	40		
5.03	GRANITE	1	1	1	1	HU	KC	GW	1	MH	70	45	STRIATED	
5.13	GRANITE	2												
5.34	GRANITE	1	1	2	2	HU	KC	BNW	.5	MH	55	60		
5.44	GRANITE	1	1	1	1	HU	KC	GW	.5	MH	80	45	PARTLY INDUCED	
5.53	GRANITE	1	1	3	1	HU	KC	GW	.5	MH	80	40		
5.60	GRANITE	1	1	3	1	HU	K	G	.5	MH	30	75		
5.62	GRANITE	1	1	3	2	HU	K	G	1	MH	100	35		
5.63	GRANITE	1	1	3	2	SU	K	G	.5	MH	240	65	PARTLY IND.	
5.74	GRANITE	1	1	3	2	SU	K	BKG	.5	MH	100	25	PARTLY INDUCED	
6.04	GRANITE	1	1	3	1	HU	K	G	.5	MH				
6.25	GRANITE	1	1	2	1	HU	K	BKG	.5	MH	110	65	HIGHLY FRACT ZONE	
6.45	GRANITE										15		SHEARED	
6.86	GRANITE	1	1	2	2	HU	K	G	.5	MH	80	75		
7.04	GRANITE	1	1	1	1	HU	K	G	.5	MH	80	50		
7.12	GRANITE	1	1	1	2	SU	K	G	.5	MH	245	60	PARTLY INDUCED	
7.34	GRANITE	1	1	1	1	HU	K	G	.5	MH	80	65	SHEAR	
7.41	GRANITE	1	1	1	1	HU	K	G	.5	MH	80	80		
7.71	GRANITE	1	1	1	2	SU	K	G	.5	S	50	45		
7.73	GRANITE	1	1	1	2	HU	K	G	.5	MH	45	65		
7.87	GRANITE	1	1	1	1	HU	KC	GW	.5	MH	60	45		
8.13	GRANITE	1	1	1	1	HU	K	G	.5	MH	50	45		
8.26	GRANITE	2												
8.59	GRANITE	1	1	1	2	HU	KC	GW	.5	MH	40	50		
8.88	GRANITE	1	1	1	2	HU	KC	GW	.5	MH	50	50		
9.16	GRANITE	1	1	2	1	HU	K	G	.5	MH	70	40		
9.19	GRANITE	1	1	2	1	HU	K	G	.5	MH	40	55		
9.22	GRANITE	1	1	2	1	HU	K	G	.5	MH	50	55		
9.27	GRANITE	2												
9.90	GRANITE	1	1	1	2	HU	KC	GW	.5	MH	70	35		
9.90	GRANITE	1	1	2	1	HU	K	G	.5	MH	160	30		
10.09	GRANITE	2												ENDS ROTATED
10.46	GRANITE	2												
10.64	GRANITE	3	3	1	2	SU	E	G	.5	H	150	15	PART INDUCED	
11.02	GRANITE	1	1	3	2	HU	KE C E	GW G	.5	S	235	40		
11.28	GRANITE	1	1	2	2	SU	E	G	.5	H	270	15		
11.80	GRANITE	2	2											
12.80	GRANITE	2	2											
13.19	GRANITE	1	1	2	2	SU	KCEQ	GW	.5	H-MS	160	25		
13.34	GRANITE	1	1	1	2	HU	K	G	.5	S	230	25		
13.45	GRANITE	1	1	2	2	SU	E	G	.5	MH	270	30		
13.46	GRANITE	1	1	3	3	SU	K	G	.5	S	170	40		
13.70	GRANITE	1	1	1	2	HU	KC	GW	.5	S-H	205	35		
13.86	GRANITE	1	1	3	2	HU	KCE	GW	.5	H-S	270	30		
13.96	GRANITE	1	1	3	3	SU	C	U	.5	H	290	40		

H1	DISCONTINUITIES AND BREAKS						MINERALIZATION				ORIENTATION		REMARKS	
	DEPTH (M)	ROCK TYPE	CONDITION			SURFACE CHARACTERISTICS			TYPE	COLOR	THICK- NESS (MM)	HARD- NESS		BETA (DEG)
1-NATURAL			3-UNCERTAIN 2-INDUCED	1-OPEN	3-OTHER 2-CLOSED	1-PLANAR	3-IRREGULAR 2-CURVED	ROUGH- NESS (MM)					WEATH- ERING	
	1.15	GRANITE	1	1	1	3	MW	K	G	.5	MH	265	35	
	2.52	GRANITE	1	1	1	8	SW	C	W	.5	S	80	8	PARTLY INDUCED, WAVY
	3.39	GRANITE	1	1	1	2	MW	KC	GW	1	S	300	22	SHEARED, B=315
	4.21	GRANITE	1	1	2	6	MW	KC	GW	1	S	275	30	PARTLY INDUCED
	4.30	GRANITE	1	1	1	2	MW	KC	GW	1	S	180	5	ONLY ABOUT 5CM OPEN NO MIDPT DEPTH MANY FR, NO ORIENT. BELOW 4.93
	4.53													
	4.53	GRANITE	1	1	1	1	SW	K	G	.5	S		55	
	4.51	GRANITE	2	2										
	4.65	GRANITE	1	1	1	3	MW	K	G	.5	S		30	
	4.84	GRANITE	2	2										
	4.84	GRANITE	1	1	1	1	MW	KCE	GW	.5	S-M		25	
	4.88	GRANITE	1	1	1	1	MW	K	G	.5	S		70	SHEARED
	4.93	GRANITE	1	1	1	2	MW	K	G	.5	S	145	65	
	4.99	GRANITE	1	1	1	2	MW	K	G	.5	S	130	65	SAND IN FRACTURE
	5.09	GRANITE	2											
	5.29	GRANITE	1	1	1	1	MW							
	5.05	GRANITE	2	2										
	5.25	GRANITE	1	1	1	1	MW	KC	GW	.5	S	105	40	B UNCERTAIN
	5.43	GRANITE	1	1	1	2	MW	KC	GW	.5	S	130	40	B UNCERTAIN
	5.49	GRANITE	1	1	1	1	MW	KC	GW	.5	S	135	65	SHEARED, B UNCERTAIN
	5.57	GRANITE	1	1	1	1	MW	KC	GW	.5	S	120	65	B UNCERTAIN
	5.63	GRANITE	1	1	1	2	MW	KC	GW	.5	S	115	80	B UNCERTAIN
	5.94	GRANITE	1	1	3	2	MW	KC	GW	.5	S	150	75	B UNCERTAIN
	5.99	GRANITE	1	1	3	2	MW	KC	GW	.5	S	150	70	B UNCERTAIN
	6.07	GRANITE	1	1	1	2	SW	K	G	.5	S	105	40	B UNCERTAIN
	6.10	GRANITE	1	1	2	2	SW	K	G	.5	S	315	35	B UNCERTAIN
	6.13	GRANITE	1	1	1	3	SW	K	G	.5	S	145	75	PART INDUCED
	6.50	GRANITE	1	1	1	1	MW	K	G	.5	S	95	43	B UNCERTAIN
	6.51	GRANITE	1	1	2	2	SW	K	G	.5	S	295	45	B UNCERTAIN
	6.59	GRANITE	1	1	1	1	SW	K	G	.5	S	300	33	B UNCERTAIN
	6.62	GRANITE	1	1	1	2	SW	K	G	.5	S	85	55	B UNCERTAIN
	6.69	GRANITE	1	1	1	1	MW	K	G	.5	S	85	48	B UNCERTAIN
	7.21	GRANITE	1	1	2	1	MW	K	G	1	S	325	30	B UNCERTAIN
	7.31	GRANITE	1	1	3	1	MW	KC	GW	.5	S	320	30	B UNCERTAIN
	7.35	GRANITE	1	1	2	1	MW	K	G	.5	S	85	15	B UNCERTAIN
	7.38	GRANITE	1	1	1	1	MW	KC	GW	.5	S	320	30	SHEARED, B UNCERTAIN
	7.57	GRANITE	1	1	1	3	SW	K	G	.5	S	130	75	
	7.63	GRANITE	1	1	3	1	MW	K	G	.5	S	325	33	
	7.84	GRANITE	1	1	1	1	MW	KC	GW	.5	S	95	50	
	7.93	GRANITE	1	1	1	2	MW	KC	GW	.5	S	320	30	SHEARED
	8.08	GRANITE	1	1	1	1	MW	K	G	.5	S	315	40	SHEARED
	8.23	GRANITE	1	1	1	1	MW	K	G	.5	S	0	85	B UNCERTAIN
	8.23	GRANITE	1	1	1	2	MW	KC	GW	1	S	305	40	B UNCERTAIN
	8.29	GRANITE	1	1	2	1	MW	KC	GW	1	S	310	35	SHEARED, B UNCERTAIN
	8.29	GRANITE	1	1	1	1	MW	KC	GW	.5	S	330	10	B UNCERTAIN
	8.59	GRANITE	1	1	1	1	MW	KC	GW	.5	S-M	90	50	B UNCERTAIN
	8.75	GRANITE	1	1	3	3	MW	KC	GW	.5	S	310	33	B UNCERTAIN
	8.72	GRANITE	1	1	3	2	SW	KC	GW	.5	M	95	50	
	9.20	GRANITE	1	1	1	2	SW	KC	GW	.5	M	100	63	
														RUBBLE 9.2-9.54; A=10-15 AND A=40-70 RUBBLE 9.54-9.85; A=20-40 AND A=60-80
	9.85	GRANITE	1	1	3	2	SW	KC	GW	.5	M	330	15	
	9.85	GRANITE	1	1	3	2	SW	K	G	.5	S	170	45	
	10.15	GRANITE	1	1	1	2	MW	K	GW	.5	S	150	65	
	10.35	GRANITE	1	1	1	3	MW	KC	GW	.5	S	225	55	
	10.39	GRANITE	1	1	3	3	SW	KC	GW	.5	S	160	85	
	10.63	GRANITE	1	1	1	2	MW	KCE	GW	1	S	300	30	
	10.94	GRANITE	1	1	2	2	MW	KC	GW	.5	M	175	22	
	11.11	GRANITE	1	1	3	3	SW	KCE	GW	.5	M	155	50	
	11.15	GRANITE	1	1	2	2	SW	K	G	.5	S	75	40	
	11.20	GRANITE	1	1	3	2	MW	KE	W	.5	S	145	65	

H4		DISCONTINUITIES AND BREAKS					MINERALIZATION				ORIENTATION		REMARKS						
		CONDITION			SURFACE CHARACTERISTICS		TYPE	COLOR	THICKNESS (MM)	HARDNESS	BETA (DEG)	ALPHA (DEG)							
DEPTH (M)	ROCK TYPE	1-NATURAL	2-INDUCED	3-UNCERTAIN	1-OPEN	3-OTHER							1-PLANAR	2-CURVED	3-IRREGULAR	ROUGHNESS (MM)	WEATHERING		
0.		3																	
.06	GRANITE	3								3	SW	C	W	.5	MH	215	60		
.15	GRANITE	1	1							2	S-MW	KC	BKGW	.5	MH	85	65	SHEARED B=135	
.36	GRANITE	1	1							1	MW	KC	BKW	.5	MH	105	35	PARTLY INDUCED	
1.05	GRANITE	2																	
1.18	GRANITE	1	1							2	MW	KC	GW	.5	MH	305	15	PARTLY INDUCED	
1.58	GRANITE	1	1							3	MW	K	BKG	.5	MH	185	45	PARTLY INDUCED	
1.75	GRANITE	2																	
1.92	GRANITE	2																	
2.34	GRANITE	1	1							2	MW	KC	BKW	.5	MH	155	80	PARTLY INDUCED	
3.14	GRANITE	2																	
3.25	GRANITE	2																	
3.46	GRANITE	2																	
3.95	GRANITE	1	1							1	SW	KC	BKW	.5	MH	100	45		
4.22	GRANITE	1	1							1	MW	KCIM	BKWY	3	S-MH	265	20	SHEARED B=0	
4.37	GRANITE	1	1							3	MW	KC	BKGW	1	MH	335	70		
4.69	GRANITE	2																	
4.89	GRANITE	1	1							1	MW	K	BK	10	S-MH	290	25	SHEARED FR. ZONE 4.69-4.89	
5.21	GRANITE	1	1							3	SW	KC	BKW	.5	MH	345	70		
5.56	GRANITE	1	1							1	SW	KC	BKG	.5	MH	310	85	SHEARED B=170	
5.97	GRANITE	1	1							2	SW	KC	BKG	.5	MH	50	80	SHEARED B=150	
6.30	GRANITE	1	1							2	SW	K	BKG	.5	MH	220	50	PART INDUCED	
6.28	GRANITE	2																	
6.40	GRANITE	1	1							1	SW	K	BKG	.5	MH	15	13	SHEARED, PART INDUCED	
6.64	GRANITE	1	1							3	SW	KC	BKGW	.5	MH	25	80	SHEARED B=170	
6.72	GRANITE	1	1							3	SW	KC	BKWB	.5	MH	75	78	SHEARED	
6.81	GRANITE	1	1							1	MW	KC	GW	1	MH	290	22		
7.13	GRANITE	2														80	88		
7.23	GRANITE	1	1							1	MW	KC	G	.5	MH	300	30		
7.47	GRANITE	1	1							2	SW	KC	BKG	.5	MH	10	85	SHEARED B=160	
7.51	GRANITE	1	1							2	SW	K	BKG	.5	MH	270	25		
8.23	GRANITE	1	1							3	SW	KCM	BKG	.5	MH	195	80		
8.50	GRANITE	1	1							2	SW	K	BKG	.5	MH	320	70	PART INDUCED	
8.82	GRANITE	1	1							2	SW	K	BKG	.5	MH	330	35	SHEARED B=120	
9.12	GRANITE	1	1							1	SW	K	BKG	.5	MH	240	12		
9.32	GRANITE	1	1							2	MW	CE	BKWB	3	MH-H	215	33		
9.59	GRANITE	1	1							2	SW	KC	GW	.5	MH	210	55		
9.95	GRANITE	1	1							2	MW	KC	GW	1	MH	285	22		
10.21	GRANITE	1	1							2	SW	KC	GW	.5	MH	300	15	PARTLY CLOSED	

H5		DISCONTINUITIES AND BREAKS					MINERALIZATION				ORIENTATION		REMARKS			
		CONDITION		SURFACE CHARACTERISTICS			TYPE	COLOR	THICKNESS (MM)	HARDNESS	BETA (DEG)	ALPHA (DEG)				
DEPTH (M)	ROCK TYPE	1-NATURAL	2-INDUCED	3-UNCERTAIN	1-OPEN	2-CLOSED							3-OTHER	1-PLANAR	2-CURVED	3-IRREGULAR
.04	GRANITE	1			1	2	SW	KC	BKW	.5	MH	80	55			
.15	GRANITE	2														
.30	GRANITE	1	1		1	1	NW	KC	BKW	.5	S-MH	30	75			
.75	GRANITE	2														
1.39	GRANITE	1	1		2	2	NW	K	BKG	.5	MH	290	25	PARTLY INDUCED		
1.39	GRANITE	1	1		1	3	NW	KC	BKGW	.5	MH	325	30	PARTLY INDUCED		
1.78	GRANITE	1	1		2	3	NW	KC	BKGW	.5	MH	95	55			
1.89	GRANITE	1	1		1	2	NW	KC	BKGW	.5	MH	250	60	PARTLY INDUCED		
1.90	GRANITE	1	1		1	3	NW	K	G	.5	MH	50	15			
1.97	GRANITE	1	1		1	1	NW	K	G	.5	MH	325	15	PARTLY, INDUCED		
2.24	GRANITE	1	1		1	2	NW	KC	GW	.5	MH	320	25			
2.43	GRANITE	1	1		1	1	NW	KM	G	.5	MH	245	25	PARTLY INDUCED		
2.45	GRANITE	2														
2.76	GRANITE	1	1		1	2	NW	KC	GW	.5	MH	350	25	PARTLY INDUCED		
2.76	GRANITE	1	1		1	1	NW	K	G	.5	MH	310	20	PARTLY INDUCED		
3.55	GRANITE	2			1	3	NW	KC	BKGW	.5	MH	70	70			
3.75	GRANITE	2														
4.24	GRANITE	1	1		3	2	NW	KM	BW	.5	MH	270	15			
4.27	GRANITE	1	2							25		245	30	SEALED FRACTURE		
4.32	GRANITE	1	1		1	1	SW	C	W	.5	MH	65	20			
4.71	GRANITE	1	1		3	2	SW	KC	BKW	.5	MH	105	70			
4.89	GRANITE	2														
5.02	GRANITE	1	1		1	1	NW	KC	BKW	.5	MH	70	20	MOSTLY SEALED		
5.28	GRANITE	1	2							1		280	10	SEALED FRACTURE		
5.39	GRANITE	1	1		2	2	NW	KC	BKW	.5	MH	75	50	PARTLY SEALED		
6.28	GRANITE	1	1		1	2	SW	K	BK	.5	MH	275	70			
6.82	GRANITE	1	1		1	1	NW	K	BKG	1	MH	315	35	SHEARED		
6.87	GRANITE	1	1		1	1	NW	K	BKG	.5	MH	310	45	SHEARED B=315		
7.06	GRANITE	1	1		3	2	S-NW	K	BK	.5	MH	240	60			
7.24	GRANITE	1	1		2	2	SW	KC	BKGW	.5	MH	90	60			
7.26	GRANITE	1	1		1	1	SW	KC	BKW	.5	MH	315	30			
7.30	GRANITE	1	1		1	2	SW	KC	BKW	.5	MH	170	45	B=DR-20 DEG TO 7.69		
7.38	GRANITE	1	1		1	2	SW	KC	BKW	.5	MH	100	45			
7.38	GRANITE	1	1		1	1	S-NW	K	GW	.5	MH	200	35	SHEARED		
7.48	GRANITE	1	1		1	1	NW	K	BK	.5	MH	105	50			
7.66	GRANITE	1	1		3	2	NW	KC	BKW	.5	MH	335	85			
7.76	GRANITE	1	1		1	1	SW	K	BK	.5	MH	45	30	B=DR-20 DEG TO 8.15		
7.79	GRANITE	1	1		1	1	NW	K	BK	.5	MH	80	45			
7.90	GRANITE	1	1		1	1	SW	K	BK	.5	MH	150	60			
7.90	GRANITE	1	1		3		N-NW	KE	BKG	1	H			PARTLY INDUCED		
8.04	GRANITE	1	1		1	1	SW	K	BK	.5	MH	160	70	PARTLY INDUCED		
8.05	GRANITE	1	1		1	1	NW	KC	BKW	.5	MH	305	30	PARTLY INDUCED		
8.24	GRANITE	1	1		1	2	NW	KC	BKGW	.5	MH	305	80	8.15-8.24 CORE LOST		
8.25	GRANITE	1	1		1	2	NW	K	BKW	.5	MH	65	30	PARTLY INDUCED		
8.53	GRANITE	1	1		1	2	NW	KC	BKGW	.5	MH	300	29	SHEARED		
8.56	GRANITE	1	1		1	1	NW	KC	BKW	.5	MH	70	20	SHEARED		
8.75	GRANITE	1	1		1	2	NW	K	BKG	.5	MH	120	70			
9.09	GRANITE	1	1		1	3	NW	KC	BKGW	.5	MH	315	25	SHEARED		
9.14	GRANITE	1	1		1	3	NW	KC	BKGW	.5	MH	70	30			
9.16	GRANITE	1	1		2	3	NW	KC	BKGW	.5	MH	310	30	SHEARED		
9.32	GRANITE	1	1		1	3	NW	KC	BKGW	.5	MH	295	30			
9.84	GRANITE	1	1		1	3	NW	K	BKG	.5	MH	190	75	PARTLY INDUCED		
11.66	GRANITE	1	1		1	1	NW	K	BKG	.5	MH	105	45	UNCERTAIN ORIENT.		

H6		DISCONTINUITIES AND BREAKS					MINERALIZATION				ORIENTATION		REMARKS
DEPTH (M)	ROCK TYPE	SURFACE CHARACTERISTICS					TYPE	COLOR	THICK- NESS (MM)	HARD- NESS	BETA (DEG)	ALPHA (DEG)	
		1-INDUCED 2-UNCERTAIN 3-NATURAL	1-OPEN 2-CLOSED 3-OTHER	1-PLANAR 2-CURVED 3-IRREGULAR	ROUGH- NESS (MM)	WEATH- ERING							
.10	GRANITE	1	1	3	1	HW	K	G	1	S	55	65	1/2 OPENED BY HAND SHEARED
.29	GRANITE	1	1	1	2	HW	K	G	.5	S	40	70	
.34	GRANITE	1	1	1	1	HW	K	G	.5	S	335	55	PARTLY INDUCED
.52	GRANITE	1	1	1	1	HW	K	G	.5	S	335	55	
.69	GRANITE	1	1	1	2	HW	K	G	.5	S	10	70	
.77	GRANITE	1	1	1	1	HW	KC	GW	1	S		78	
1.08	GRANITE	1	1	2	1	HW	K	G	.5	S		80	
1.18	GRANITE	1	1	1	1	HW	K	G	.5	S		87	
1.41	GRANITE	1	1	1	1	HW	KC	GW	.5	S		85	
1.58	GRANITE	1	1	3	1	HW	KC	GW	.5	S		75	
1.64	GRANITE	1	1	3	1	HW	KC	GW	.5	S		75	
2.24	GRANITE	1	1	1	2	HW	K	G	.5	S		60	
2.48	GRANITE	1	1	3	1	HW	KC	GW	.5	S		65	
2.97	GRANITE	1	1	2	1	HW	K	G	.5	S		50	
2.24	GRANITE	1	1	1	2	HW	K	G	.5	S		60	
2.48	GRANITE	1	1	3	1	HW	KC	GW	.5	S		65	
2.97	GRANITE	1	1	2	1	HW	K	G	.5	S		50	
3.18	GRANITE	1	1	3	1	HW	KC	GW	.5	S		65	
4.15	GRANITE	1	1	3	1	HW	KC	GW	.5	S			
4.38	GRANITE	1	1	1	1	HW	KC	BKG	2	MH	90	55	SHEARED
4.50	GRANITE	1	1	3	2	HW	KCF	BKG	1	MH	60	80	SHEARED
4.51	GRANITE	1	1	3	2	HW	KC	BW			190	40	2 SHEARED FR. B1=60 A1=80;B2=190,A2=40
4.65	GRANITE	1	1	1	2	S-HW	KC	BKGW	1	MH	100	60	SHEARED
4.72	GRANITE	1	1	2	2	HW	KC	BKGW	1	MH	90	80	SHEARED
5.19	GRANITE	1	1	2	2	HW	KC	BKG	1	MH	120	55	
5.30	GRANITE	1	1	1	1	HW	KC	BKBNG	2	MH	100	65	
5.51	GRANITE												FR.ZONE 5.51-.77
5.77	GRANITE	2											
6.09	GRANITE	2											RUBBLE TO 6.2
6.25	GRANITE	1	1	1	2	HW	KC	BKG	.5	MH	120	80	
6.61	GRANITE	1	1	1	1	HW	KC	G	2	MH	65	80	
6.92	GRANITE	1	1	2	1	HW	K	G	1	MH	0	85	SHEARED,PART INDUCE
7.04	GRANITE	1	1	1	1	HW	KC	GW	3	MH	170	27	
7.16	GRANITE	1	1	1	1	HW	K	G	.5	MH	265	70	PARTLY INDUCED
7.48	GRANITE	1											PERCUS.HOLE IN CORE
7.55	GRANITE	1	1	3	2	SW	KC	BKG	.5	MH	150	32	
7.61	GRANITE	1	1	1	1	SW	KC	GW	.5	MH	95	15	
7.66	GRANITE	1	1	1	2	SW	KC	BKGW	.5	MH	295	50	
8.12	GRANITE	1	1	1	3	HW	KC	BKGW	1	MH	35	75	
8.19	GRANITE	1	1	1	2	SW	KC	BKGW	.5		270	9	
8.36	GRANITE	1	1	2	2	SW	KC	GW	.5	MH	210	75	
8.54	GRANITE	1	2				C		20				WEATHERED CALCITE
8.68	GRANITE	1	2				C		20				WEATHERED CALCITE
8.69	GRANITE	1	1	1	2	SW	KCEF	BKBG	.5	MH-H	25	85	SHEARED SEVERAL WEATHERED CALCITE FRACTURES
9.10	GRANITE	1	1	1	1	HW	KC	GW	1	MH	10	65	
9.32	GRANITE	1	1	1	1	HW	K	G	1	MH	195	45	
9.90	GRANITE	2											9.70-9.90 SEVERAL EPIDOTE-SEALED FRAC
9.99	GRANITE	1	1	1	2	SW	CI	W	.5	MH	00	80	
10.10	GRANITE	2											
10.20	GRANITE	1	1	3	2	SW	K	BK	.5	MH	170	50	
10.49	GRANITE	2											
10.69	GRANITE	1	1	1	1	SW	KC	BKG	.5	MH	195	40	

H7		DISCONTINUITIES AND BREAKS						MINERALIZATION				ORIENTATION		REMARKS		
		SURFACE CHARACTERISTICS						TYPE	COLOR	THICKNESS (MM)	HARDNESS	BETA (DEG)	ALPHA (DEG)			
DEPTH (M)	ROCK TYPE	1-NATURAL	2-INDUCED	3-UNCERTAIN 1-OPEN	2-CLOSED	3-OTHER 1-PLANAR	2-CURVED							3-IRREGULAR	ROUGHNESS (MM)	WEATHERING
0.	GRANITE		2												0.00 - .15 RUBBLE	
.15	GRANITE		1		1	3	2	2	SW	K	B	.5	MH	280	22	
.40	GRANITE		1		1	3	2	2	MW	K	B	.5	MH	260	80	
.49	GRANITE		1		1	3	3	3	MW	K	BKG	.5	MH	150	60	
.54	GRANITE		1		1	2	1	1	MW	E	G	1	H	140	45	
.79	GRANITE		1		1	3	3	3	SW	K	BG	.5	MH	150	75	PART INDUCED
1.08	GRANITE		1		1	1	1	1	SW	K	BKG	.5	MH	175	80	ROTATED
1.24	GRANITE		3			1	2	2	SW	K	BKG	.5	MH	305	75	PART INDUCED
1.43	GRANITE					2	2	2	S-MW	KF	BKKG	1	MH	215	75	
1.61	GRANITE		1		1	3	3	3	SW	K	BKG	.5	MH	220	70	PARTLY INDUCED
1.87	GRANITE		2											215	75	
1.90	GRANITE		2											245	80	
2.13	GRANITE		2													
2.15	GRANITE		2													ROTATED
2.18	GRANITE		1		1	1	1	1	SW	KC	BKG	.5	MH	35	70	ROTATED
2.20	GRANITE		1		2	1				C	W	.5	MH	315	35	
2.40	GRANITE		1		1	1	1	1	SW	K	G	.5	MH	300	43	PARTLY INDUCED
2.58	GRANITE		1		1	1	1	1	MW	K	G	.5	MH	285	15	
2.99	GRANITE															HIGHLY FRACT ZONE
2.80	GRANITE		1		1	1	2	2	SW	K	BKG	.5	MH	290	18	
3.18	GRANITE		1		1	1	1	1	SW	K	BKG	.5	MH	125	80	2.99-3.18 RUBBLE
3.36	GRANITE		1		1	1	1	1	MW	KC	BKKG	.5	MH	120	65	ROTATED, SH.B=150
3.94	GRANITE		1		1	1	1	1	MW	KCF	BKBNG	.5	MH	110	70	SHEARED B=135
4.11	GRANITE		1		1	3	2	2	SW	KC	BKW	.5	MH	170	55	NO LOG 3.51 T03.94
4.34	GRANITE		1		1	2	1	1	SW	KC	GW	.5	MH	95	65	SHEARED B=140
4.48	GRANITE		1		1	1	2	2	MW	KC	GBKW	.5	MH	130	70	ROTATED
4.65	GRANITE		1		1	3	3	3	SW	KC	GBKW	.5	MH	230	75	ROTATED, SH.B=130
4.67	GRANITE		1		1	1	1	1	MW	KC	GW	.5	MH	95	70	SHEARED B=145
4.85	GRANITE		1		1	1	1	1	MW	KC	GBKW	.5	MH	115	70	SHEARED B=140
4.93	GRANITE		1		1	1	1	1	SW	K	BKG	.5	MH	155	80	SHEARED B=140
5.10	GRANITE		1		1	1	2	2	SW	K	G	.5	MH	110	75	
5.15	GRANITE		1		1	1	2	2	SW	K	BKG	.5	MH	185	85	
5.41	GRANITE		1		1	1	1	1	MW	KC	GBKW	.5	MH	315	20	ROTATED
5.68	GRANITE		1		1	1	3	3	SW	K	BK	.5	MH	280	55	
5.87	GRANITE		1		1	3	2	2	S-MW	KC	BKG	.5	MH	340	70	
5.92	GRANITE		1		1	1	1	1	MW	KC	GBKW	.5	MH	100	45	
6.07	GRANITE		1		1	1				K	BK	2	MH	350	25	
6.11	GRANITE		1		1	2	1	1	MW	K	BKG	.5	MH	250	70	ROTATED
6.22	GRANITE		1		1	1	1	1	SW	K	BKG	.5	MH	220	18	
6.31	GRANITE		1		1	1	1	1	MW	KC	GBKW	.5	MH	105	45	
6.50	GRANITE		1		1	1	1	1	SW	KE	BKG	.5	MH-H	320	22	
6.67	GRANITE		2													
7.01	GRANITE		1		1	1	2	2	SW	KC	BKGW	.5	MH	310	35	
7.24	GRANITE		1		1	1	1	1	MW	KC	BKGW	.5	MH	315	17	SAME FRACTURE
7.39	GRANITE		1		1	1	1	1	MW	KC	BKGW	.5	MH	315	17	SAME FRACTURE
7.54	GRANITE		1		1	1	1	1	MW	KC	BKW	.5	MH	105	45	FR. ZONE TO 7.78
7.78	GRANITE		1		1	1	1	1	MW	KC	BKGW	.5	MH	150	10	
8.07	GRANITE		2													
8.30	GRANITE		1		1	1	1	1	SW	KC	BKGW	.5	MH-H	315	25	
8.97	GRANITE		1		2					KE				305	20	SEALED
9.05	GRANITE		1		1	2	1	1	MW	KE	BKGW	.5	MH	315	23	PARTLY INDUCED
9.49	GRANITE		1		1	1	2	2	MW	KC	BKW	.5	MH	135	65	PART SHEARED B=330
9.54	GRANITE		1		1	1	1	1	MW	KC	BKW	.5	MH	260	53	
10.10	GRANITE		1		1	1	1	1	MW	KC	BKW	.5	MH	105	55	SHEARED ANGLE=310
10.20	GRANITE		1		1	1	1	1	SW	KE	BKG	.5	MH-H	305	30	
10.23	GRANITE		1		1	1	2	2	SW	K	BK	.5	H	115	35	
10.32	GRANITE		1		1	1	1	1	SW	KCE	BKGW	.5	MH-H	300	30	FR. ZONE TO 10.49
10.49	GRANITE		2													CORE ROTATED
10.74	GRANITE		1		1	1	2	2	MW	KCE	BKUG	.5	MH-H	125	60	
10.83	GRANITE		1		1	1	1	1	MW	K	BKG	.5	MH-S	315	30	
10.95	GRANITE		1		1	1	1	1	SW	K	BK	.5	MH-H	100	55	PARTLY INDUCED
11.03	GRANITE		1		1	1	1	1	SW	K	BKG	.5	MH-H	315	25	
11.12	GRANITE		1		1	1	1	1	MW	K	BKG	.5	MH-S	315	27	SHEARED ANGLE=320

M1		DISCONTINUITIES AND BREAKS					MINERALIZATION				ORIENTATION		REMARKS					
		CONDITION		SURFACE CHARACTERISTICS			TYPE	COLOR	THICKNESS (MM)	HARDNESS	BETA (DEG)	ALPHA (DEG)						
DEPTH (M)	ROCK TYPE	1-NATURAL	2-INDUCED	3-UNCERTAIN	1-OPEN	2-CLOSED							3-OTHER	1-PLANNAR	2-CURVED	3-IRREGULAR	ROUGHNESS (MM)	WEATHERING
.01	GRANITE	2	2															
.09	GRANITE	2	2															
.41	GRANITE	2	2															
1.02	GRANITE	1	1			1	3	SU	K	G	.5	S	200	80				
1.46	GRANITE	2	2															
2.28	GRANITE	2	2															
2.89	GRANITE	1	1			1	1	MU	KC	GW	.5	S	155	30				
3.05	GRANITE	1	1			1	2	SU	KH	GW	.5	S	65	50				
3.31	GRANITE	1	1			1	2	MU	K	G	.5	S	280	85				
3.64	GRANITE	1	1			3	3	SU	K	G	.5	S	150	55				
3.76	GRANITE	1	1			1	1	SU	K	G	.5	S	130	45				
3.80	GRANITE	1	1			2	1	MU	KCE	GW	.5	MS	275	20				
4.45	GRANITE	1	1			1	1	SU	K	G	.5	S	275	25			SHEARED	
4.63	GRANITE	1	1			1	1	MU	KC	GW	.5	M	210	35				
4.82	GRANITE	1	1			2	2	SU	C	U	.5	H	20	65				
4.96	GRANITE	1	1			1	3	SU	KC	GW	.5	S	70	75				
4.98	GRANITE	1	1			3	2	SU	KC	GW	.5	M	80	50				
5.30	GRANITE	1	1			1	3	SU	K	G	.5	S	95	70				
5.53	GRANITE	1	1			3	1	MU	KC	GW	.5	S	75	55			SHEARED	
5.76	GRANITE	1	1			1	2	MU	KC	GW	.5	S-M	285	15				
5.94	GRANITE	2	2															
6.55	GRANITE	1	1			1	2	MU	KE	G	.5	M	200	40				
6.58	GRANITE	1	1			3	2	SU	K	G	.5	S	210	70				
6.70	GRANITE	1	1			1	2	MU	KE	G	.5	M	280	10				
6.78	GRANITE	1	1			3	3	CE	CE	GW	.5	M	260	60				
6.89	GRANITE	3	3			3	1	MU	E	G	.5	H	345	75			PARTLY INDUCED	
6.98	GRANITE	1	1			1	1	MU	KC	GW	.5	S-H	75	60				
6.98	GRANITE	1	1			1	1	MU	KE	G	.5	S-H	270	15				
7.81	GRANITE	1	1			1	2	MU	KC	GW	.5	S	95	65				
7.84	GRANITE	1	1			1	3	MU	K	G	.5	S	285	65				
8.19	GRANITE	1	1			3	2	MU	K	G	.5	MH	275	25				
8.28	GRANITE	1	1			1	2	MU	K	G	.5	S	85	55			SHEARED	
8.50	GRANITE	1	1			2	2	MU	K	G	.5	S	60	45				
8.79	GRANITE	1	1			1	1	MU	KC	GW	.5	MH	75	55			SHEARED	
9.00	GRANITE	1	1			1	2	MU	KC	GW	.5	S	105	75				
9.07	GRANITE	1	1			3	2	MU	KCF	GW	.5	MH	75	60				
9.21	GRANITE	1	1			1	2	MU	C	U	.5	MH	55	65			ONLY THRU 1/2 CORE	
9.25	GRANITE	1	1			1	2	SU	K	G	.5	S	15	65				
9.29	GRANITE	1	1			1	1	MU	KC	GW	.5	S	280	20				
10.26	GRANITE	1	1			1	2	MU	K	G	.5	MH	190	50			PARTLY INDUCED	
10.46	GRANITE	1	1			1	2	MU	C	U	.5	MH	60	35				
10.50	GRANITE	1	1			1	1	MU	K	G	.5	MH	170	60			SHEARED	
10.59	GRANITE	1	1			1	1	MU	K	G	.5	MH	160	50				
10.78	GRANITE	1	1			1	1	MU	KC	GW	.5	MH	90	55				
10.82	GRANITE	1	1			2	2	SU	K	U	.5	MH	260	15				
11.13	GRANITE	1	1			1	1	MU	K	G	.5	MH	160	40				
11.25	GRANITE	2																
11.31	GRANITE	1	1			1	1	MU	KC	GW	.5	MH	90	55			SHEARED	
11.58	GRANITE	1	1			1	2	SU	C	U	.5	MH	240	35				
11.74	GRANITE	1	1			1	1	MU	K	G	.5	MH	60	30				
11.88	GRANITE	1	1			2	2	SU	C	U	.5	MH	240	25			PARTLY INDUCED	
12.06	GRANITE	1	1			1	2	MU	KC	GW	.5	MH	300	25				
12.21	GRANITE	1	1			2	2	MU	KCN	GW	.5	MH	300	20				
12.33	GRANITE	1	1			1	1	MU	K	G	.5	MH	150	35				
12.37	GRANITE	1	1			1	1	MU	K	G	.5	MH	60	45				
12.69	GRANITE	1	1			1	1	MU	KC	GW	.5	MH	60	45				
13.12	GRANITE	1	1			1	2	MU	KC	GW	.5	MH	230	20				
13.23	GRANITE	1	1			1	3	MU	K	G	.5	MH	180	50				
13.29	GRANITE	1	1			1	2	MU	KC	GW	.5	MH	180	45				
13.31	GRANITE	1	1			3	1	MU	KC	GW	.5	MH	310	20				
13.45	GRANITE	3	3			1	1	MU	K	G	.5	MH	160	45				
13.64	GRANITE	1	1			1	1	MU	KC	GW	.5	MH	40	45				
13.69	GRANITE	1	1			3	3	SU	K	G	.5	MH	165	60				
14.00	GRANITE	1	1			1	1	MU	KC	GW	.5	MH	55	30				
14.03	GRANITE	1	1			1	2	MU	KC	GW	.5	S	55	30				
14.20	GRANITE	1	1			1	2	MU	K	G	.5	S	320	20			SHEARED	
14.49	GRANITE	1	1			1	3	MU	KC	GW	.5	MH	85	50				

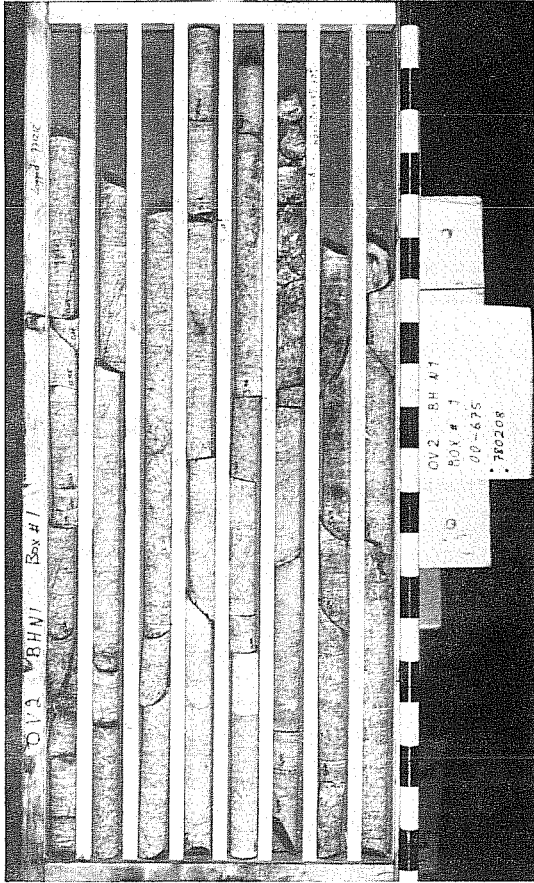
M2		DISCONTINUITIES AND BREAKS					MINERALIZATION				ORIENTATION		REMARKS				
		CONDITION		SURFACE CHARACTERISTICS			TYPE	COLOR	THICKNESS (MM)	HARDNESS	BETA (DEG)	ALPHA (DEG)					
DEPTH (M)	ROCK TYPE	1-NATURAL	2-INDUCED	3-UNCERTAIN	1-OPEN	2-CLOSED							3-OTHER	1-PLANNED	2-CURVED	3-IRREGULAR	ROUGHNESS (MM)
.08	GRANITE	2			2												
.24	GRANITE	2			2												
.61	GRANITE	1			1			3	1	MW	KC	GW	.5	S	185	75	
.70	GRANITE	2			2												
1.38	GRANITE	1			1			3	2	MW	K	G	.5	S	45	65	
1.43	GRANITE	2			2												
1.59	GRANITE	1			1			1	2	MW	KC	GW	.5	S	255	60	SHEARED
2.73	GRANITE	1			1			3	3	SW	C	W	.5	M	60	20	
2.83	GRANITE	1			1			3		SW	KE	G	.5	S-M	280	85	
3.06	GRANITE	1			1			1	1	MW	CE	GW	.5	M	150	85	
3.23	GRANITE	1			1			1	2	SW	C	W	.5	M	0	85	
3.25	GRANITE	1			1			1	2	MW	KCE	GW	.5	M-S	100	20	
3.41	GRANITE	1			1			1	2	MW	C	W	.5	M	110	50	
3.77	GRANITE	1			1			1	3	SW	E	G	.5	M	70	40	
4.14	GRANITE	1			1			2	1	MW	KC	GW	.5	S	285	15	
4.24	GRANITE	2			2												
4.70	GRANITE	1			1			1	1	MW	KC	GW	.5	S-M	160	60	
4.71	GRANITE	1			1			1	2	MW	KE	G	.5	S	270	20	
4.99	GRANITE	1			1			3	2	SW	KE	G	.5	S	270	40	
5.50	GRANITE	1			1			3	2	SW	K	G	.5	S	290	50	
5.75	GRANITE	2			2												
5.81	GRANITE	1			1			3	3	SW	E	G	.5	M	330	60	
5.81	GRANITE	1			1			1	3	SW	C	W	.5	M	210	10	
5.98	GRANITE	1			1			1	5	SW	K	G	.5	S	180	45	
5.99	GRANITE	1			1			1	2	MW	K	G	.5	S	240	25	
6.13	GRANITE	2			2												
6.27	GRANITE	1			1						E	G	20		180	30	SEALED EP ZONE
6.56	GRANITE	2			2												
6.59	GRANITE	1			1			3	3	MW	KC	GW	.5	S	300	5	
6.75	GRANITE	1			1			2	3	MW	KC	GW	.5	S	130	10	
6.83	GRANITE																MANY FR. 6.83-6.91
6.87	GRANITE	1			1			1	2	MW	C	RW	.5	M	20	30	
6.89	GRANITE	1			1			1	2	MW	K	G	.5	S	280	15	
6.91	GRANITE	3			3			3	4	SW	K	G	.5	S		90	
6.91	GRANITE	1			1			1	1	SW	KC	GW	.5	S-M	275	10	
6.93	GRANITE	1			1			3	2	SW	C	W	.5	MH	35	50	
7.03	GRANITE	1			1			2	2	SW	C	W	.5	MH	60	35	ONLY THRU 1/2 CORE
7.03	GRANITE	1			1			2	2	MW	K	G	.5	S	100	30	
7.14	GRANITE	1			1			1	2	MW	KC	GW	.5	S	280	25	
7.15	GRANITE	1			1			1	1	MW	K	G	1	S	250	20	
7.37	GRANITE	3			3			3	2	SW	K	G	.5	MH	360	80	PARTLY INDUCED
7.59	GRANITE	2			2												
7.93	GRANITE	1			1			2	1	MW	KC	GW	.5	MH	25	75	
8.21	GRANITE	1			1			1	1	MW	KC	GW	.5	S	300	50	SHEARED
8.21	GRANITE	1			1			1	2	MW	KC	GW	.5	MH	45	65	
8.48	GRANITE	1			1			1	2	MW	K	G	1	S	350	70	

M4		DISCONTINUITIES AND BREAKS					MINERALIZATION				ORIENTATION		REMARKS		
		CONDITION		SURFACE CHARACTERISTICS			ROUGHNESS (MM)	WEATHERING	TYPE	COLOR	THICKNESS (MM)	HARDNESS		BETA (DEG)	ALPHA (DEG)
DEPTH (M)	ROCK TYPE	1-NATURAL	2-INDUCED	3-UNCERTAIN	1-OPEN	2-CLOSED							3-OTHER		
.04	GRANITE				2										
.09	GRANITE	1	1		1	1	NW	K	BK	.5	MH	70	25		
.10	GRANITE	1	1		1	2	SU	C	W	.5	MH	350	15		
.18	GRANITE	1	1		1	1	SU	K	BK	.5	MH	125	60		MOSTLY CLOSED PARTLY INDUCED
.29	GRANITE	1	1		1	1	SU	K	BK	.5	MH	80	60		
.32	GRANITE	1	1		1	1	SU	KC	BK	.5	MH	260	20		
.35	GRANITE	1	1		1	1	SU	K	BK	.5	MH	75	50		SHEARED
.44	GRANITE	1	1		2	1	SU	KC	BKW	.5	MH	90	40		B=150
.46	GRANITE	1	1		1	1	SU	KC	BK	.5	MH	85	55		
.49	GRANITE	1	1		1	1	SU	KC	BK	.5	MH	80	45		
.76	GRANITE	1	1		2	1	NW	KC	BK	1	MH	65	65		
.79	GRANITE	1	1		1	1	S-NW	KC	BKW	.5	MH	70	55		
.85	GRANITE	1	1		1	1	S-NW	KC	BKW	.5	MH	55	55		
.97	GRANITE	1	1		1	2	NW	KH	BK	.5	S-MH	285	35		END OF FRACTURE .98
.98	GRANITE	1	1		1	1	NW	KC	BKW	.5	MH	150	25		
1.05	GRANITE	1	1		2	1	M-NW	KC	BKW	.5	MH	270	45		2 FR;SHEARED,B=315
1.25	GRANITE	1	1		2	1	SU	KC	BKW	.5	MH	80	50		
1.28	GRANITE	1	1		1	2	NW	KC	BKW	.5	MH	75	70		SHEARED,B=145
1.34	GRANITE	1	1		1	2	NW	KC	BKW	.5	MH	80	55		
1.46	GRANITE	1	1		1	2	SU	KC	BKW	.5	MH		90		
1.76	GRANITE	1	1		1	1	NW	KC	BKG	3	S-MH	270	15		
1.86	GRANITE	1	1		3	2	SU	KC	BKW	.5	MH	130	80		
.86	GRANITE	1	1		2	1	SU	KC	BKW	.5	MH	65	55		OPENED BY LOGGER
1.88	GRANITE	2													
1.90	GRANITE	2													
2.09	GRANITE	1	1		2	2	NW	KC	BKW	.5	MH	65	35		
2.36	GRANITE	1	1		1	1	SU	K	BK	.5	MH	270	75		
2.42	GRANITE	1	2					K	BKG	1		180	45		SEALED WITH K
2.46	GRANITE	1	1		1	1	SU	K	BK	.5	MH	300	70		
2.58	GRANITE	1	2					E		5	H	175	50		
2.62	GRANITE	2													
2.69	GRANITE	1	2					K	G	2	MH	165	30		
3.05	GRANITE	1	1		1	2	NW	K	BKG	.5	MH	295	30		
3.11	GRANITE	1	2							.5		305	10		
3.42	GRANITE	1	1		3	2	NW	KC	BKW	.5	MH	270	40		
3.54	GRANITE	1	1		1	1	NW	K	BKG	.5	MH	285	40		SHEARED,B=320
3.61	GRANITE	1	1		1	1	NW	K	BK	.5	MH	55	85		
3.68	GRANITE	1	2					K	G	3	MH	185	30		
4.11	GRANITE	1	1		2	1	SU	KC	BKW	.5	MH	90	50		PARTLY INDUCED
4.17	GRANITE	1	2						G			160	10		
4.31	GRANITE	1	2					C	W	.5	MH	90	50		
4.42	GRANITE	1	1		2	1		KC	GW	.5	MH	300	40		
4.59	GRANITE	1	2					K	G	1		155	25		
4.68	GRANITE	1	1		2	1	NW	K	G	1	MH	180	25		
4.68	GRANITE	1	2					KE							SEALED FR,4.68-4.84
4.74	GRANITE	2													
4.76	GRANITE	1	2					E		5		175	35		
4.84	GRANITE	2													
5.03	GRANITE	1	1		2	2	SU	K	BK	.5	MH	185	20		
5.15	GRANITE	2													
5.17	GRANITE	1	2					E		4		230	15		
5.31	GRANITE	1	2					E		8		165	25		
5.31	GRANITE	1	1							.5			90		PARTLY OPEN
5.34	GRANITE	2													
5.51	GRANITE	1	1			1	SU	KC	BK	.5	MH	60	3		MOSTLY INDUCED
5.62	GRANITE	1	1			2	SU	KC	BKW	.5	MH	115	55		
5.73	GRANITE	1	1		1	1	MH	KC	BKW	.5	MH	85	60		
5.82	GRANITE	1	2					K		.5		270	40		SEALED FRACTURE

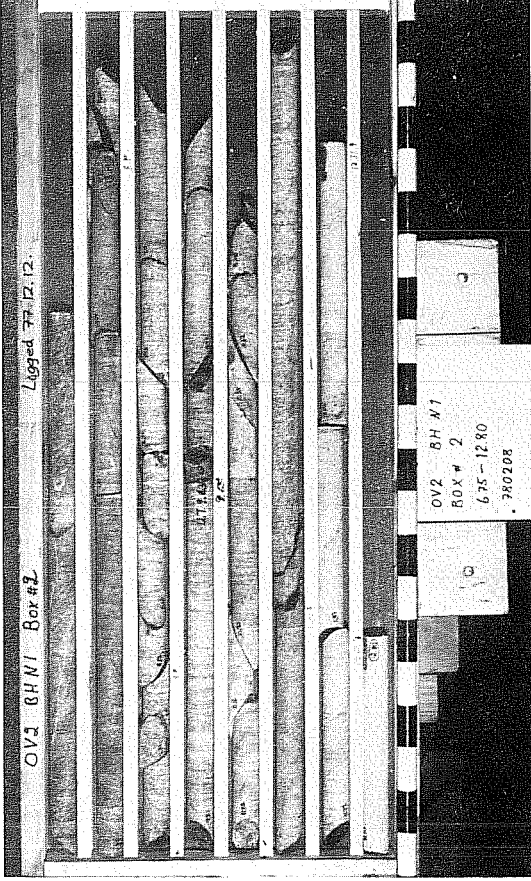
M4		DISCONTINUITIES AND BREAKS					MINERALIZATION				ORIENTATION		REMARKS						
		CONDITION		SURFACE CHARACTERISTICS			TYPE	COLOR	THICK- NESS (MM)	HARD- NESS	BETA (DEG)	ALPHA (DEG)							
DEPTH (M)	ROCK TYPE	1- NATURAL	2- INDUCED	3- UNCERTAIN	1- OPEN	2- CLOSED							3- OTHER	1- PLANAR	2- CURVED	3- IRREGULAR	ROUGH- NESS (MM)	WEATH- ERING	
5.84	GRANITE	1			2								K		.5		275	55	SEALED FRACTURE
5.87	GRANITE	1	1			1					2	HU	KC	BKW	.5	MH	80	55	
6.01	GRANITE	1	2												.5		125	40	WITH K OR EP
6.18	GRANITE	1	1		1	1					1	HU	KC	BKW	.5	MH	250	70	SHEARED
6.20	GRANITE	1	1		1	1					1	HU	KC	BKW	.5	MH	95	45	SHEARED, B=80
6.35	GRANITE	1	2										K		1				SEALED FRACTURE
6.45	GRANITE	1	1		1	1					1	SU	K	BK	.5	MH	260	60	
6.54	GRANITE	1	2										K		1		110	70	SEALED FR, A=55-70
7.00	GRANITE	1	1		3	1					1	HU	KC	BKW	2	MH	60	60	
7.05	GRANITE	1	1		1	1					1	SU	KC	BKGW	.5	MH	110	45	
7.10	GRANITE	1	1		1	2					2	SU	KC	BKG	.5	MH	75	45	
7.18	GRANITE	1	1		2	1					1	S-HU	KC	BKW	.5	MH	90	40	
7.21	GRANITE	1	1		1	1					1	HU	KC	BKW	.5	S-MH	95	45	SHEARED, B=120
7.31	GRANITE	1	2										K		1		80	35	SEALED FRACTURE
7.35	GRANITE	1	1		1	1					1	HU	KC	BKW	.5	MH	90	40	SHEARED, B=165
7.48	GRANITE	1	1		1	1					1	HU	KC	BKW	1	MH	115	45	
7.51	GRANITE	1	1		1	1					1	SU	KC	BKW	.5	MH	105	50	SHEARED, B=165
7.57	GRANITE	1	1		1	1					1	SU	KC	BKW	.5	MH	105	50	
7.65	GRANITE	1	1		1	1					1	SU	KC	BKW	.5	MH	100	50	SHEARED, B=160
7.71	GRANITE	1	1		1	2					2	SU	KC	BKW	.5	MH	110	40	SHEARED, B=180
7.88	GRANITE	1	1		2	1					1	HU	KC	BK	.5	MH	110	55	
7.97	GRANITE	1	2										K	G	4		320	65	SEALED FRACTURE
8.14	GRANITE	1	1		1	1					1	HU	K	BK	.5	MH	105	60	SHEARED, B=155
8.35	GRANITE	1	1		1	1					1	HU	K	BK	.5	MH	255	75	
8.40	GRANITE	1	1		1	1					1	S-HU	KC	BKW	.5	MH	85	40	
8.45	GRANITE	1	1		3	2					2	SU	K	BK	.5	MH	70	70	
8.47	GRANITE	1	1		2	1					1	HU	K	BK	.5	MH	85	45	
8.53	GRANITE	1	1		3	1					1	SU	K	BK	.5	MH	85	50	
8.61	GRANITE	1	1		2	1					1	HU	KC	BKGW	.5	MH	105	70	SHEARED, B=155
8.76	GRANITE	1	2										K		1				MANY SEALED FRACT; B=70-90, A=50-55
8.80	GRANITE	1	1		3	2					2	SU	K	BK	.5	MH	210	70	
8.85	GRANITE	1	2										K		1				MANY SEALED FRACT, 8.85-8.88; B=110-115, A=45-55
9.43	GRANITE	1	1		1	1					1	SU	C	W	.5	MH	20	80	
9.51	GRANITE	1	1		3	2					2	SU	K	BK	.5	MH	90	65	
9.54	GRANITE	1	1		1	2					2	SU	K	BK	.5	MH	80	55	
9.77	GRANITE	1	1		1	2					2	SU	K	BK	.5	MH	75	70	
10.05	GRANITE	2																	
10.09	GRANITE	1	2										KE		1		80	50	1 SEALED FRACTURE
10.83	GRANITE	1	2										KE		1		75	60	10 SEALED FRACTURES 10.09-10.83; A=50-60
10.83	GRANITE	1	1		1	2					2	HU	K	BK	.5	MH	75	45	
10.91	GRANITE	1	1		1	1					1	HU	KC	BKW	2	MH	320	45	SHEARED, B=315
11.04	GRANITE	1	1		1	1					1	HU	KC	BKW	.5	MH	80	55	
11.09	PEGMATITE																360	65	30MM
11.12	GRANITE																		
11.23	GRANITE	1	1		1	1					1	SU	K	BK	.5	MH	65	65	
11.30	GRANITE	1	2										E		1		285	45	1 SEALED FRACTURE
11.46	GRANITE	1	1		1	2					2	HU	KC	BKW	.5	MH	65	60	
11.50	GRANITE	1	1		1	2					2	SU	K	BK	.5	MH	50	50	PARTLY INDUCED
11.88	GRANITE	1	1		2	2					2	HU	KC	BKW	.5	MH	275	25	
12.55	GRANITE	1	1		1	2					2	S-HU	K	BK	.5	MH	320	80	PARTLY INDUCED
12.82	GRANITE	1	1		1	1					1	HU	KC	BKG	.5	MH	75	70	SHEARED, B=130
12.88	GRANITE	1	1		3	2					2	HU	KC	BKW	.5	MH	175	75	
12.94	GRANITE	1	1		3	3					3	SU	K	BK	.5	MH	270	60	
13.09	GRANITE	1	1		2	2					2	HU	K	BKG	1	MH	295	30	
13.58	GRANITE	1	2										C		1		110	60	SEALED FRACTURE

M5		DISCONTINUITIES AND BREAKS					MINERALIZATION				ORIENTATION		REMARKS		
		CONDITION		SURFACE CHARACTERISTICS			ROUGHNESS (MM)	WEATHERING	TYPE	COLOR	THICKNESS (MM)	HARDNESS		BETA (DEG)	ALPHA (DEG)
DEPTH (M)	ROCK TYPE	1-NATURAL	2-INDUCED	3-UNCERTAIN	1-OPEN	3-CLOSED							3-OTHER		
.03	GRANITE	3				3	2	SW	K	BKG	.5	MH	220	55	
.13	GRANITE	1				2	2	MW	K	BK	.2	MH	295	65	
.56	GRANITE	1				2	2	S-MW	K	BK	.5	MH	200	60	
.79	GRANITE	1				1	2	SW	K	BK	.5	MH	325	55	
.84	GRANITE	1				1	2	SW	K	BK	.5	MH	270	50	
.93	GRANITE	1											345	55	
.98	GRANITE	2													
1.34	GRANITE	1				1	1	MW	KC	BKW	.5	MH	180	35	
1.52	GRANITE	1				1	2	MW	KC	BKGW	.5	MH	215	45	
1.58	GRANITE	1				1	2	SW	K	BK	.5	MH	180	85	
1.59	GRANITE	1				1	2	MW	K	BK	.5	MH	170	65	
1.61	GRANITE	1				1	1	MW	K	BK	.5	MH	180	65	SHEARED, B=150
1.65	GRANITE	1				1	1	MW	K	BK	.5	MH	190	50	SHEARED, B=135
1.70	GRANITE	1				1	1	MW	K	BK	.5	MH	225	50	TWO SUBPARALLEL FRACTURES
1.74	GRANITE	1				1	2	MW	K	BKG	.5	MH	75	40	SHEARED=155
1.80	GRANITE	1				1	2	MW	K	BK	.5	MH	160	50	
2.80	GRANITE	1				1	1	MW	KC	BK	.5	MH	80	40	
2.21	GRANITE	2													
2.26	GRANITE	1				1	1	MW	K	BKG	.5	MH	165	20	
2.33	GRANITE	1				1	2	SW	K	BK	.5	MH	215	75	
2.50	GRANITE	2													
2.87	GRANITE	1				1	1	SW	K	BK	.5	MH	70	50	
3.33	GRANITE	1				1	2	MW	KC	BK	.1	MH	315	45	SHEARED, B=300
3.41	GRANITE	1				1	2	MW	K	BK	.5	MH	315	60	SHEARED, B=310
3.47	GRANITE	1				1	2	SW	KC	BK	.5	MH	65	40	
3.54	GRANITE	1				1	2	MW	K	G	.5	MH	30	35	SHEARED B=310
3.58	GRANITE	1				1	1	SW	KC	BK	.5	MH	70	50	
3.58	GRANITE	1				1	2	SW	K	BK	.5	MH	235	65	
3.69	GRANITE	1				1	3	MW	KE	BKG	.5	H	230	75	PARTLY LOST
3.69	GRANITE	1				1	3	SW	K	BK	.5	MH		90	
3.95	GRANITE	1				1	1	SW	K	BK	.5	MH	85	35	PART INDUCED
4.09	GRANITE	1				1	1	MW	KC	BKW	.5	MH	80	35	SHEARED, B=160
4.29	GRANITE	1				1	2	SW	K	BK	.5	MH	230	65	
4.31	GRANITE	1				1	1	SW	K	BK	.5	MH	80	40	SHEARED, B=155
4.43	GRANITE	1				2			K		1		75	45	SEALED FRACTURE
4.53	GRANITE	1				2			K		1		270	15	SEALED FRACTURE
4.55	GRANITE	1				2			KI		1		95	45	SEALED FRACTURE
4.69	GRANITE	1				1	2	SW	K	BK	.5	MH	250	65	
4.70	GRANITE	1				1	1	SW	K	BK	.5	MH	90	40	
4.81	GRANITE	1				1	2	M-HW	C	RU	1	MH	35	75	MICROCLINE
4.88	GRANITE	1				2			E		2		315	50	SEALED FR; MICROCLIN
4.98	GRANITE	1				1	2	MW	K	BKG	.5	MH	295	25	SHEARED, B=0
5.07	GRANITE	1				1	1	MW	KC	BKGW	.5	MH	35	20	
5.11	GRANITE	1				1	1	S-MW	KC	BKW	.5	MH	85	40	
5.11	GRANITE	1				1	2	MW	K	G	.5	MH	360	50	SHEARED, B=315
5.12	GRANITE	1				1	1	MW	KC	G	.5	MH	310	40	SHEARED, B=320
5.18	GRANITE	1				1	2	SW	K	BK	.5	MH	90		
5.29	GRANITE	1				1	2	SW	KC	BKW	.5	MH	60	65	
5.44	GRANITE	1				1	1	SW	K	BK	.5	MH	280	85	
5.70	GRANITE	1				1	1	SW	K	BK	.5	MH	255	75	
5.85	GRANITE	1				1	1	SW	KC	BKW	.5	MH	240	70	
5.93	GRANITE	1				1	1	SW	K	BK	.5	MH	250	70	
5.98	GRANITE	1				1	2	SW	KC	BKW	.5	MH	230	75	PARTLY INDUCED

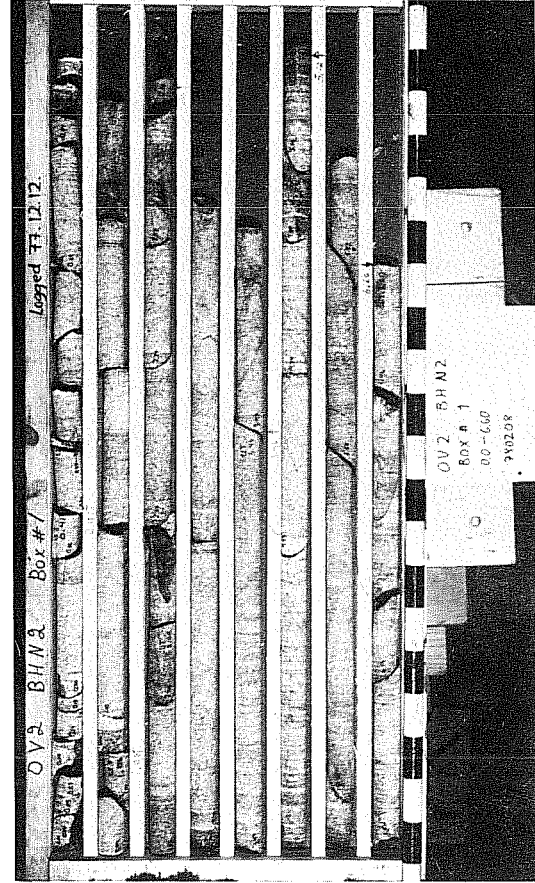
APPENDIX B. Photographs of Time-Scale Experiment Core Samples



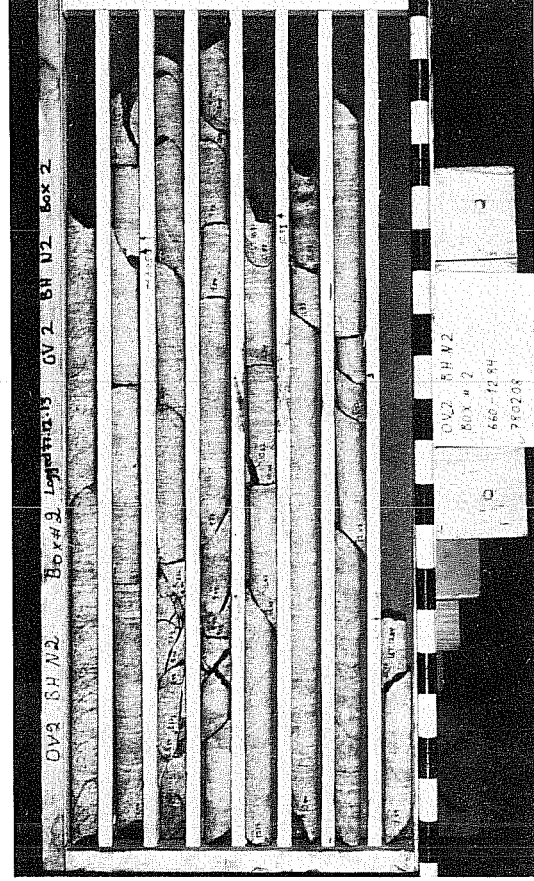
Borehole N1, 0 - 6.75 m (CBB 796-8615)



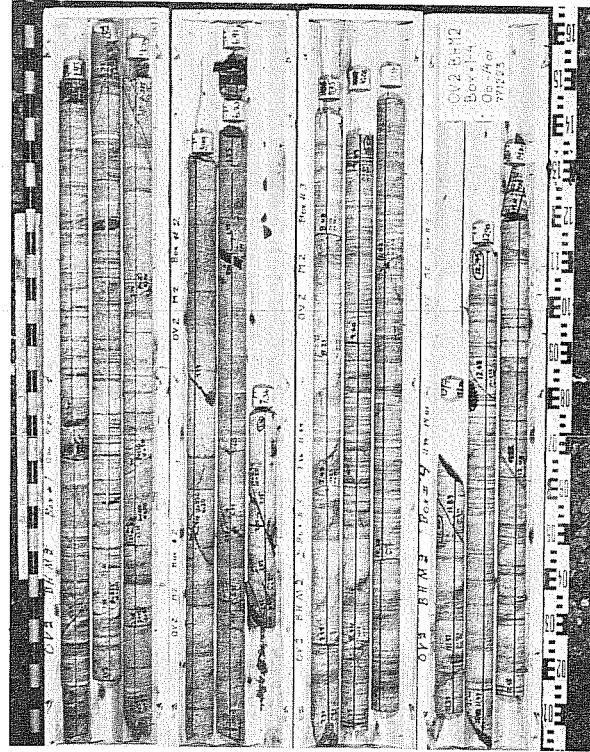
Borehole N1, 6.75 - 12.80 m (CBB 796-8528)



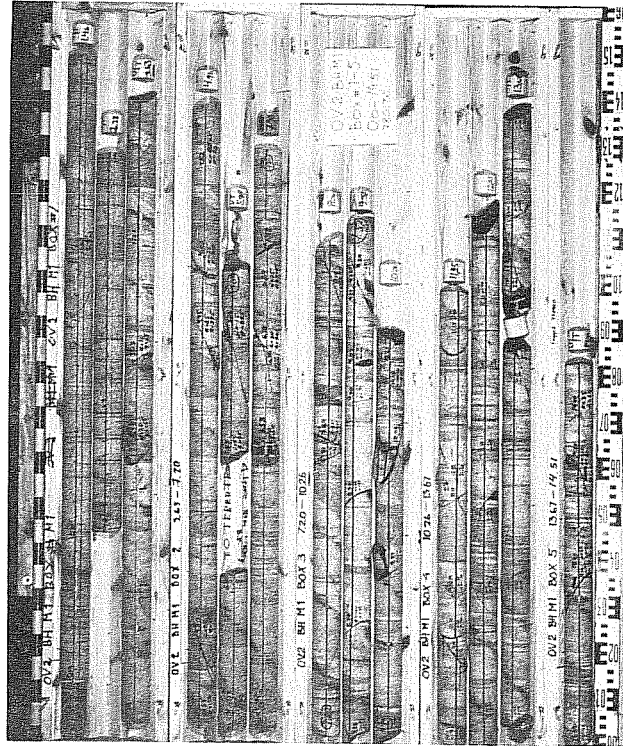
Borehole N2, 0 - 6.60 m (CBB 796-8530)



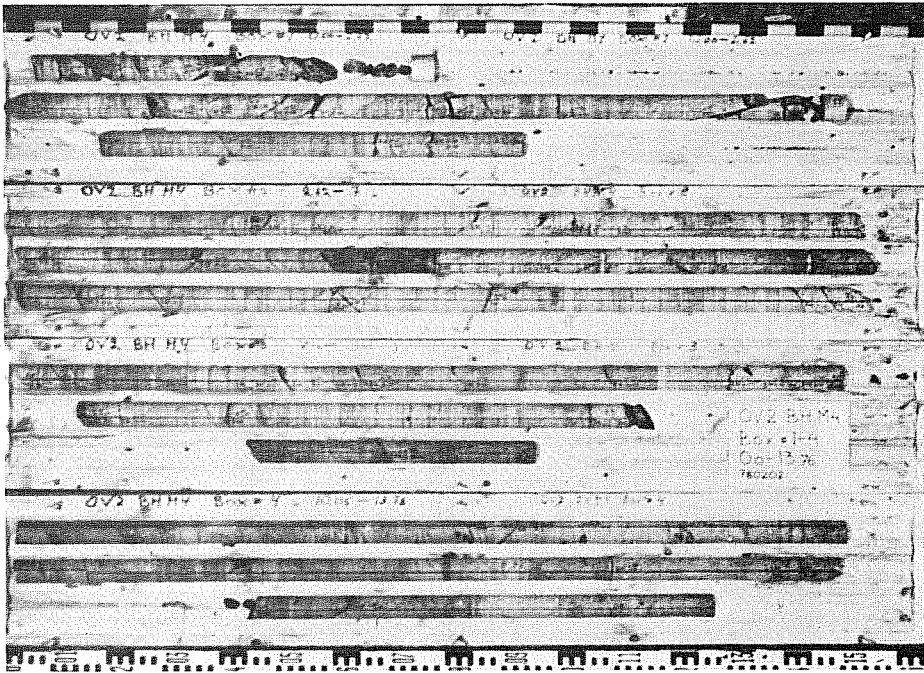
Borehole N2, 6.60 - 12.84 m (CBB 796-8613)



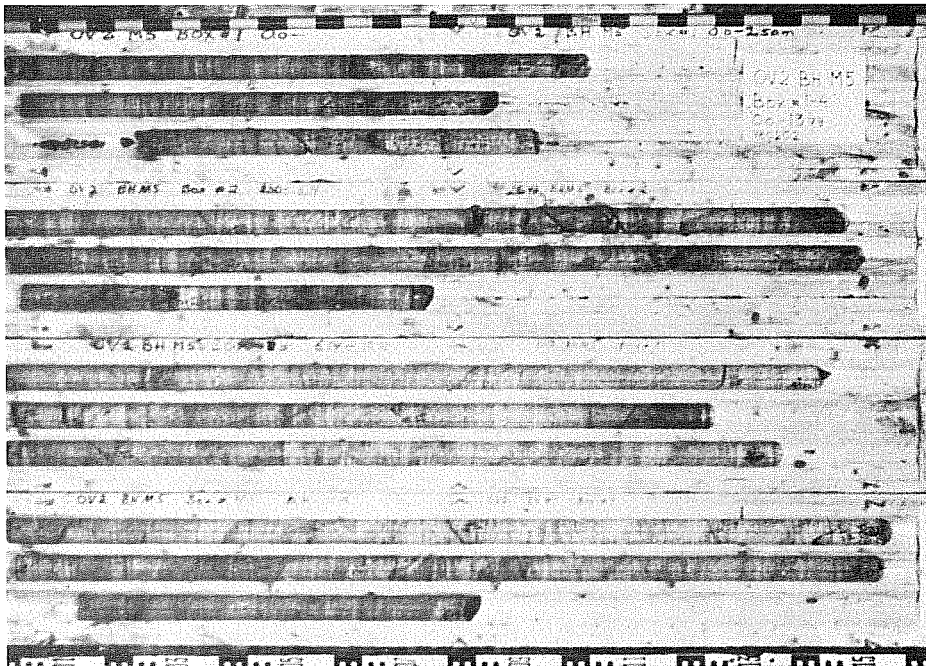
Borehole M2, 0 - 14.01 m (XBC 784-3875)



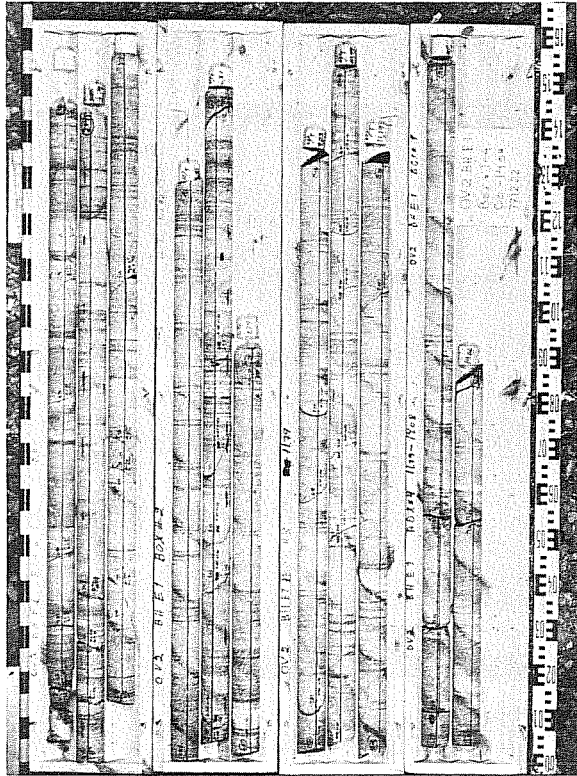
Borehole M1, 0 - 14.51 m (XBC 784-3865)



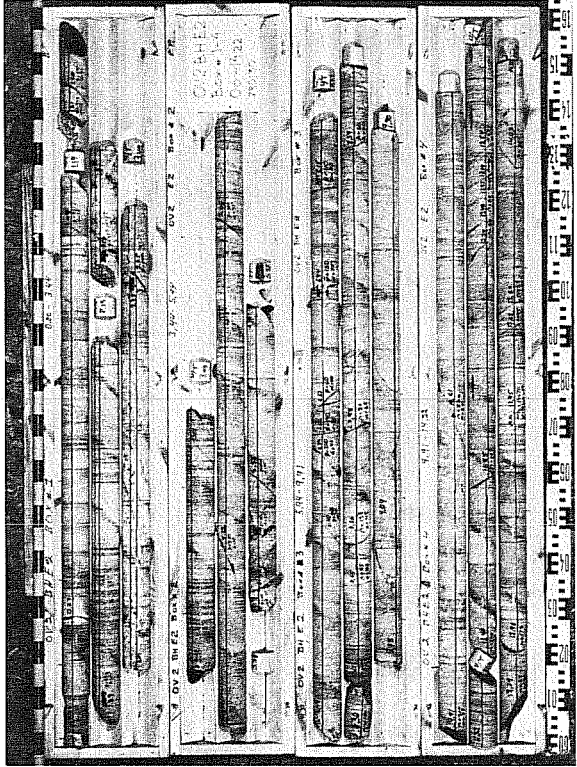
Borehole M4, 0 - 13.76 m (XBC 784-4012)



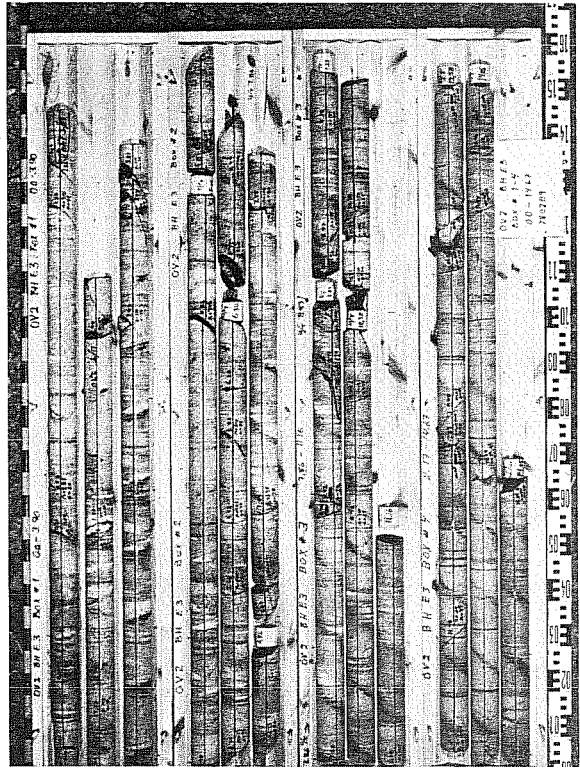
Borehole M5, 0 - 13.79 m (XBC 784-3963)



Borehole E1, 0 - 14.08 m (XBC 784-3871)



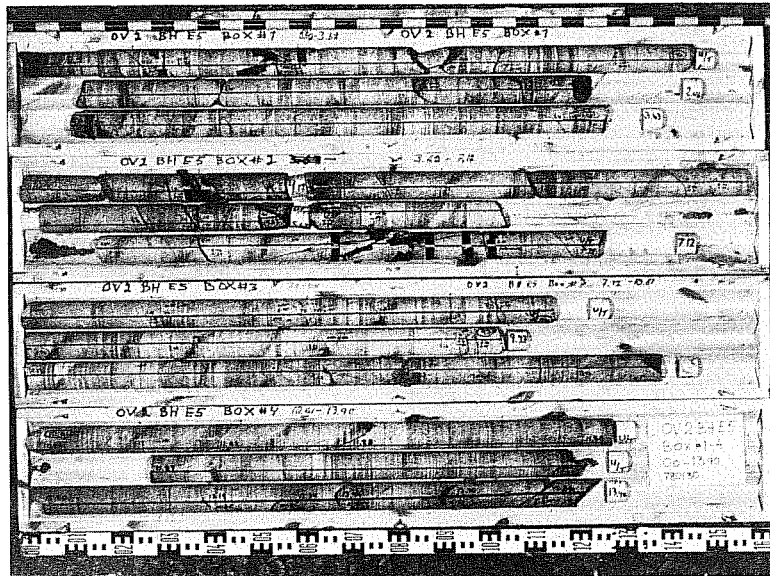
Borehole E2, 0 - 14.22 m (XBC 784-3873)



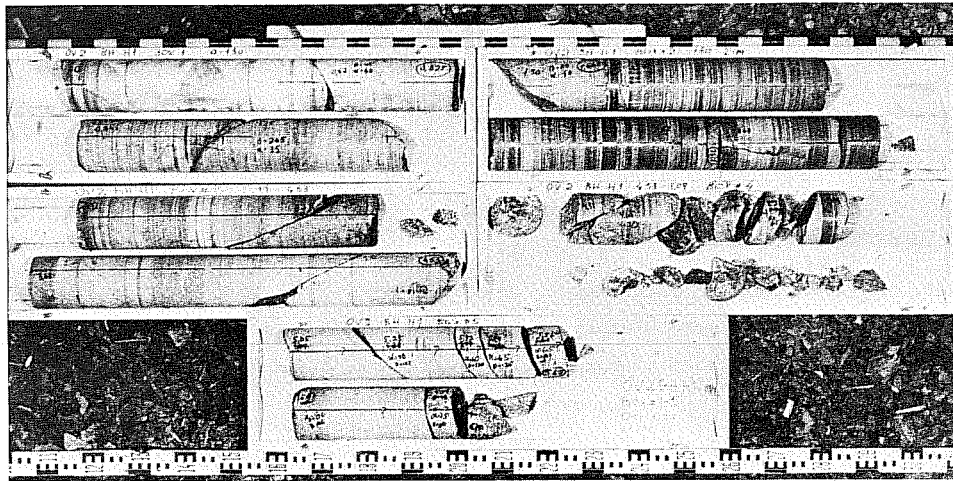
Borehole E3, 0 - 14.67 m (XBC 784-3874)



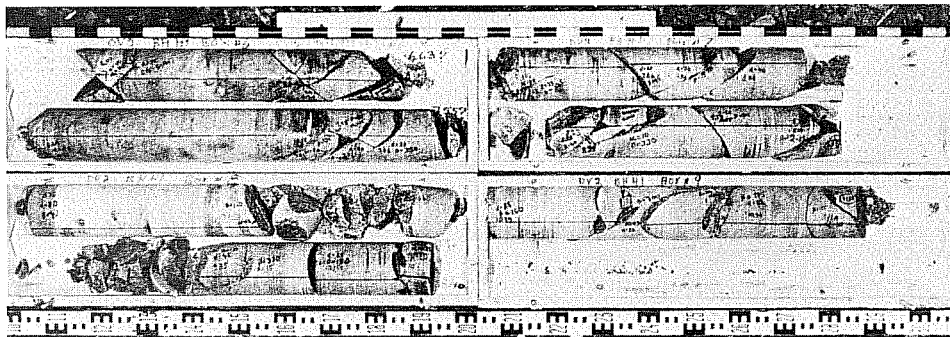
Borehole E4, 0 - 14.58 m (XBC 784-3877)



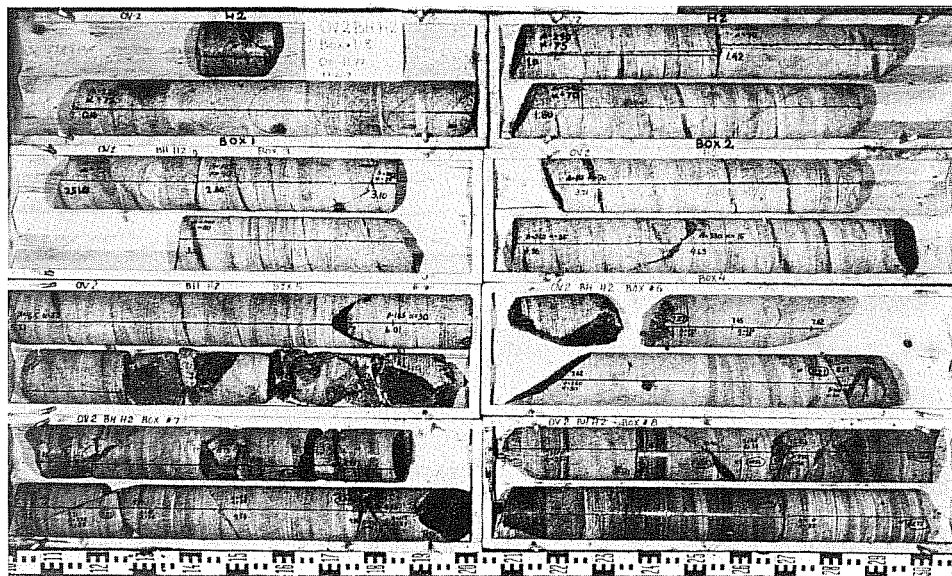
Borehole E5, 0 - 13.90 m (XBC 784-3876)



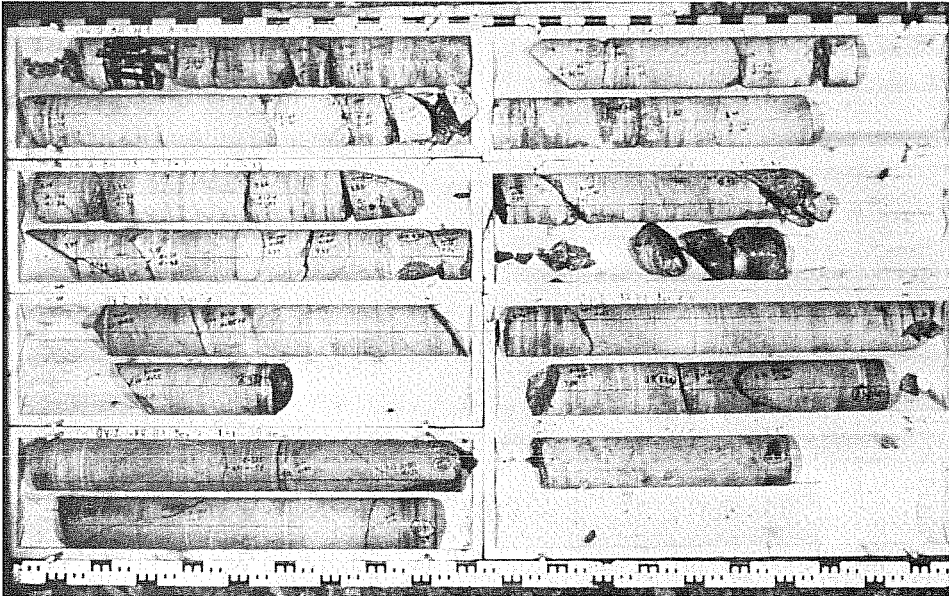
Borehole H1, 0 - 6.07 m (XBC 784-3881)



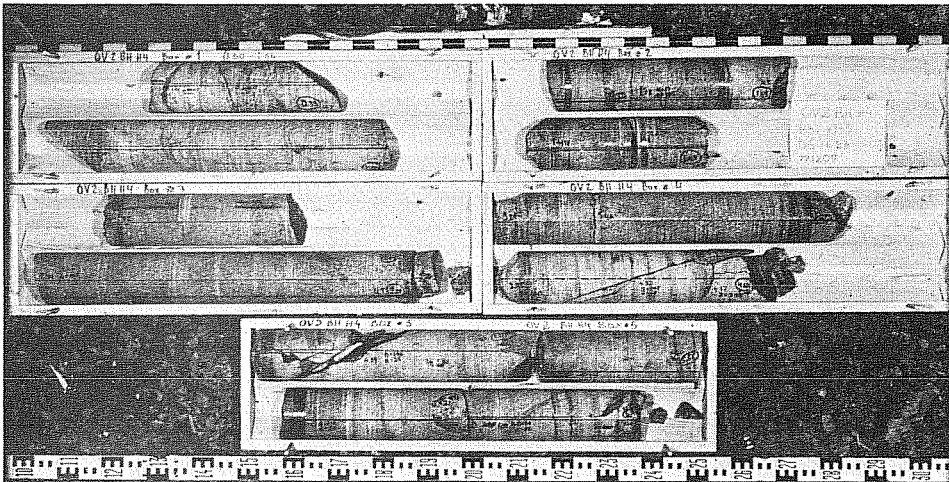
Borehole H1, 6.07 - 11.18 m (XBC 784-3882)



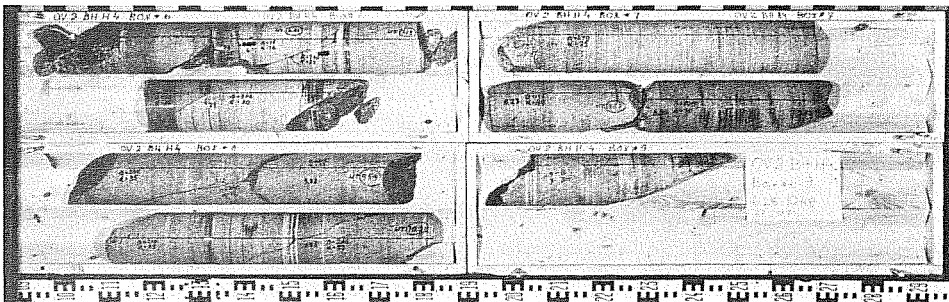
Borehole H2, 0 - 11.77 m (XBC 784-3870)



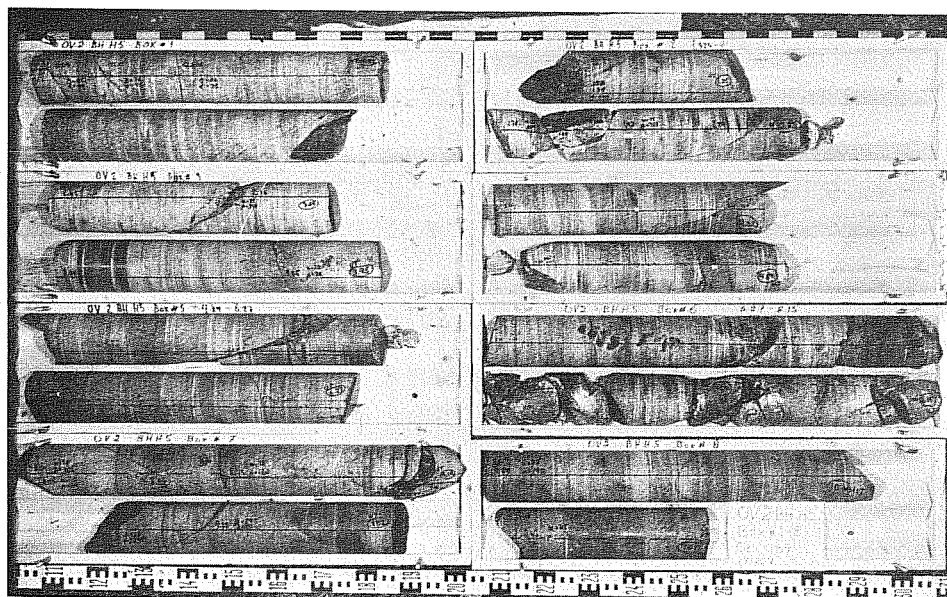
Borehole H3, 0 - 10.85 m (XBC 784-3879)



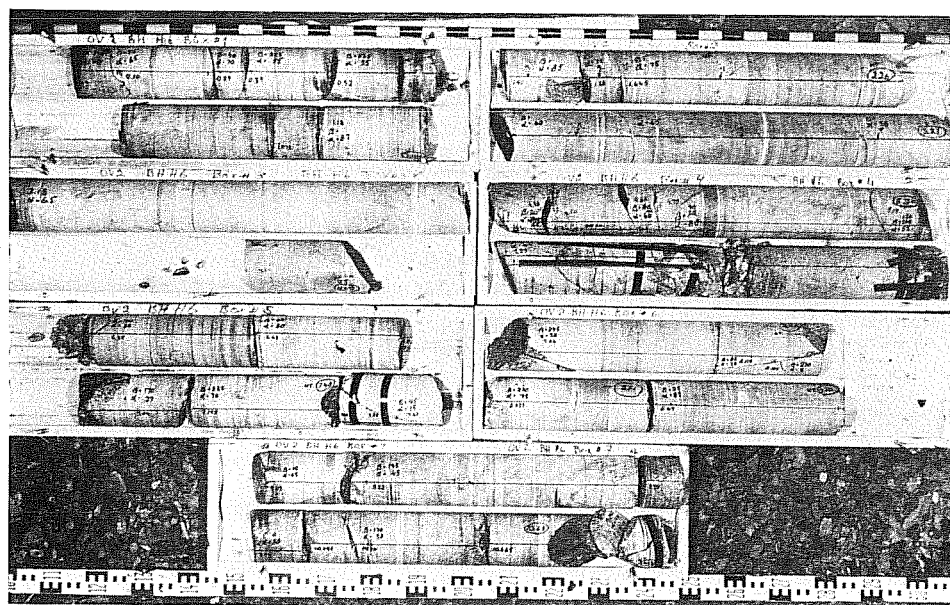
Borehole H4, 0 - 6.28 m (XBC 784-3890)



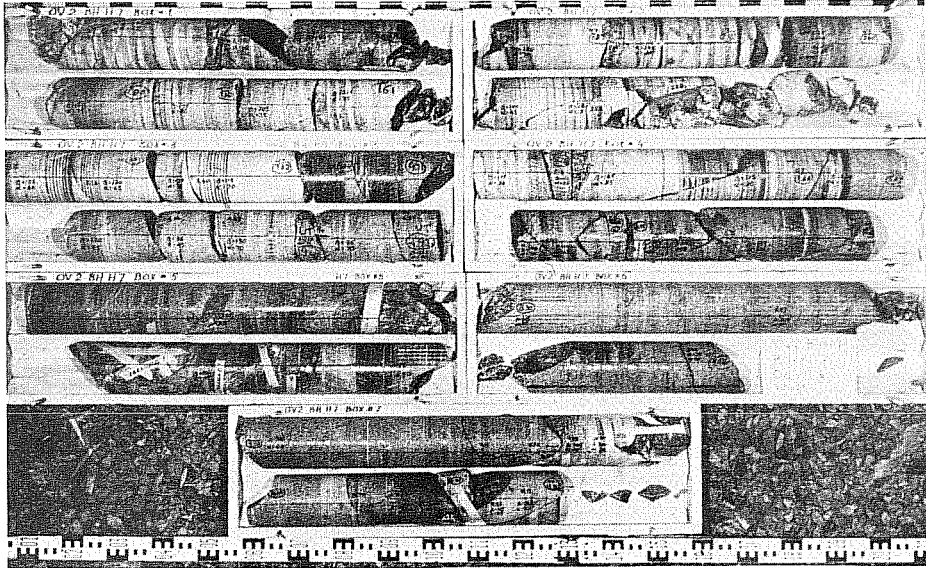
Borehole H4, 6.28 - 10.48 m (XBC 784-3891)



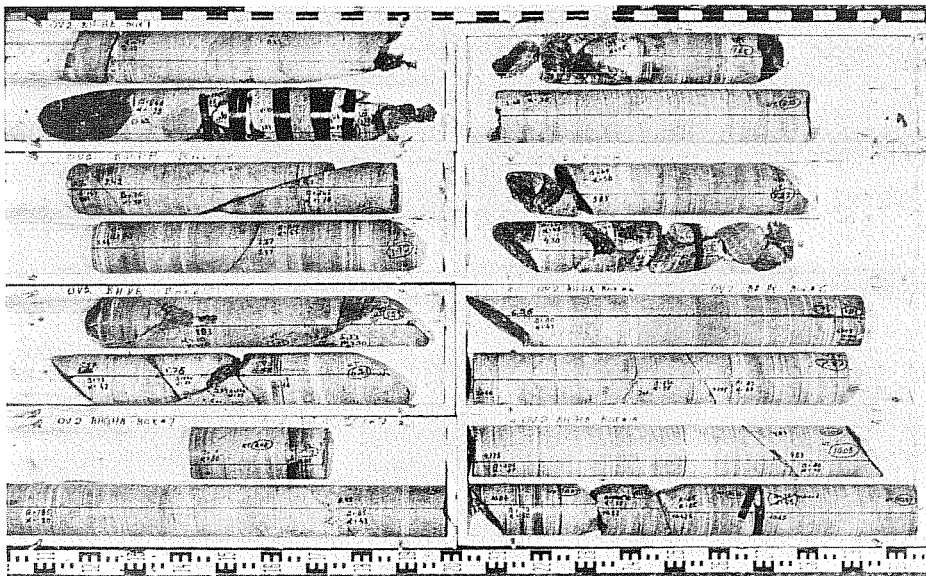
Borehole H5, 0 - 11.07 m (XBC 784-3889)



Borehole H6, 0 - 10.82 m (XBC 784-3880)

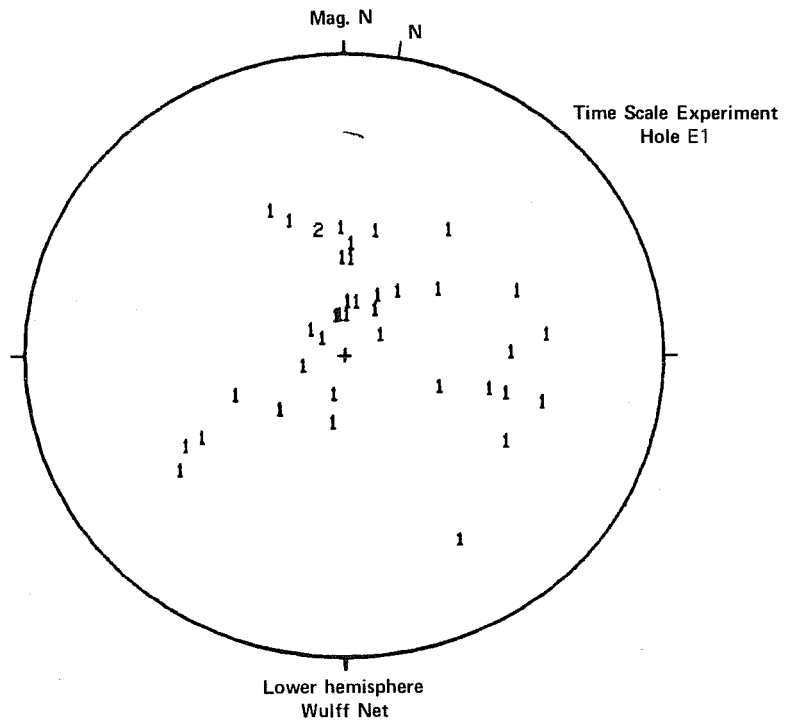


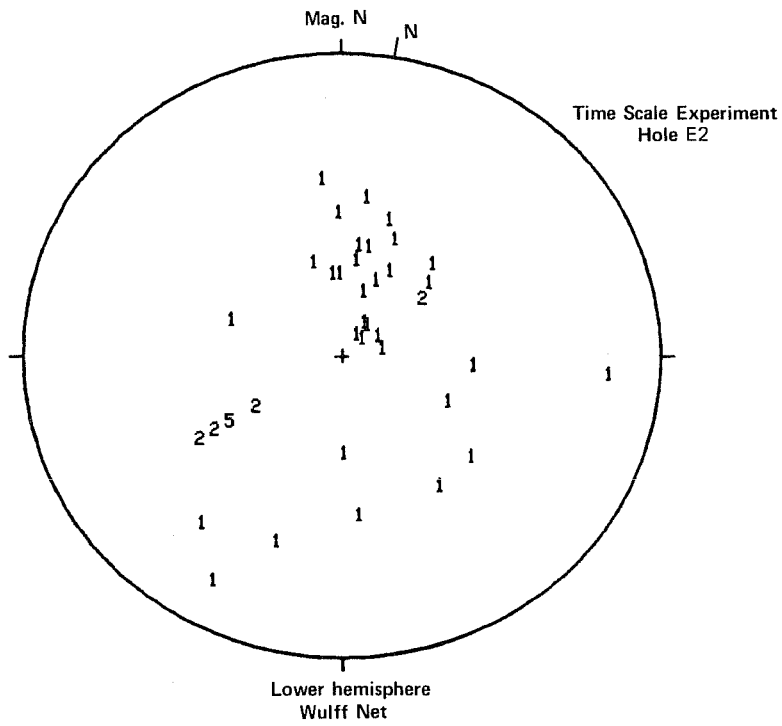
Borehole H7, 0 - 11.18 m (XBC 784-3894)



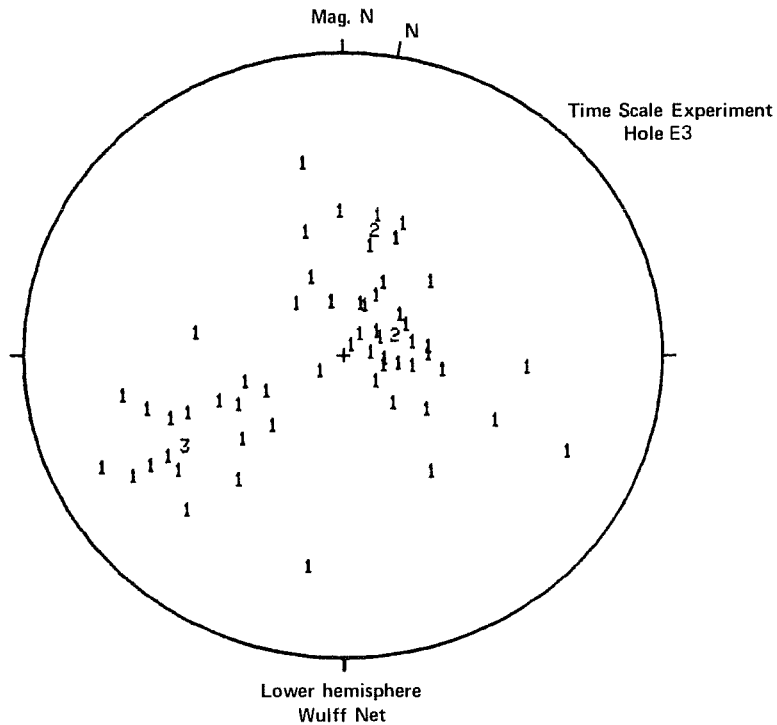
Borehole H8, 0 - 10.97 m (XBC 784-3888)

APPENDIX C. Stereonet Plots of Fracture Poles for Time-Scale Experiment Boreholes

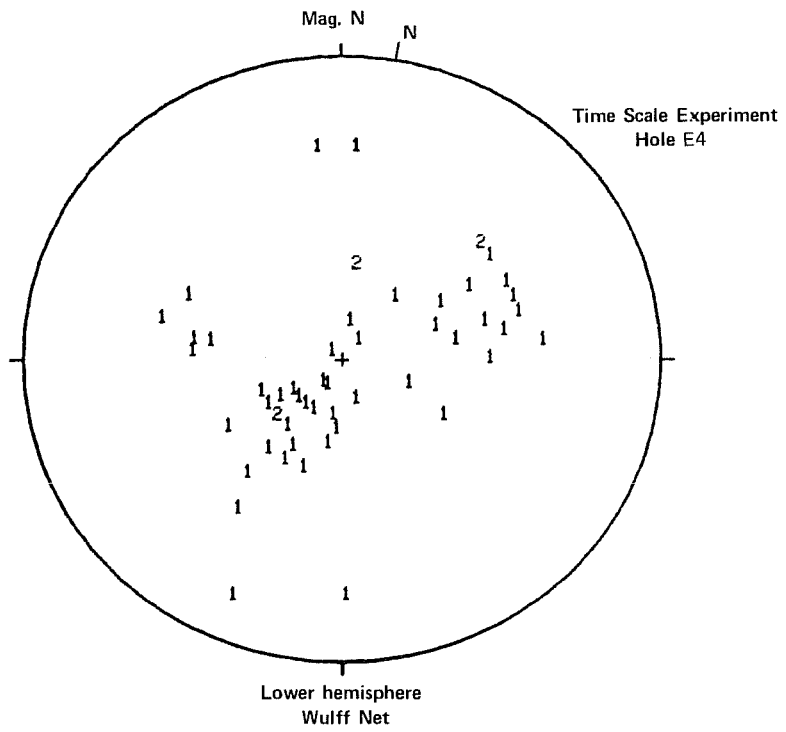




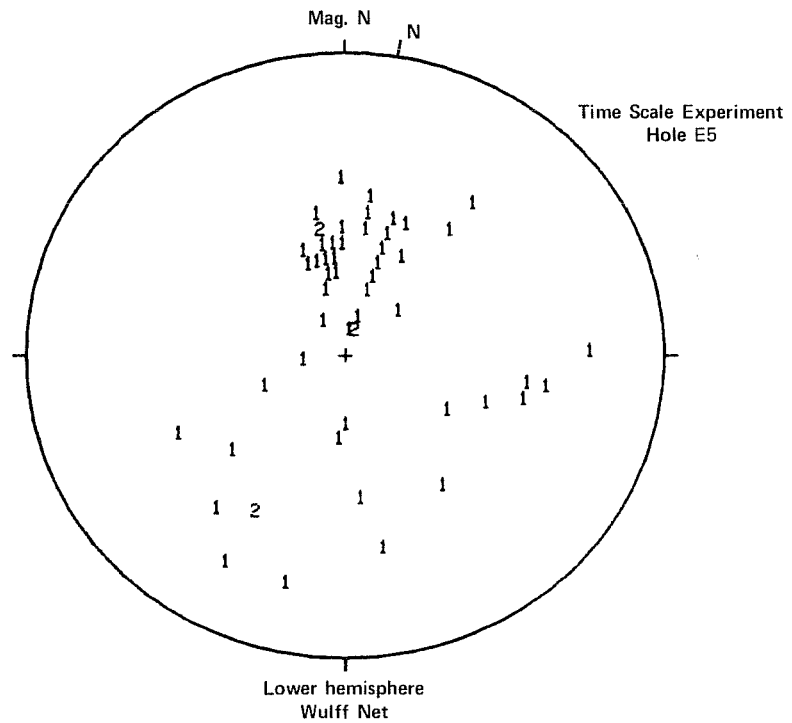
XBL 798-11225



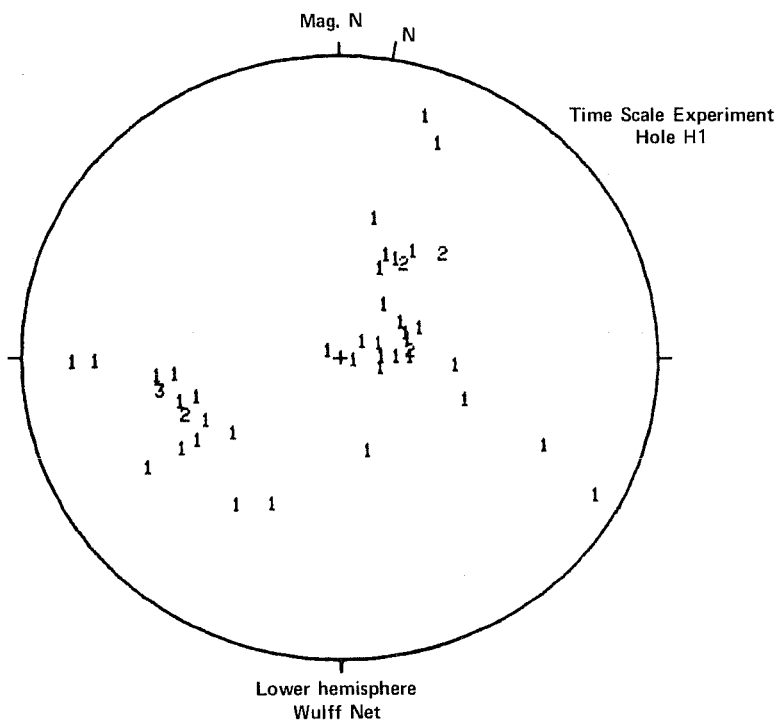
XBL 798-11226



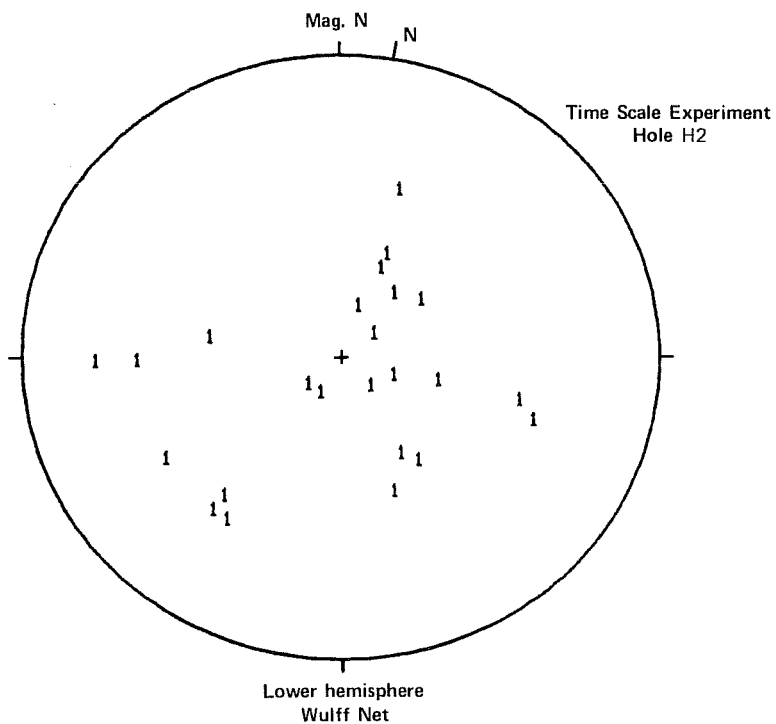
XBL 798-11227



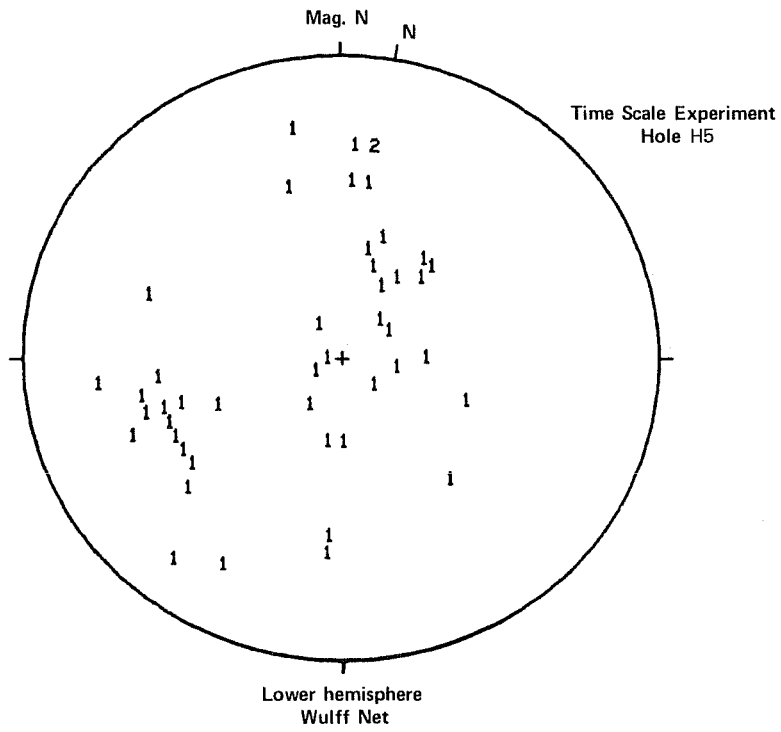
XBL 798-11228



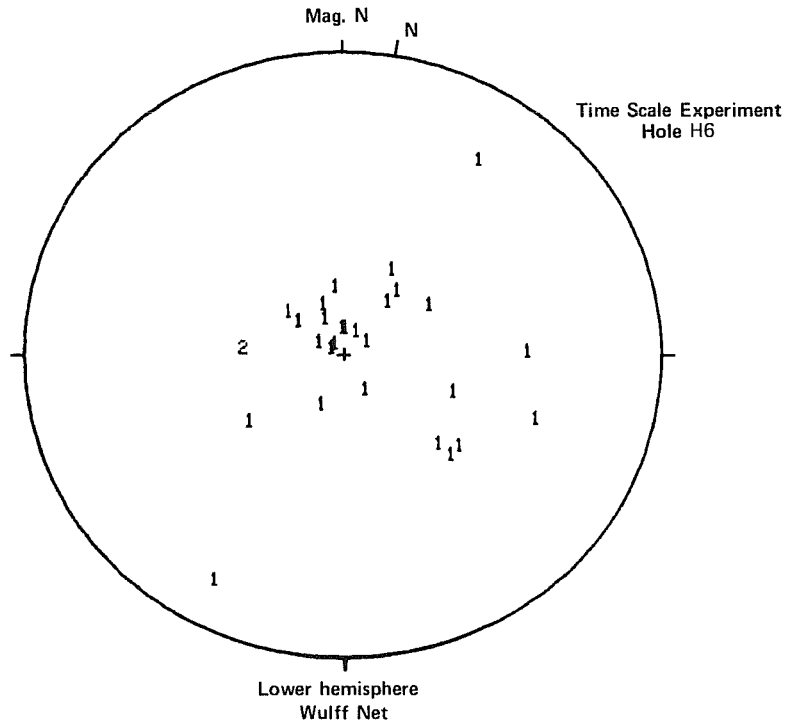
XBL 798-11229



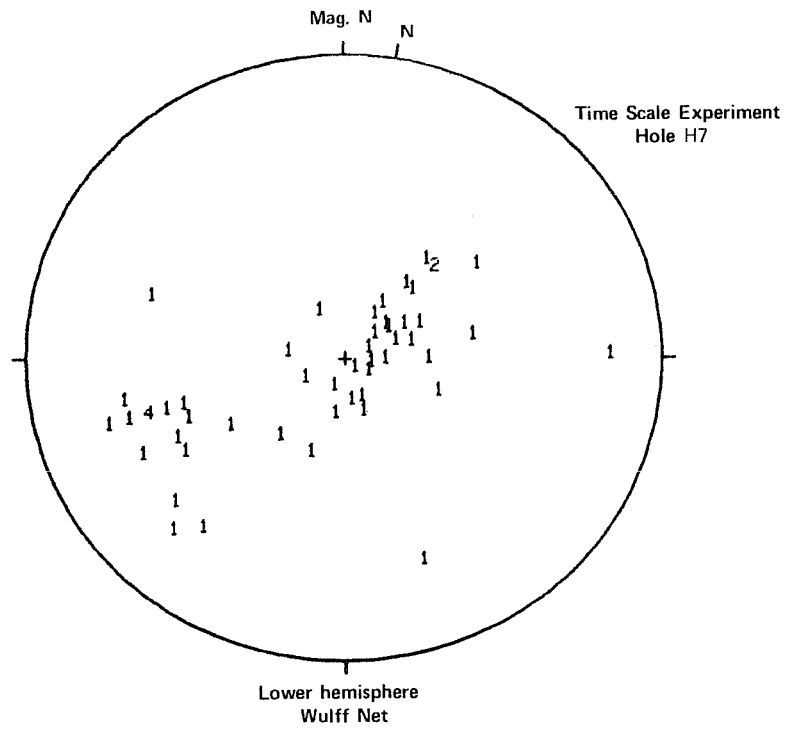
XBL 798-11230



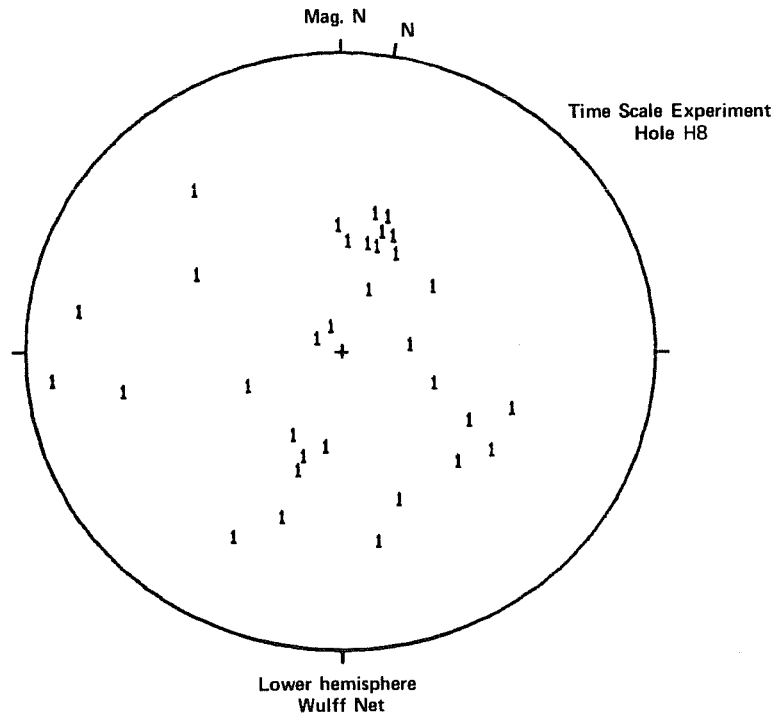
XBL 798-11234



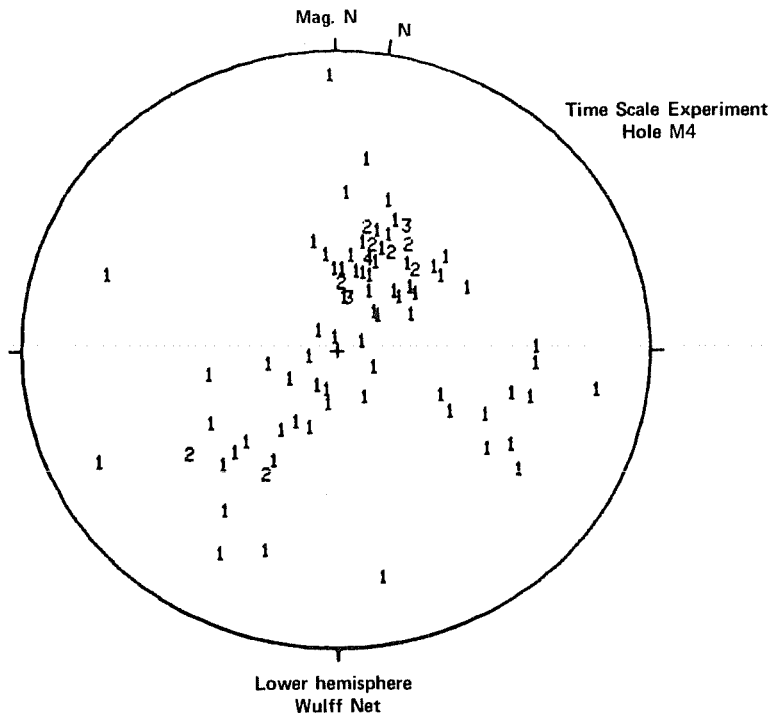
XBL 798-11233



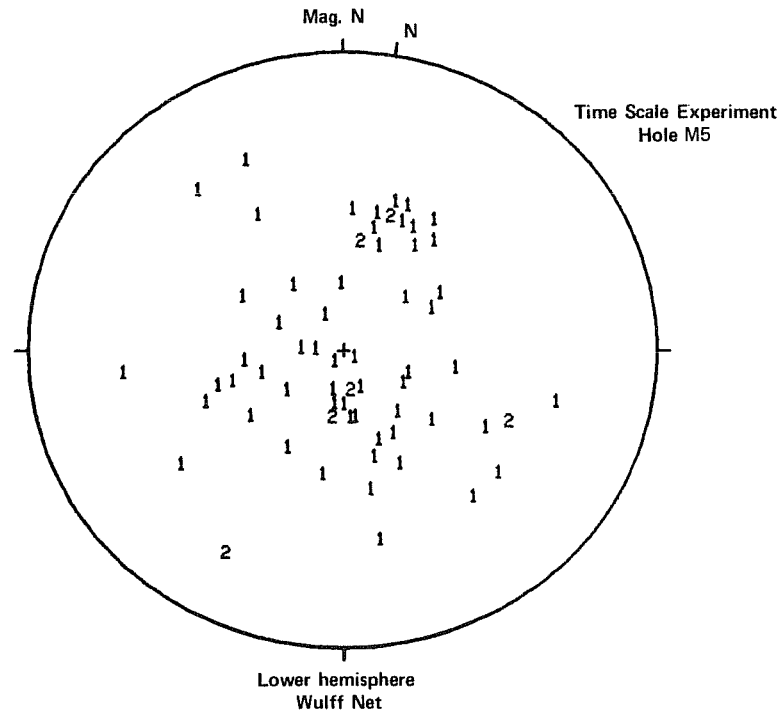
XBL 798-11235



XBL 798-11219



XBL 798-11222



XBL 798-11223

This report is part of a cooperative Swedish-American project supported by the U.S. Department of Energy and/or the Swedish Nuclear Fuel Supply Company. Any conclusions or opinions expressed in this report represent solely those of the author(s) and not necessarily those of The Regents of the University of California, the Lawrence Berkeley Laboratory, the Department of Energy, or the Swedish Nuclear Fuel Supply Company.

Reference to a company or product name does not imply approval or recommendation of the product by the University of California or the U.S. Department of Energy to the exclusion of others that may be suitable.

TECHNICAL INFORMATION DEPARTMENT

LAWRENCE BERKELEY LABORATORY

UNIVERSITY OF CALIFORNIA

BERKELEY, CALIFORNIA 94720

62

284707

ANDREW DUBOIS
EARTH SCIENCES DIV
BLDG 90, RM 1070D
LBL

62